THESIS

MEMBRANE AND DIFFUSION BEHAVIOR OF A COMPACTED SAND-BENTONITE MIXTURE FOR HYDRAULIC AND CHEMICAL CONTAINMENT APPLICATIONS

Submitted by

Amara Joy Meier

Department of Civil and Environmental Engineering

In partial fulfillment of the requirements

For the Degree of Master of Science

Colorado State University

Fort Collins, Colorado

Spring 2016

Master's Committee:

Advisor: Charles D. Shackelford

Christopher A. Bareither
Gregory L. Butters

ABSTRACT

MEMBRANE AND DIFFUSION BEHAVIOR OF A COMPACTED SAND-BENTONITE MIXTURE FOR HYDRAULIC AND CHEMICAL CONTAINMENT APPLICATIONS

Due to the ability of sodium bentonite (Na-bentonite) to exhibit high swell, low hydraulic conductivity, *k* ($\leq 10^{-10}$ m/s), and semipermeable membrane behavior when exposed to water and dilute chemical solutions, Na-bentonite is commonly used as a component for engineered barriers (e.g., geosynthetic clay liners (GCLs)), or as an engineered barrier (e.g., compacted Na-bentonite buffers) used to contain solid wastes and liquid contaminants. Compacted sand-bentonite (SB) mixtures typically comprising 5 to 20 % Na-bentonite (by dry weight) are commonly used as alternatives to compacted clay liners (CCLs) for containment of solid wastes and liquid contaminants when a suitable natural clay source is not readily or economically available. In addition, membrane behavior, or the ability of a porous material to selectively restrict the passage of dissolved chemical species (solutes), has been shown to exist in many of these bentonite-based barriers, including GCLs, bentonite amended natural clays used for CCLs, and soil-bentonite backfills for *in situ* vertical cutoff walls. However, compacted SB mixtures suitable for use as engineered hydraulic and chemical containment barriers previously have not been evaluated for membrane behavior. As a result of these considerations, the purpose of this study was to evaluate simultaneously the membrane and diffusion behavior of a SB mixture that would be suitable for use as an engineered barrier for hydraulic and chemical containment applications.

Accordingly, membrane tests were conducted on duplicate specimens of a compacted SB mixture comprising 15 % bentonite that was shown to exhibit sufficiently low *k* ($\leq 2.7 \times 10^{-11}$ m/s) to be suitable for use as a hydraulic and chemical containment barrier. In addition, the simultaneous diffusion of the principal salt species evaluated in the study, viz., Cl^- and K^+, was evaluated for one of the specimens. The results indicated that both specimens exhibited virtually the same magnitude of membrane behavior, with measured values of the membrane efficiency coefficients, ω, ranging from 0.395 ± 0.053 to 0.063 ± 0.012 when exposed to KCl solutions with source concentrations, C_{ot}, ranging from 5 mM KCl to 80 mM KCl, respectively. In addition, the diffusion of both Cl^- and K^+ was found to be restricted relative to the case in which the specimen would not exhibit membrane behavior (i.e., $\omega = 0$). Despite the imposition of chemical conditions in the tests that were more complex than those imposed previously, the measured values of ω and the effective diffusion coefficients, D^*, for Cl^- were in good agreement with those reported in the literature for other bentonite-based engineered barriers when exposed to similar or the same types of salts and salt concentrations. Thus, this study provides the first results to illustrate that a compacted SB mixture that is suitable for use as a hydraulic and chemical containment barrier behaves as a semipermeable membrane that can restrict aqueous-phase diffusion of chemical species to an extent that the chemical containment function of the barrier is improved.

ACKNOWLEDGEMENTS

First and foremost, I would like to extend my sincere gratitude to my advisor, Dr. Charles Shackelford for always encouraging and challenging me to rise to my highest potential, and for working tirelessly with me on the work presented in this study. I would also like to thank Dr. Christopher Bareither and Dr. Gregory Butters for serving on my MS committee. Additionally, my fellow graduate students: Kristin Sample-Lord, David Castelbaum, Catherine SooJung Hong, and Shan Tong for all their support both in and out of the lab. For all things lab-related, I'd like to thank Joe Wilmetti for his brilliance and hard work to help keep my tests running. Finally, I'd like to thank my parents, Kami and Randy Meier, my sisters, Kiara, Alycia, Kassandra, and Miranda Meier, and Cole Christiansen, for being my strongest sources of motivation and providing unrelenting love, patience, insights, and encouragements, without which I couldn't have made it this far.

Financial support for this project was provided by the U.S. Department of Energy, under Cooperative Agreement Number DE-FC01-06EW07053 entitled, "The Consortium for Risk Evaluation with Stakeholder Participation III" awarded to Vanderbilt University. The opinions expressed in this document are solely those of the author and are not necessarily consistent with the policies or opinions of the sponsors.

TABLE OF CONTENTS

LIST OF TABLES

LIST OF FIGURES

CHAPTER 1. INTRODUCTION

1.1 Background

1.1.1 *Engineered Bentonite-Based Barriers*

Engineered barriers, such as compacted clay liners (CCLs) and geosynthetic clay liners (GCLs), typically are used for hydraulic and chemical containment applications, such as those associated with municipal solid waste and hazardous waste landfills, for the purpose of preventing undesired negative impacts to the surrounding environment. For this purpose, these engineered barriers typically are required to exhibit a sufficiently low hydraulic conductivity, k, such as $\leq 10^{-9}$ m/s, in order to minimize the amount of contaminated liquid (e.g., leachate) permeating through a bottom barrier or the amount of fresh liquid (e.g., water derived from precipitation) percolating through a cover to minimize the amount of leachate generated within a waste pile.

Sodium bentonite (Na-bentonite) commonly is used in hydraulic and chemical (e.g., waste) containment applications either as an additive component in an engineered barrier (for example, GCLs, bentonite amended CCLs, and soil-bentonite backfills (SBBs) for *in situ* vertical cutoff walls) or as an engineered barrier, such as in the case of highly compacted Na-bentonite buffers for the disposal of high-level radioactive waste (HLRW). In these applications, Na-bentonite is preferred because Na-bentonite typically exhibits high swell, low hydraulic conductivity, k, (e.g., $\leq 10^{-10}$ m/s), and semipermeable membrane behavior (i.e., solute restriction) when exposed to water and dilute aqueous solutions (van Olphen 1963; Kemper and Rollins 1966; Barbour and Fredlund 1989; Cey et al. 2001; Malusis et al. 2001; Malusis and Shackelford 2002a; Shackelford and Lee 2003; Shackelford et al. 2003; Yeo et al. 2005; Henning et al. 2006; Dominijanni and Manassero 2008; Evans et al. 2008; Kang and Shackelford 2009; Bohnhoff and Shackelford 2013;

Tang et al. 2014a). In addition, compacted sand-bentonite (SB) mixtures are often considered as an alternative to CCLs comprising natural clay when a suitable source of natural clay is not readily or economically available. In such cases, the bentonite content (*BC*) of the SB mixtures for most practical applications involving non-hazardous or non-radioactive wastes typically has been less than about 5 to 10 % by dry weight of the mixture in order to minimize the cost associated with the commercially available bentonite (Lundgren 1981; Daniel 1987; Garlanger et al. 1987; Kenney et al. 1992; Chapuis et al. 1992; O'Sadnick et al. 1995; Alston et al. 1997; Gleason et al. 1997; Howell and Shackelford 1997). However, values of *BC* ranging from 10 to 30 % may be required in cases where hazardous or radioactive waste is involved due to the greater environmental risk associated with these wastes and/or, in the case of radioactive waste, the long design periods (e.g., 1,000 yr for low-level radioactive waste and 10,000 yr for high-level radioactive waste) associated with the containment (e.g., Akgün et al. 2015; Tong and Shackelford 2016). Also, Kenney et al. (1992) determined that $11\ \% \leq BC \leq 17\ \%$ was required to impart an adequate bentonite distribution and achieve a suitably low *k* value. In that study, SB mixtures comprising up to 17 % bentonite behaved as an "ideal mixtures," such that the mixture exhibited seepage barrier properties representative of a continuous saturated Na-bentonite matrix at the micro-level, and also exhibited the dimensional stability attributed to the load-bearing capacity of sand at the macro-level.

Finally, Dixon et al. (1985) indicated that a *BC* of up to 50 % may be required for buffers used in HLRW containment applications. Dixon et al. (1985) also concluded that 100 % Na-bentonite, unless compacted to very high dry densities (> 2.0 Mg/m^3), would likely not be sufficient in fulfilling the requirement for a buffer material for radioactive waste containment, because the dry density of pure clays compacted *in situ* can be as low as 1.3 Mg/m^3. Therefore, Dixon et al. (1985) recommended *BCs* up to 50 % for radioactive containment application because adding sand to clay increases the attainable dry density of the otherwise 100 % Na-bentonite buffer.

In all of these cases involving compacted SB mixtures, the sand can play an important role as well. For example, Dixon et al. (1985) reported that the sand component of compacted sand-clay mixtures serves to decrease the creep potential and increase the strength of the mixture. Additionally, when mixed with a highly swelling clay such as Na-bentonite, sand can decrease the shrinkage potential of the barrier (Mitchell 1976). The addition of sand also lowers the porosity of the mixture and increases the maximum possible dry density (Dixon et al. 1985). Finally, Howell and Shackelford (1997) found that the addition of powdered bentonite versus granular bentonite increases the compaction dry density for specimens compacted at or above the optimum water content.

1.1.2 *Containment Properties of Compacted Sand-Bentonite Mixtures*

1.1.2.1 *Hydraulic Behavior of Compacted Sand-Bentonite Mixtures*

The hydraulic conductivity, *k*, is representative of the capability of a porous medium (e.g., soil) to conduct flow via in response to a hydraulic gradient (i.e. advection). The value of *k* is a function of both the soil matrix and the permeant liquid. In particular, the effects of specimen length, *BC*, and chemistry of the permeant liquid on measured values of *k* have been evaluated previously (Lundgren 1981; Alther 1982, 1987; Garlanger et al. 1987; Haug and Wong 1992; Kenney et al. 1992; Chapuis et al. 1992; Shackelford 1994; O'Sadnick et al. 1995; Mollins et al. 1996; Gleason et al. 1997; Howell et al. 1997; Stern and Shackelford 1998; Lo et al. 2004; Tong 2015).

For example, the results of a comprehensive study of these effects on compacted SB specimens comprising the same soils as used in this study (i.e., powdered Na-bentonite and Ottawa sand) are presented in Tong (2015). The measured values of k were found to be not significantly affected by the specimen length, L, for values of L in the range 29.1 mm $\leq L \leq$ 58.3 mm. However, values of k based on permeation with tap water decreased by approximately 1 to 1.5 orders of magnitude as the values of BC increased from 5 % to 15 %. Additionally, measured values of k increased by less than one order of magnitude as the electrical conductivity, EC, of the permeant liquid increased from 13 mS/m to 240 mS/m.

Permeating compacted SB mixtures with chemical solutions has been shown to increase the measured value of k (Gipson 1985; Alther 1987; Shackelford 1994; Gleason et al. 1997; Stern and Shackelford 1998; Lo et al. 2004). In this regard, Stern and Shackelford (1998) concluded that increasing the bentonite content, BC, of the mixture can reduce the increase in k when the mixture is permeated with a chemical solution. They determined that compacted SB mixtures comprising 20 % bentonite maintained the lowest value of k when permeated with 500 mM $CaCl_2$ compared to mixtures comprising 10 % and 15 % bentonite.

1.1.2.2 *Diffusion Behavior of Compacted Sand-Bentonite Mixtures*

Diffusion of chemical species through compacted SB mixtures has been explored previously by Gillham et al. (1984). Based on the results of that study, the authors determined that the porosity, n, and bulk (dry) density, ρ_b, of compacted SB mixtures with BCs greater than 5 % increased and decreased, respectively, with increasing BC. They also reported a strong influence of ρ_b on measured values of the effective diffusion coefficient, D^*, with values of D^* increasing with decreasing ρ_b and/or increasing BC. As a result, Gillham et al. (1984) concluded that high values of *BC* (> 10 %) are not necessarily more effective at minimizing diffusive mass flux through a soil mixture. However, they also noted that the observed trends of increasing D^* with increasing *BC* and decreasing ρ_b could be eliminated with increased compaction energy.

1.1.3 *Semipermeable Membrane Behavior*

Membrane behavior in clay barrier materials refers to the ability of the clay to selectively restrict the passage of dissolved chemical species (solutes). Solute restriction is attributed to anion repulsion from the electrically charged diffuse double layers (DDL) between hydrated clay particles. Membrane behavior often is observed in highly active clays such as Na-bentonite due to overlapping DDLs (Kemper and Massland 1964; Kemper and Rollins 1966; Fritz 1986; Keijzer et al. 1999; Malusis and Shackelford 2002a,b; Malusis et al. 2001; Shackelford and Lee 2003; Shackelford et al. 2003; Yeo et al. 2005; Henning et al. 2006; Dominijanni and Manassero 2008; Kang and Shackelford 2009, 2010, 2011; Di Emidio 2010; Mazzieri et al. 2010; Shackelford 2011; Bohnhoff 2012; Dominijanni et al. 2013; Shackelford 2013). If a clay exhibits membrane behavior, chemico-osmosis occurs, such that liquid flows from lower solute concentration (higher water activity) to higher solute concentration (lower water activity). The degree to which a clay exhibits semipermeable membrane behavior is referred to as the chemico-osmotic or membrane efficiency, and is designated in terms of a coefficient, typically designated as either σ or ω, which ranges from zero for no solute restriction (no membrane behavior) to unity for complete solute restriction (ideal membrane behavior). In engineering literature, σ is used predominately to represent stress, such that use of ω to represent the membrane efficiency coefficient is preferred. As a result, ω will be used exclusively hereafter to designate the membrane efficiency coefficient.

Previous studies have established that ω decreases as the average of the solute concentrations that bound a specimen, C_{ave}, increases, with a typical trend in ω versus log (C_{ave}) being approximately semi-log linear with nonlinear trends at the limiting values C_{ave} (Kemper and Rollins 1966; Shackelford et al. 2003; Dominijanni et al. 2013; Meier et al. 2014). However, membrane behavior of compacted sand-bentonite mixtures has not been studied extensively, and virtually not at all in terms of the use of compacted SB mixtures for waste containment applications. Therefore, a brief review of the results of studies focused on the membrane behavior of other bentonite-based barriers is provided for additional background for this study.

1.1.3.1 *Geosynthetic Clay Liners (GCLs)*

Geosynthetic clay liners have been tested extensively for membrane behavior (Malusis and Shackelford 2002a; Malusis and Shackelford 2002b; Shackelford and Lee 2003; Malusis and Shackelford 2004; Dominijanni and Manassero 2008; Kang and Shackelford 2011; Malusis et al. 2014; Meier et al. 2014). Membrane testing on GCLs has been performed by circulating salt solutions and de-ionized water (DIW) across the top and bottom specimen boundaries, respectively, where the concentrations of the source circulation solutions were designated as C_{ot} and C_{ob} (= 0) with respect to the top and bottom specimen boundaries.

For example, GCL specimens have been shown to exhibit membrane behavior when exposed to values of C_{ot} ranging from 3.9 mM to 47 mM KCl (Malusis and Shackelford 2002a; Malusis et al. 2014). Values for ω measured in a rigid-wall cell ranged from 0.07 to 0.68 for as C_{ot} ranged from 47mM KCl to 3.9 mM KCl, respectively (Malusis and Shackelford 2002a).

Shackelford and Lee (2003) tested the effects of diffusion on chemico-osmotic membrane behavior in clays. The authors performed a combined chemico-osmotic/diffusion experiment on a

GCL specimen comprising 100 % bentonite with a 5 mM $CaCl_2$ solution. The results of the study indicated that membrane behavior in clays can be partially or fully destroyed due to the compression of diffuse double layers, DDLs, resulting from diffusion of invading salt cations.

Malusis and Shackelford (2004) compared measured solute flux breakthrough curves (FBCs) for GCL specimens versus predicted FBCs based on three different scenarios, i.e., advective-dispersive transport that neglects membrane behavior, advective-dispersive transport that accounts for the concentration dependency of D^* resulting from membrane behavior, and fully coupled transport that accounts for hyperfiltration, chemico-osmosis, and the concentration dependency of D^* resulting from membrane behavior. The predicted FBCs based on the fully coupled transport theory yielded better agreement with the experimentally measured FBCs compared to the other two scenarios used for predicting the measured FBCs. The advective-dispersive theory overestimated the steady-state solute fluxes and, therefore, underestimated solute transit times. However, Malusis and Shackelford (2004) determined that the partially coupled advective-dispersive theory could be used to predict somewhat conservative FBCs, provided diffusion is a dominant solute transport mechanism and the concentration dependency of D^* is taken into account.

The same GCL evaluated by Malusis and Shackelford (2002a) and Malusis and Shackelford (2004) was tested by Kang and Shackelford (2011) using a flexible-wall cell that allowed for an evaluation of the effect of increasing effective stress, σ', on the measured values of ω. Kang and Shackelford (2011) reported measured values of ω based on given value of C_{ot} for KCl generally increased as σ' increased from 34.5 kPa (5 psi) to 241 kPa (35 psi). For example, as σ' increased from 34.5 kPa (5 psi) to 241 kPa (35 psi), values of ω for a C_{ot} of 3.9 mM KCl increased from 0.43 to 0.68, respectively, whereas values of ω for a C_{ot} of 47 mM KCl increased from 0.01 to 0.79. Kang and Shackelford (2011) concluded that membrane behavior in GCLs can offer improved containment performance that can be enhanced by increasing σ′.

Meier et al. (2014) also reported values of ω for a GCL ranging from 0.096 to essentially nil as values of C_{ot} ranged from 20 mM KCl to 400 mM KCl, respectively. Therefore, the value for C_{ot} at which membrane behavior was essentially destroyed (i.e., threshold concentration) was determined to be 400 mM KCl, which is higher than the value of 84 mM KCl estimated by extrapolation of the semi-log linear trend in the measured values of ω versus the log (C_{ave}). They concluded that membrane behavior likely is more persistent and significant at higher salt concentrations than previously estimated based on semi-log linear extrapolation.

1.1.3.2 *Soil-Bentonite Backfills (SBBs) for Vertical Cutoff Walls*

Yeo et al. (2005) reported the results of tests conducted in rigid-wall cells to measure the membrane efficiency of SBBs. Two base soils for the backfills were tested, a natural clay with 89 % fines (i.e., % < 75 μm by dry weight) and a mixture of sand with 5 % Na-bentonite (by dry weight). In accordance with standard practice for soil-bentonite vertical cutoff walls, the base soils were mixed with a 5 % Na-bentonite slurry to achieve a standard slump of 100 mm. The final *BC*s for the SBB specimens, which included the bentonite derived from mixing the base soils with the bentonite slurry, were 2.12 % and 7.20 % for the natural clay SBB and the sand-bentonite SBB, respectively. Both SBB specimens behaved as semipermeable membranes at a low source salt concentration (C_{ot} = 3.88 mM KCl) and at the tested void ratios, *e*, ranging from 0.61 to 1.0 and 0.81 to 1.2, such that corresponding values of ω ranged from 0.024 to 0.018 and 0.166 to 0.118 for the natural clay and sand-bentonite SBBs, respectively. The higher ω values for the sand-bentonite SBB were attributed to the higher overall bentonite content of that mixture. Yeo et al. (2005) also concluded that membrane behavior is enhanced at higher consolidation stress (i.e., lower *e* and *k*). Overall, the existence of membrane behavior in a hypothetical SBB vertical cutoff wall was shown to reduce the total liquid flux to as low as 68 % of that which would occur in the absence of membrane behavior, thereby potentially improving the performance of the vertical cutoff wall in cases where solute restriction is desirable.

Samples of SBBs recovered from two field constructed vertical cutoff walls were tested for membrane behavior by Henning et al. (2006). The field samples contained 2 % to 4 % bentonite, and the results indicated that membrane behavior was exhibited by both field constructed backfills. Although the measured values for ω of ≤ 0.0172 for the field samples were lower than those previously reported for backfills prepared in the laboratory by Yeo et al. (2005), membrane behavior was found to contribute to a reduction in liquid flux ranging from 1 % to10 % and from 7 % to 8 % for the two sites, as the void ratios decreased from 0.70 to 0.40 and from 0.89 to 0.60, respectively. Henning et al. (2006) concluded that the potential benefit due to membrane behavior could be more significant for barriers with higher clay contents and lower void ratios.

1.1.3.3 *Compacted Clay Liners*

Kang and Shackelford (2010) performed membrane testing on compacted specimens of unamended and bentonite amended natural clay. They determined that the unamended CCL was suitable for waste containment ($k < 10^{-9}$ m/s), but exhibited negligible membrane behavior ($\omega \leq 0.014$) compared to significant membrane behavior ($\omega \leq 0.973$) for a compacted specimen of the natural clay amended with 5 % bentonite. However, the 5 % bentonite-amended specimens were highly sensitive to increasing salt concentrations. For example, ω was 0.97 for a C_{ot} of 3.9 mM, whereas ω was only 0.03 for C_{ot} of 20 mM KCl. Therefore, the authors recommended amended bentonite contents greater than 5 % in order to achieve more sustainable values of ω over a wider range of salt concentrations. Kang and Shackelford (2010) also illustrated that chemico-osmotic counter flow was greater than the outwardly directed advective flow, such that outward liquid flux of solutes was minimized at low, source salt concentrations ($\leq$ 10 mM KCl).

Membrane testing on compacted specimens of bentonite amended Fukakusa Clay (FC) also was performed by Tang et al. (2014a). The unamended FC was found to be unsuitable for use in waste containment applications due to high k ($> 10^{-9}$ m/s). However, nearly ideal values of ω (i.e., ~ 1.0) were reported for C_{ot} = 0.5 mM KCl for the bentonite-amended FC specimens, and values of ω remained at greater than 0.20 at higher salt concentrations ($\leq$ 10 mM KCl). The authors concluded that ω for the unamended FC specimens could be ignored due to a significant decrease in ω as C_{ot} increased. They also determined that increasing the amended bentonite content from 5 % to 20 % did not have a significant effect on the pore size within the specimens, although values of ω increased slightly (e.g., from 0.20 for 5 % bentonite to 0.23 for 20 % bentonite when exposed to 10 mM KCl).

A subsequent study reported by Tang et al. (2014b) that involved the same soil mixtures as studied by Tang et al. (2014a) evaluated the effect of degree of compaction on the measured membrane behavior. They reported that a 20 % increase in the degree of compaction (i.e., from 80 % to 100 %) resulted in roughly 30 % higher values of ω for salt solutions with $\leq$ 50 mM KCl.

Dominijanni and Manassero (2008) numerically evaluated the effect of solute restriction on the overall solute flux through both CCLs and Na-bentonite based GCLs. They noted that, in the absence of consideration of solute restriction due to semipermeable membrane behavior, the advective-diffusive solute flux through the GCL would be greater than that through the CCL due to the relative thinness of the GCL. However, when the membrane behavior (solute restriction) of the GCL was taken into account, the solute flux decreased with decreasing salt concentration and, consequentially, the solute flux through the GCL ultimately was lower than that through the CCL. Therefore, Dominijanni and Manassero (2008) concluded that the ability of the GCL to restrict contaminant transport was underestimated when using the advective-diffusive transport theory to compare the performance of unamended CCLs with GCLs at low salt concentrations, i.e., < 100 mM (also see Shackelford 2013). This conclusion is the same as that drawn for a GCL in the aforementioned study by Malusis and Shackelford (2004).

1.1.3.4 *Compacted Natural Sodium Bentonites*

Bentonite specimens were tested for membrane behavior by Kemper and Rollins (1966) and Kemper and Quirk (1972) with Na^+-saturated Wyoming bentonite. The authors determined that values of ω increased with decreasing values of the volumetric water content (θ) of the soil, and decreasing average boundary salt concentration. Dominijanni et al. (2013) also reported a decrease in ω from 0.68 to 0.05 with increasing values of C_{ot} from 5.16 mM to 109.3 mM NaCl, respectively, for a Na-bentonite specimen with n = 0.81.

1.1.3.5 *Compacted Polymerized Bentonites*

In an effort to increase the resistance of bentonite to diffusing salt species and, therefore, improve the sustainability of membrane behavior in bentonite, a Na-bentonite modified with a polyacrylate polymer, referred to as a bentonite-polymer composite (BPC) or a bentonite-polymer nanocomposite (BPN), was evaluated by Bohnhoff and Shackelford (2013) for membrane behavior at increasing salt solutions (4.7 mM to 54 mM KCl). The BPC specimens were prepared from a consolidated bentonite-monomer slurry containing 30 % to 50 % bentonite (by dry weight).

Scalia et al. (2001) showed that BPC specimens permeated with solutions ranging from 5 mM to 500 mM $CaCl_2$ maintained low values of k (< 3 x 10^{-12} m/s) compared to higher values of k (> 2 x 10^{-7} m/s) exhibited by natural (unmodified) Na-bentonite specimens permeated under the same conditions. Additionally, the values of k remained low (< 8 x 10^{-11} m/s) following prolonged permeation (> 2 years) of BPC specimens with 5 mM to 500 mM $CaCl_2$ (Scalia et al. 2014).

Measured values of ω for BPC specimens were 109 % to 433 % of those previously reported for specimens containing traditional Na-bentonite, depending on test conditions and specimen properties. For example, values of ω corresponding to C_{ot} of 20 mM KCl ranged from 0.21 to 0.28 and from 0.43 to 0.48 for traditional GCL specimens and BPC specimens, respectively, tested in rigid-wall cells. Overall, the BPC specimens exhibited improved membrane behavior over a wider range of salt concentrations compared to GCLs with natural Na-bentonite.

Another type of polymer-modified bentonite was tested by Di Emidio et al. (2014) referred to as HYPER clay that was developed through treatment of a Na-bentonite with an anionic polymer in an effort to enhance the hydraulic performance of the clay when exposed to inorganic solutions. When exposed to concentrations of 1 mM and 5 mM $CaCl_2$, values of ω for the HYPER clay were 0.65 and 0.13, respectively, which were greater than the values of ω of 0.29 and zero for a non-polymer enhanced bentonite specimen under the same testing conditions.

1.1.3.6 *Compacted Sand-Bentonite Mixtures*

Membrane behavior in compacted SB specimens comprising 20 % bentonite was measured by Barbour and Fredlund (1989) via osmotic consolidation upon exposure to a range of NaCl concentration solutions. The authors determined that values of ω decreased with increasing values of C_{ot}, and that osmotically induced consolidation did not result in significant volume change with respect to the specimen. The hyperfiltration method for measuring membrane behavior was conducted by Saindon and Whitworth (2005) on compacted SB specimens with a dilute salt solution (i.e., 1 mM NaCl). The compacted SB specimens were compacted under a relatively low pressure (i.e., 345 kPa), and values of ω ranged from 0.03 to 0.04 for specimens comprising 12 % $\leq BC \leq$ 50 %, respectively. Despite the relatively low values of ω, Saindon and Whitworth (2005) concluded that the magnitude of membrane behavior could have significant effects on contaminant fate and transport due to concomitant solute rejection.

1.2 Objectives of Research

Based on the aforementioned review, the only category of bentonite-based barrier commonly used in engineered hydraulic and chemical containment applications that has not been evaluated for semipermeable membrane behavior is compacted sand-bentonite (SB) mixtures. Accordingly, the objectives of this research were to:

(a) evaluate the existence and magnitude of semipermeable membrane behavior in a compacted SB mixture suitable for use as a low hydraulic conductivity barrier upon exposure to a range of salt solutions consistent with those previously used to evaluate membrane behavior of other bentonite-based barriers; and

(b) simultaneously, evaluate the ability of the same compacted (SB) mixture to restrict the diffusion of the primary chemical species (i.e., Cl^- and K^+) in the system.

REFERENCES

Akgün. H., Ada. M., and Koçkar. M.K., 2015. "Performance Assessment of a Bentonite-Sand Mixture for Nuclear Waste Isolation at the Potential Akkuyu Nuclear Waste Disposal Site, Southern Turkey." *Environmental Earth Sciences*, 73, 6101-6116.

Alther. G.R., 1982. "The Role of Bentonite in Soil Sealing Applications." *Bulletin of Association of Environmental and Engineering Geologists*, 19, 401-409.

Alther, G.R., 1987. "The Qualifications of Bentonite as a Soil Sealant." *Engineering Geology*, 23(3/4), 177-191.

Alston, C., Daniel, D.E., and Devroy, D.J., 1997. "Design and Construction of Sand-Bentonite Liner for Effluent Treatment Lagoon, Marathon, Ontario." *Canadian Geotechnical Journal*, 34(6), 841-852.

Barbour, S., and Fredlund, D., 1989. "Mechanisms of Osmotic Flow and Volume Change in Clay Soils." *Canadian Geotechnical Journal*, 26(4), 551-562.

Bohnhoff, G., 2012. "Membrane Behavior, Diffusion, and Compatibility of a Polymerized Bentonite for Containment Barrier Applications." PhD Dissertation, Colorado State University, Fort Collins, CO.

Bohnhoff, G.L., and Shackelford, C.D., 2013. "Improving Membrane Performance via Bentonite Polymer Nanocomposite." Applied Clay Science, 86, 83-98.

Cey B.D., Barbour S.L., and Hendry M.J., 2001. "Osmotic Flow through a Cretaceous Clay in Southern Saskatchewan, Canada." Canadian Geotechnical Journal, 38, 1025-1033.

Chapuis, R.P., Lavoie, J., and Girard, D., 1992. "Design, Construction, Performance, and Repair of the Soil-Bentonite Liners of Two Lagoons," *Canadian Geotechnicat Journal*, 29(4), 638-649.

Daniel, D.E., 1987. "Earthen Liners for Land Disposal Facilities." *Geotechnical Practice for Waste disposal '87*, Woods. R.D. eds., GSP 13, ASCE, 21-39.

Dominijanni, A. and Manassero, M., 2008. "Influence of Membrane Behavior on Contaminant Transport Through Geosynthetic Clay Liners." *Characterization, Monitoring, and Modeling of GeoSystems*, Alshawabkeh, A.N. Reddy, K.R., and Khire, M.V. Eds., GeoCongress 2008, ASCE, Reston, Virginia, USA, 814-821.

Dominijanni, A., Manassero, M, and Puma, S., 2013. "Coupled Chemical-Hydraulic-Mechanical Behavior of Bentonites." *Gèotechnique,* 63(3), 191-205.

Dixon, D.A., Gray, M.N., and Thomas, A.W., 1985. "A Study of the Compaction Properties of Potential Clay-Sand Buffer Mixtures for Use in Nuclear Fuel Waste Disposal." *Eng. Geol*., 21, 247-255.

Fritz, S., 1986. "Ideality of Clay Membranes in Osmotic Processes: A Review." *Clays and Clay Minerals*, 34(2), 214-223.

Garlanger, J.E., Cheung, F.K., and Bishar, S.T. 1987. "Quality Control Testing for a Sand-Bentonite Liner." *Geotechnical Practice for Waste Disposal '87,* Woods, R.D., eds., ASCE, New York, NY, 488-499.

Gillham, R.W., Robin, M.J.L., and Dytynyshyn, D.J., 1984. "Diffusion of Nonreactive and Reactive Solutes through Fine-Grained Barrier Materials." *Canadian Geotechnical Journal*, 21, 541-550.

Gipson, A.H., Jr. 1985. "Permeability Testing on Clayey Soil and Silty Sand-Bentonite Mixture Using Acid Liquor." *Hydraulic Barriers in Soil and Rock*, STP 874, Johnson, A.I., Frobel, R.K., Cavalli, N.J., and Pettersson, C.B., eds., ASTM, West Conshohocken, Pa., 140-54.

Gleason, M.H., Daniel, D.E., and Eykholt, G.R. 1997. "Calcium and Sodium Bentonite for Hydraulic Containment Applications." *Journal of Geotechnical and Geoenvironmental Engineering*, 123(5), 438-445.

Haug, M.D. and Wong, L.C. 1992. "Impact of Molding Water Content on the Hydraulic Conductivity of Compacted Sand-Bentonite." *Canadian Geotechnical Journal*, 29(2), 253-262.

Henning, J., Evans, J., and Shackelford, C. (2006). "Membrane Behavior of Two Backfills from Field-Constructed Soil-Bentonite Cutoff Walls." *Journal of Geotechnical and Geoenvironmental Engineering*, 132(10), 1243–1249.

Howell, J.L. and Shackelford, C.D. 1997. "Hydraulic Conductivity of Sand Admixed with Processed Clay Mixtures." Proceedings, *14th International Conference on Soil Mechanics and Foundation Engineering*, Hamburg, Germany, Sept. 6-12, Balkema, A.A. Rotterdam, The Netherlands, Vol. 1, 307-310.

Kang, J., and Shackelford, D., 2009. "Clay Membrane Testing Using a Flexible-Wall Cell under Closed-System Boundary Conditions." *Applied Clay Science*, 44(1-2), 43-58.

Kang, J. and Shackelford, C., 2010. "Membrane Behavior of Compacted Clay Liners." *Journal of Geotechnical and Geoenvironmental Engineering*, 136(10), 1368-1382.

Kang, J. and Shackelford, C., 2011. "Consolidation Enhanced Membrane Behavior of a Geosynthetic Clay Liner." *Geotextiles and Geomembranes*, 29, 544-556.

Keijzer, T., Kleingeld, P., and Loch, J., 1999. "Chemical Osmosis in Compacted Clayey Material and the Prediction of Water Transport." *Engineering Geology*, 53(2), 151-159.

Kemper, W., and Maasland, D., 1964. "Reduction in Salt Content of Solution Passing through Thin Films Adjacent to Charged Surfaces." *Proceedings of the Soil Science Society of America*, 28(3), 318-323.

Kemper, W. and Rollins, J., 1966. "Osmotic Efficiency Coefficients across Compacted Clays." *Proceedings of the Soil Science Society of America*, 30(5), 529-534.

Kenney, T.C., van Veen, W.A., Swallow, M.A., and Sungaila, M.A. 1992. "Hydraulic Conductivity of Compacted Bentonite-Sand Mixtures." *Canadian Geotechnical Journal*, 29(3), 364-374.

Lo, I., Luk, A., and Yang, X. 2004. "Migration of Heavy Metals in Saturated Sand and Bentonite/Soil Admixture." *Journal of Environmental Engineering*, 130(8), 906–909.

Lundgren, T.A. 1981. "Some Bentonite Sealants in Soil Mixed Blankets." Proceedings, *10th International Conference on Soil Mechanics and Foundation Engineering*, Stockholm, Sweden, June 15-19, Balkema, A. A. eds., Rotterdam, The Netherlands, Vol. 2, 349-354.

Malusis, M., and Shackelford, C., 2002a. "Chemico-Osmotic Efficiency of a Geosynthetic Clay Liner." *Journal of Geotechnical and Geoenvironmental Engineering*, 128(2), 97-106.

Malusis, M., and Shackelford, C., 2002b. "Coupling Effects during Steady-State Solute Diffusion through a Semipermeable Clay Membrane." *Environmental Science and Technology*, 36(6), 3212-1319.

Malusis, M. and Shackelford, C., 2004. "Explicit and Implicit Coupling during Solute Transport through Clay Membrane Barriers." *Journal of Contaminant Hydrology*, 72, 259-285.

Malusis, M., Shackelford, C., and Olsen, H., 2001. "Flow and Transport through Clay Membrane Barriers." *Geoenvironmental Engineering, Geoenvironmental Impact Management*, R. Yong and H. Thomas, Eds., *Thomas Telford Publ*., London, UK, 334-341.

Mazzieri, F., Di Emidio, G., and Van Impe, P., 2010. "Diffusion of Calcium Chloride in a Modified Bentonite: Impact on Osmotic Efficiency and Hydraulic Conductivity." *Clays and Clay Minerals*; 58(3), 351-363.

Meier, A., Sample-Lord, K., Castelbaum, D., Kallase, S., Moran, B., Ray, T., and Shackelford, C., 2014. "Persistence of Semipermeable Membrane Behavior for a Geosynthetic Clay Liner." *Proceedings, 7th International Conference on Environmental Geotechnics*, A. Bouazza, S. Yuen, and B. Brown, Eds., Nov. 10-14, 2014, Melbourne, Australia (ISBN 978-1-922107-23-7), 496-503.

Mitchell, J.K. and Younger, J.S., 1967. "Abnormalities in Hydraulic Flow through Fine-Grained Soils." *Permeability and Capillarity of Soils*, STP 417, ASTM, Philadelphia, Pa., 106-141.

Mollins, L.H., Stewart, D.I., and Cousens, T.W., 1996. "Predicting the Properties of Bentonite-Sand Mixtures." *Clay Minerals*, 31(2), 243-252.

O'Sadnick, D.L., Simpson, B.E., and Kasel, G.K., 1995. "Evaluation and Performance of a Sand/Bentonite Liner." *Geoenvironment 2000*, Acar, Y. B. and Daniel, D. E. eds., ASCE, New York, NY, 688-701.

Shackelford, C.D., 1994. "Waste Soil Interactions that Alter Hydraulic Conductivity." *Hydraulic Conductivity and Waste Contaminant Transport in Soil*, Daniel, D.E. and Trautwein, S.J. eds., STP 1142, ASTM, West Conshohoken, PA, 111-168.

Shackelford, C., 2011. "Membrane Behavior in Geosynthetic Clay Liners." *Geo-Frontiers 2011: Advances in Geotechnical Engineering*, J. Han and D. Alzamora, Eds., Geotechnical Special Publication 211, ASCE, Reston, VA, 1961-1970.

Shackelford, C., 2013. "Membrane Behavior in Engineered Bentonite-Based Containment Barriers: State of the Art." *Proceedings of Coupled Phenomena in Environmental Geotechnics (CPEG)*, M. Manassero, A. Dominijanni, S. Foti, and G. Musso, eds., July 1-3, Torino, Italy, CRC Press/Balkema, Taylor & Francis Group, London, 45-60.

Shackelford, C.D, Benson, C.H., Katsumi, T., Edil, T.B., and Lin, L., 2000. "Evaluating the Hydraulic Conductivity of GCLs Permeated with Non-standard Liquids." *Geotextiles and Geomembranes*, 18(2-4), 133-161.

Shackelford, C., and Lee, J., 2003. "The Destructive Role of Diffusion on Clay Membrane Behavior." *Clays and Clay Minerals*, 51(2), 187-197.

Shackelford, C., Malusis, M., and Olsen, H., 2003. "Clay Membrane Behavior for Geoenvironmental Containment." *Soil and Rock America Conference 2003*, P. J. Culligan, H. H. Einstein, and A. J. Whittle, Eds., Verlag Glückauf GMBH, Essen, Germany, Vol. 1, 767-774.

Stern, R.T. and Shackelford, C.D. 1998. "Permeation of Sand-Processed Clay Mixtures with Calcium Chloride Solutions." *Journal of Geotechnical and Geoenvironmental Engineering*, 124(3), 231-241.

Tang, Q., Katsumi, T., Inui, T., and Li, Zhenze (2014). "Membrane Behavior of Bentonite-Amended Compacted Clay." *Soils and Foundations,* Japanese Geotechnical Society, 54(3), 329-344.

Tong, S., 2015. "Standardized Hydraulic Conductivity Testing of Compacted Sand-Bentonite Mixtures." MS Thesis, Colorado State University, Fort Collins, CO.

Tong, S., and Shackelford, C., 2016. "Standardized Hydraulic Conductivity Testing of Compacted Sand-Bentonite Mixtures." *Geotechnical Testing Journal* (in-review).

van Olphen, H., 1963. *An Introduction to Clay Colloid Chemistry*. John Wiley & Sons, Inc., New York.

Yeo, S., Shackelford, C., and Evans, J., 2005. "Membrane Behavior of Model Soil-Bentonite Backfills." *Journal of Geotechnical and Geoenvironmental Engineering*, 131(4), 418-429.

CHAPTER 2. MEMBRANE BEHAVIOR AND DIFFUSION OF COMPACTED SAND-BENTONITE LINERS

2.1 Introduction

Engineered barriers, such as compacted clay liners (CCLs), and geosynthetic clay liners (GCLs), typically are used in municipal solid waste and hazardous waste containment applications for the purpose of preventing the migration of chemical contaminants to the surrounding environment. Sodium bentonite (Na-bentonite) commonly is used as an additive component in engineered barriers (e.g., GCLs, bentonite amended CCLs, and soil-bentonite backfills for vertical cutoff walls) or as an engineered barrier (e.g. highly compacted Na-bentonite buffers for high-level radioactive waste disposal) in hydraulic and chemical containment applications. In such applications, the use of Na-bentonite is favored because Na-bentonite typically exhibits low hydraulic conductivity, k ($\leq 10^{-10}$ m/s), high swell, and semipermeable membrane behavior (e.g., solute restriction) when exposed to water and dilute chemical solutions (Van Olphen 1963; Kemper and Rollins 1966; Barbour and Fredlund 1989; Cey et al. 2001; Malusis et al. 2001; Malusis and Shackelford 2002a; Shackelford and Lee 2003; Shackelford et al. 2003; Yeo et al. 2005; Henning et al. 2006; Dominijanni and Manassero 2008; Evans et al. 2008; Kang and Shackelford 2009; Bohnhoff and Shackelford 2013; Tang et al. 2014a). Additionally, compacted sand-bentonite (SB) mixtures are often considered as an alternative to bentonite amended CCLs comprising natural clay when a suitable source of natural clay is not readily or economically available. In such cases, the required bentonite content (*BC*) typically is less than 5 % to 10 % by dry weight, for SB mixtures to achieve a suitably low k ($\leq 10^{-9}$ m/s) for applications involving non-hazardous or non-radioactive wastes.

Semipermeable membrane behavior in bentonite-based barriers refers to the ability of the Na-bentonite to selectively restrict the passage of aqueous chemical species due to anion repulsion resulting from the overlap of the electrically charged diffuse double layers (DDL) surrounding adjacent clay particles. The extent to which solutes are restricted due to membrane behavior is referred to as the chemico-osmotic or membrane efficiency, and is represented by the chemico-osmotic or membrane efficiency coefficient, ω. Values of ω range from zero for no solute restriction to unity for complete solute restriction (i.e., ideal membrane). Values of ω for clay barriers that exhibit some membrane behavior typically are less than unity due to the natural variation in pore sizes, which results in some (larger) pores permitting the migration of solutes (Shackelford 2013). Additionally, previous studies have determined that ω decreases with increasing average solute concentration across the specimen, C_{ave}, due to the compression of DDLs and the concomitant increase in pore sizes (Shackelford and Lee 2003; Malusis et al. 2014; Shackelford 2013). Typically, the trend in ω versus log (C_{ave}) is approximately semi-log linear with nonlinear trends at the limiting (maximum and minimum) values of C_{ave} (Kemper and Rollins 1966; Shackelford et al. 2003; Dominijanni et al. 2013; Meier et al. 2014). However, membrane behavior of compacted sand-bentonite mixtures for waste containment application has not been studied extensively. Additionally, to the author's knowledge, the measurement of diffusion coefficients corresponding to compacted SB mixtures exhibiting membrane behavior has not been studied previously. Therefore, this study focused on determining the extent and magnitude of membrane behavior of specimens of a compacted SB mixture comprising 15 % bentonite that were prepared in accordance with standard procedures for use as a barrier for hydraulic and chemical containment applications. In addition, the diffusive behavior of the two principal salt species, chloride (Cl^-) and potassium (K^+), was evaluated simultaneously for one of the compacted specimens to determine the effect, if any, of membrane behavior in restricting the diffusion of these two chemical species.

2.2 Materials and Methods

2.2.1 Liquids

The liquids used in this study included de-ionized water (DIW), tap water (TW), and potassium chloride solutions (KCl) (certified A.C.S.; Fisher Scientific, Fair Lawn, NJ) with measured concentrations ranging from 5 mM to 80 mM KCl. The electrical conductivity, *EC*, at 25 ^oC of the DIW and TW was measured using an Orion Conductivity Cell (Orion 013005MD, Waltham, MA), and the measured values were 1 mS/m and 14.6 mS/m, respectively. The pH of the DIW and TW also was measured using an Orion Ross Ultra pH/ATC Triode (Orion 8157BNUMD, Waltham, MA), and the measured values were 7.0 and 7.1, respectively. The results of chemical analysis on the tap water are provided in Table 2.1.

Tian and Benson (2015) evaluated how values of *k* for geosynthetic clay liners (GCLs) are affected by the permeation of liquids characteristic of leachate generated from low-level radioactive waste (LLRW) disposal facilities The authors determined that values of *k* for GCL specimens measured from permeation with leachates containing radionuclides were essentially the same as values of *k* measured from permeation with non-radioactive leachate. Therefore, the use of a chemical solution comprising simple salts was determined to be an acceptable alternative to the use of a radioactive solution when simulating testing conditions consistent with LLRW disposal facilities. Accordingly, potassium chloride (KCl) was chosen as the salt for this study to allow for comparison of the results of this study with those of previous studies pertaining to membrane and diffusion testing of GCLs and CCLs (Malusis and Shackelford 2002a,b; Kang and Shackelford 2009; Kang and Shackelford 2010).

The KCl solutions were prepared and stored in 20-L carboys (Nalgene®; Thermo Fisher Scientific, Rochester, NY). Concentrations of chloride were measured using ion chromatography, or IC (Dionex® 4000i 131 IC Module, Dionex Co., Sunnyvale, CA) whereas concentrations of potassium were measured using inductively coupled plasma-atomic emission spectrometry or ICP-AES (IRIS® Advantage/1000 ICAP Spectrometer, Thermo Jarrel Ash Co., Franklin, MA). A biocide (OK-20 Antimicrobial, Dow Chemical Company, Midland, MA) was added to all the liquids at 500 ppm to control any biological activity. The addition of 500 ppm biocide to the TW and KCl solutions resulted in a slight increase in *EC* values (i.e., $\Delta EC \leq 7$ mS/m) and a decrease in pH values (i.e., $\Delta \mathrm{pH} \leq 2$). The resulting measured concentrations, *EC*, and pH of the KCl solutions (with biocide) used in this study are summarized in Table 2.2. The *EC* of KCl solutions ranged from 76.3 mS/m to 1156 mS/m for the KCl solutions with target concentration ranging from 5 mM to 80 mM KCl, respectively. The measured values of pH ranged from 4.5 to 4.8.

2.2.2 Soils

Two soils were used in this study, viz., Ottawa silica fine sand (F-60, U.S. Silica, Frederick, MD) and a powdered bentonite (Natural Gel, Wyo-Ben Inc., Billings, MT). The mineralogical composition and physical and chemical properties of the soils are summarized in Table 2.3. The particle-size distributions for the sand and bentonite (ASTM D 422) are shown in Fig. 2.1. The sand was poorly graded and classified as SP according to the Unified Soil Classification System (ASTM D 2487). The bentonite classified (ASTM D 2487) as high-plasticity clay (CH) according to ASTM D 2487, with 98 % of the bentonite comprising fine-grained (< 75 μm) particles. Also, 87 % of the bentonite was clay-sized particles based on the standard definition (i.e., < 5 μm), whereas 82.8 % of the bentonite was clay-sized particles based on the practical definition (i.e., < 2 μm). Also, as indicated in Table 2.3, the predominant bound cation for the bentonite was sodium (Na^+), such that the bentonite was considered to be a sodium bentonite (Na-bentonite).

Mineralogical analysis of the bentonite based on X-ray diffraction was conducted by Mineralogy, Inc. (Tulsa, OK). The results indicated the bentonite composition as 70 % montmorillonite, 15 % plagioclase feldspar, 9 % quartz, 3 % potassium feldspar, 2 % illite (mica), and 1 % calcite.

The Atterberg limits of the powdered bentonite hydrated with DIW were measured according to ASTM D 4318, and the resulting flow curve is presented in Fig. 2.2. The liquid limit, *LL*, was 426 % and the plastic limit, *PL*, was 33 %, resulting in a plasticity index, *PI*, of 393 %. The resulting activity, *A*, of the bentonite (i.e., $A = PI$ (%)/% < 2 μm) was 0.47. Table 2.3 also provides a comparison of properties for the Natural Gel bentonite used in this study versus the Natural Gel bentonite analyzed in previous studies. The discrepancy in mineralogical composition and physical and chemical properties for the same Natural Gel bentonite product can be attributed, in part, to inherent variations in the bentonite deposit and mining activity spanning a 10-year period.

2.2.3 Sand-Bentonite Mixture

The Na-bentonite was dry mixed with the sand to result in a bentonite content of 15 % by dry weight. The mixing process was consistent with that reported in previous studies (e.g., Howell and Shackelford 1997), and is described in the following section.

The G_s of the sand-bentonite mixture was calculated as 2.68. The calculation was based on a weighted harmonic mean of the individually measured G_s values for bentonite and sand and the respective mass percentages of the sand and bentonite in the mixtures.

The Atterberg limits of the sand-bentonite mixture hydrated with DIW resulted in *LL* and *PL* measured at 55 % and 17 %, respectively. The sand-bentonite mixture hydrated with tap water yielded *LL* and *PL* values of 50 % and 15 %, respectively.

2.2.4 Specimen Preparation

2.2.4.1 Wetted Soil Mixtures

Dry sand and bentonite were mixed thoroughly together using a combination of dynamic mixing (e.g. oscillating, shaking, rolling, etc.) and hand mixing in order to achieve a homogenous dry mixture containing 15 % bentonite content (*BC*) by dry weight. The *BC* of 15 % was chosen on the basis that a $BC > 5$ % was recommended by Kang and Shackelford (2010) for sustainable membrane behavior over a wide range of salt concentrations. Additionally, Kenney et al. (1992) determined 11 % $\leq BC \leq$ 17 % was most effective for a mixture to have adequate bentonite distribution and achieve a suitably low k value ($\leq 10^{-9}$ m/s), and *BC*s ≥ 20 % were considered unreasonably high by Lundgren (1981), Garlenger et al. (1987), and O'Sadnick et al. (1995) for practical engineering application due to economic feasibility.

The dry sand and bentonite mixture was transferred to a 7.6 L (2 gal) bucket in layers that were approximately 7 mm in thickness. In order to hydrate the soil mixture to the targeted water content, each layer of dry mixture was hydrated with tap water (without biocide) via a spray bottle, which then was covered with another portion of dry soil sprayed with tap water, and so on. In order to maintain consistency, the total mass of dry soil and tap water required for each batch was divided by the number of layers (e.g., five to eight layers), such that each layer consisted of approximately the same mass of soil and water. Large batches (~ 3.6 kg) with up to eight layers were prepared.

The hydrated sand-bentonite mixture was sealed in a 7.6 L (2 gal) bucket with a lid and placed in a moisture room set at 23° C and 75 % relative humidity for curing. After a 24-h curing period, the hydrated sand-bentonite mixture was again thoroughly mixed with a hand spade until visibly homogeneous. The bucket containing the hydrated soil mixture was re-sealed and remained in the moisture room for an additional 24 h before a sample was taken to verify the water content of the mixture. Following the 48-h curing period, the sand-bentonite mixture was considered ready for specimen preparation via dynamic compaction.

2.2.4.2 Compaction Properties

Prior to compaction, the hydrated sand-bentonite mixture was passed through a No. 4 sieve (4.75 mm) as specified in ASTM D 698, to further homogenize the soil and break up any lumps (clods) that may have formed during the curing period. Then, the wetted sand-bentonite mixture was compacted in general accordance with the standard (Proctor) compaction procedure (i.e., ASTM D 698), except the wetted sand-bentonite mixture was compacted in molds that were one quarter the thickness of the standard compaction mold used in ASTM D 698 (i.e., 29.1 mm versus 116.4 mm). The thinner molds, henceforth referred to as quarter-size molds, were desired for specimen preparation in order to limit the durations required to achieve steady-state diffusion during membrane/diffusion testing (Cotten et al. 1998). The use of the quarter-size molds also required an adjustment to the standard compaction procedure, whereby compaction was achieved using only one lift of wetted sand-bentonite mixture and 19 blows of the standard hammer weight of 24.5 N (5.5 lb), which resulted in approximately 587 kN-m/m^3 (12,260 ft-lb/ft^3) or 99 % of the standard compaction energy of 593 kN/m^3 (12,385 ft-lb/ft^3) applied to a specimen prepared in a full-size mold.

Based on the aforementioned compaction procedure, a compaction curve for quarter-size sand-bentonite specimens comprising the 15 % bentonite (by dry weight) was generated as shown in Fig. 2.3. As described in Howell et al. (1997), the resulting compaction data were fitted with a third-order polynomial to determine the optimum water content, w_{opt}, and maximum dry unit weight, $\gamma_{d,max}$. As indicated in Fig. 2.3, the resulting values for w_{opt} and $\gamma_{d,max}$ were 12.2 % and 17.4 kN/m^3, respectively.

According to Kenney et al. (1992), mixing sand-bentonite mixtures at water contents greater than w_{opt} allows the bentonite to blend more readily with the sand. Additionally, laboratory trials for this study determined that the mixture water content, w_{mix}, decreased on average 0.67 percentage points during the sieving and compaction (see Table 2.4). Therefore, the dry sand-bentonite mixture was hydrated with tap water via the aforementioned layering method until w_{mix} was at least one percentage point greater than the w_{opt} of 12.2 % (i.e., $w_{mix} \geq 13.2$ %), such that w of each test specimen was > 12.2 % (see Fig. 2.4). Approximately 450 g of dry soil was sprayed with approximately 55 g of tap water, which then was covered with another ~450 g of soil sprayed with ~55 g of tap water, and so on. In an effort to improve specimen reproducibility, roughly 550 g of the sieved, wetted mixture was added to each compaction mold, which resulted in consistent values of the dry unit weight, γ_d, for each 102-mm (4-in) diameter specimen, such that 17.5 kN/m^3 $\leq \gamma_d \leq$ 17.8 kN/m^3 (111 lb/ft^3 $\leq \gamma_d \leq$ 113 lb/ft^3).

2.2.4.3 Hydraulic Conductivity Specimen Preparation and Testing Procedure

Evidence suggests values of *k* for compacted SB mixtures are relatively insensitive to the compaction (molding) water content (e.g., Haug and Wong 1992; Kraus et al. 1997). However, an acceptable zone (AZ) as described by Daniel and Benson (1990) was developed for the compacted SB mixture in this study. In general, an AZ represents the zone of acceptable values of the molding (compaction) water content, *w*, and dry unit weight, γ_d, required for a specified engineering property, which in this case is a suitably low value of *k*. In this study, the boundaries for the AZ shown in Fig. 2.4 were defined as the zero air voids (ZAV) curve, for a G_s of 2.68 as the upper bound, and a curve representing the relationship between *w* and γ_d for a constant degree of saturation of 64.4 %, which corresponds to the degree of saturation at w_{opt} and $\gamma_{d,max}$, or S_o, as the lower bound (Benson et al. 1999; Yesiller and Shackelford 2011).

Compacted sand-bentonite test specimens containing 15 % bentonite (by dry weight) were prepared via the aforementioned mixing and compaction methods (see sections 2.2.4.1-2.2.4.2) for measurement of *k* in accordance with ASTM D 5084 using a flexible-wall (FW) permeameter (cell). Test specimens were compacted in quarter-size compaction molds such that the thickness and diameter of specimens were 29.1 mm (1.15 in) and 102 mm (4.0 in), respectively. The measured values of the water content, *w*, and γ_d for the test specimens fell within the designated AZ as illustrated in Fig. 2.4a.

After a test specimen was extruded from the quarter-size compaction mold, the specimen was placed in the FW cell. A schematic of the FW cell is shown in Fig. 2.5a. Filter paper (Whatman™ 42 Grade Ashless Filter Paper, GE Healthcare UK Limited, Buckinghamshire, UK) and a hydrated porous stone were placed between the test specimen and the base pedestal. A second piece of filter paper and hydrated porous stone were placed on top of the test specimen, followed by the top cap. A latex membrane was stretched around the sides of the specimen, filter paper, porous disks, base pedestal, and top cap. O-rings and vacuum grease were used to secure the latex membrane to the top cap and base pedestal. Following placement of the test specimen, the remainder of the cell was assembled, including an acrylic cylinder sealed with the base pedestal and a top cap as illustrated in Fig. 2.5a. Finally, the FW cell was filled with tap water via the cell water valve, and any visible air bubbles were forced out of the cell through a top vent valve.

Once the FW cell was assembled, the cell water, headwater, and tailwater valves on the FW cell were connected to separate accumulators on a panel board (M100000 Standard Panel and M116000 Standard Add-Panel, Trautwein, Houston, TX) via flexible tubing and stainless steel connections as illustrated schematically in Fig. 2.5b. An image of the apparatus is shown in Fig. 2.6. The three accumulators were pressurized independently via controls on the panel board.

Specimens were back-pressure saturated with tap water in accordance with ASTM D 5084 until a *B* value of at least 0.95 was achieved. For this back-pressure stage, pressure transducers (DPG8001-100 General Purpose Digital Pressure Gauge, Omega Engineering Inc., Stamford, CT) with an accuracy of ± 0.25 % were connected to valves 4 and 5 (see Figure 2.7b) in order to measure the pore-water pressure at the specimen boundaries during the back-pressure stage. The initial applied cell-water pressure was 137.9 kPa (20 psi), and this pressure was increased daily by 34.5 kPa (5.0 psi) to a final applied pressure of 344.7 kPa (50 psi). The initially applied headwater and tailwater pressures were 103.4 kPa (15 psi), and these pressures were increased daily by 34.5 kPa to a final applied pressure of 310.3 kPa (45 psi). Thus, the effective stress of the specimens at the end of the back-pressure stage was 34.5 kPa (5.0 psi).

Following back-pressure saturation, an average hydraulic gradient of 30 was applied to the specimen by increasing the headwater pressure to 318 kPa (46.2 psi) while maintaining the tailwater and cell-water pressures at 310 kPa (45 psi) and 345 kPa (50 psi), respectively. An average effective stress of 30.4 kPa (4.4 psi) was maintained across the specimen. Once the gradient was applied to the specimen, hydraulic conductivity testing began via the constant head (constant-gradient) method described in ASTM D 5084 (i.e. Method A), resulting in the permeant liquid flowing from the bottom to the top of the specimen. Tap water spiked with biocide was used as the permeant liquid to reduce the likelihood of measuring unconservatively low k values due to bio-clogging (e.g., see Tong 2015). The gradient was applied by maintaining an applied constant air-pressure head difference of 8.3 kPa (1.2 psi) across the specimen (i.e., $-\Delta h_p = 0.85$ m (2.8 ft)) that was considerably greater than the change in elevation head attributed only to rising and falling water levels (i.e., $-\Delta h_z = 0.07$ m (0.23 ft)), with the change in total head during permeation being attributed entirely to the change in applied air-pressure head (i.e., $-\Delta h \approx -\Delta h_p = 0.85$ m (2.8 ft). The resulting average value for the hydraulic gradient of ≤ 29.2 was less than 30 in accordance with ASTM D 5084 for soils with k values $< 10^{-9}$ m/s. Values for k were calculated based on the following equation (Method A, ASTM D 5084):

$$k = \frac{\Delta V \cdot L}{A \cdot \Delta h \cdot \Delta t} = \frac{(V_{in} + V_{out}) \cdot L}{(\Delta h_1 + \Delta h_2) \cdot A \cdot \Delta t} \tag{2.1}$$

where ΔV is the average incremental volume of flow for a given time interval Δt taken as the average of the incremental volumes of inflow (V_{in}) and outflow (V_{out}) (i.e., $\Delta V = (\Delta V_1 + \Delta V_2)/2$), L is the specimen length (thickness) in the direction of flow, A is the specimen cross-sectional area, and Δh is the average head loss across the specimen, representing the average of Δh_1 and Δh_2 (i.e.,

$\Delta h = (\Delta h_1 + \Delta h_2)/2)$ is the average head loss across the specimen at the start of the permeation period and Δh_2 is the average head loss across the specimen at the end of the permeation period.

The criteria for terminating each test were in accordance with ASTM D 5084, i.e. the last four values for k and the ratio of the volumetric outflow rate to the volumetric inflow rate, or Q_{out}/Q_{in} , were required to be steady (no visible upward or downward trend) and Q_{out}/Q_{in} for the last four data points was required to be within 1.00 ± 0.25. Testing continued beyond the time based on the termination criterion, such that the test durations ranged from 66 to 158 d, whereas the time to meet the termination criterion ranged from 34 to 94 d. Testing was prolonged in an effort to collect sufficient volume of effluent (≥ 20 mL) for the purpose of chemical analysis of the outflow.

Following permeation with the biocide-tagged tap water, chemical compatibility testing was performed on the test specimens in accordance with ASTM D 7100 (Method 3), such that the permeant liquid was switched to 80 mM KCl, also tagged with 500 ppm of the biocide, with all other test conditions remaining constant. Chemical compatibility testing on soils with high swell, such as those with Na-bentonite, is important because the chemical constituents in permeant liquid have been shown to increase values of k relative to those measured when DIW or dilute aqueous solutions have been used as the permeant liquid (Gipson 1985; Alther 1987; Shackelford 1994; Gleason et al. 1997; Stern and Shackelford 1998; Lo et al. 2004).The 80 mM KCl permeant liquid was chosen specifically to determine the k value for the sand-bentonite specimens when permeated with the same aqueous solution used in the last stage of membrane behavior and diffusion testing. The hydraulic system remained unchanged from the tap water permeation stage, i.e. the constant head method was applied in order to induce flow, therefore, values of k for the 80 mM KCl permeation stage were also calculated using Eq. 2.1. Because the compatibility stage of hydraulic conductivity followed the initial permeation of the specimens with TW, the specimens can be considered as prehydrated specimens. i.e., specimens that have been hydrated with water prior to permeation with chemical solutions.

2.2.4.4 Membrane and Diffusion Test Specimen Preparation

The measured inner diameter of the quarter-sized mold was 102 mm (4.0 in), whereas the inner diameter of the rigid-wall cell in which compacted specimens were tested was 71.0 mm (2.8 in). Therefore, a stainless steel ring with a sharpened edge and an inner diameter of 71 mm was pushed into the compacted sand-bentonite mixture to provide a specimen with the appropriate diameter for testing. After the ring had been pushed all the way through the compacted sand-bentonite mixture, the test specimen was extruded from the ring. Due to disturbance during extrusion, this procedure reduced the dry unit weight of the test specimen, γ_d, relative to that based on compaction by approximately 3.5 %. The reduction in γ_d for the test specimens is conservative, in that specimens at lower γ_d would be expected to result in higher measured values of k and D^* and lower measured values of ω relative to specimens at higher γ_d.

Prior to extrusion of the specimens from the compaction molds, the measured values of w and γ_d were within the designated AZ as illustrated in Fig. 2.4b. The measured values for γ_d following the diameter reduction procedure are also shown in Fig. 2.4b (note that the water content did not change during diameter reduction).

The extruded test specimen was placed on the base pedestal of the rigid-wall cell inside the confining acrylic cylinder, and secured in place with the top cap via threaded rods and nuts. Once secure, the distance between the top cap and the base pedestal was 29.1 mm. Initially, the specimen was permeated with tap water via constant-head permeation. The constant head (gradient) was applied in increments of 1.4 kPa (0.2 psi) on a periodic basis (i.e., every few days) in an effort to avoid particle migration and/or side-wall leakage (e.g., see Tong 2015), until a final applied gradient of 168 was achieved. However, due to the slow nature of this testing procedure, the test was switched to constant-flow permeation after from three to five milliliters of effluent had been collected via constant-head permeation, and the specimen was visibly in good contact with the side-walls (see Fig. 2.7). Constant-flow permeation induced a larger volume of flow through the specimen over a shorter period of time, thereby effectively saturating the specimen and partially flushing the specimen of soluble salts. During permeation, flow occurred from the bottom specimen boundary to the top specimen boundary and tap water was periodically flushed across the top specimen boundary to remove entrapped air as the specimen became saturated. The specimen was considered sufficiently saturated when approximately one pore volume of flow (PVF) of effluent was collected from the specimen. Approximately three months were required for this permeation/saturation of each specimen.

2.2.5 Membrane Behavior and Diffusion Testing Apparatus and Procedure

A schematic of the apparatus used in this study, which is similar to that described by Malusis et al. (2001), is shown in Fig. 2.8. The primary components of the testing apparatus include a flow pump with two, dual-acting syringes (actuators) used to circulate liquids across the top and bottom boundaries of the specimen at an equal and constant rate, a rigid-wall cell used to contain the compacted specimen of the sand-bentonite mixture, and stainless-steel tubing that connected the syringes to the rigid-wall cell. A schematic of the rigid-wall cell is given in Fig. 2.9. The apparatus maintained constant-volume conditions of the specimen throughout the duration of the test. The stainless-steel tubing was used to minimize volume change within the system and to provide chemical resistance to the KCl solutions.

The circulation outflow liquid from the bottom of the cell was collected and stored in sampling tubes for chemical analysis. Pressures in the boundary liquids were measured via in-line (gage) pressure transducers (PX26 and PX 209 Series, Omega, Stamford, CT). The chemico-osmotic pressure difference across the specimen generated as a result of semipermeable membrane behavior was measured via a differential pressure transducer (PX26 Series, Omega, Stamford, CT). The measured pressures were recorded via a data acquisition (DAQ) system consisting of a circuit board (SCB-68, National Instruments, Austin, TX), DAQ device (National Instruments, Austin, TX), and LabVIEW software (National Instruments, Austin, TX).

The rigid-wall cell comprised a base pedestal, a top piston, and a confining acrylic cylinder with an inner diameter of 71.0 mm. Vacuum grease and O-rings on the base pedestal and top piston created an airtight seal with the acrylic cylinder. The specimen was confined axially between the base pedestal and top piston, with the latter secured into place to control the specimen thickness and prevent volume change. The top piston and base pedestal included two ports each for liquid circulation, with a third central port connected to the in-line pressure transducers. Electrolyte solutions and/or tap water were circulated across each specimen boundary through porous disks (GenPore porous sheet TO-6, General Polymer Corp., Reading, PA) via inflow and outflow ports. Filter paper (Whatman™ 42 Grade Ashless Filter Paper, GE Healthcare UK Limited, Buckinghamshire, UK) was placed between the porous disks and the specimen to prevent clogging of the disks.

The hydraulic flow-pump system was the same as the system described by Malusis et al. (2001). The flow pump consisted of a dual-carriage syringe pump (Model 55-1382 or 944, Harvard

Apparatus, Holliston, MA), two stainless-steel syringes, and stainless-steel tubing. The two syringes displaced liquid at the same rate into the top piston and base pedestal via the inflow ports (valve 1, Fig. 2.8). The liquids circulated through the porous disks and exited via the outflow ports (valve 2). The inflow and outflow rates were constant and equal such that the incremental volume of liquid entering the cell was equal to the incremental volume exiting the cell. Therefore, the volume change in the circulation system was zero, such that liquid flow through the specimen was prevented during circulation.

Operation of the flow pump system consisted of circulation and sampling/refilling cycles. The circulation cycle was used to measure the membrane and diffusion behavior of the specimen. The refilling cycle was used to collect samples of the circulation outflows from the top and bottom boundaries of the specimens while simultaneously replenishing the circulation inflow liquids for the subsequent circulation cycle.

During the circulation cycle, the syringes were open to the cell by opening valves 1 through 4 to the cell and closing valves 5 and 6 (see Fig. 2.8). The syringe displacement rate during the circulation cycle corresponded to 2.3 x 10^{-10} m^3/s, which resulted in approximately 40 mL of liquid circulated every two days. Thus, each circulation cycle lasted two days.

During the sampling/refilling cycle, the syringes were closed to the cell by closing valves 1 and 2 and opening valves 3 through 6 to the reservoirs (Fig. 2.8). The displacement direction of the flow pump was reversed such that the circulation outflow liquid from the back chambers of the syringes was expelled and collected, while fresh liquids filled the front chambers of the syringes from the reservoirs. The chemical properties of the collected circulation liquids, i.e. EC, pH, C_t and C_b, were measured and the resulting measured values were used to determine the membrane and diffusion behavior of the specimen. In contrast to the two-day duration of each circulation cycle, the sampling/replenishment cycle was accomplished in less than five minutes.

The concentration difference across the specimen (ΔC) was maintained virtually constant during the circulation cycle via continuous circulation of fresh liquid across the top and bottom specimen boundary. Boundary liquid pressures at the top and bottom of the specimen (u_{top}, u_{bottom}), and the pressure difference across the specimen (ΔP) were measured every fifteen minutes via in-line pressure transducers and a differential pressure transducer, respectively. When valves 7 through 9 (Fig. 2.8) were open, the in-line and differential pressure transducers were connected directly to the boundary liquid in the cell. The pressure difference across the specimen was measured via the differential pressure transducer and calculated for comparison from the difference between u_{top} and u_{bottom}.

Flushing excess soluble salts from the soil pore fluid via permeation prior to membrane testing enhances the potential for measureable membrane behavior (Shackelford 2013). Therefore, prior to membrane and diffusion testing, specimens RW-1 and RW-2 were permeated with tap water under open-system conditions (e.g., advective flow conditions) in the rigid-wall cell for 47 days to 102 days in an attempt to flush soluble salts from the specimen and saturate the specimen with tap water. However, little effluent was collected during this stage (~ 50 mL or 1.0 PVF) due to the low hydraulic conductivity of the sand-bentonite mixture, and the *EC* of the outflow at the end of the permeation stage was approximately 381 mS/m and 172 mS/m (compared to the *EC* of the tap water spiked with biocide of ~21.6 mS/m). As a result, specimens tested in this study were not considered flushed of all soluble salts compared to those tested for membrane behavior in previous studies, where permeation stages were significantly longer (≥ 6 months) and the *EC* of the outflow was significantly lower (20 mS/m to 70 mS/m) (Shackelford and Lee 2003; Kang and

Shackelford 2009; Kang and Shackelford 2010). Therefore, the initial pore-fluid conditions of the compacted sand-bentonite specimens tested in this study prior to semipermeable membrane testing were less favorable towards the likelihood of significant membrane behavior relative to those of previously tested GCL and CCL specimens, but more consistent with the expected conditions in field applications. Following this permeation stage, the steady-state baseline pressure difference, ΔP_{TW}, was established by simultaneously circulating tap water across the top and bottom boundaries of the specimen.

Ideally, ΔP_{TW} should be zero since the concentration gradient across the specimen was zero ($C_{ot} = C_{ob}$), such that there was no tendency for membrane pressures to develop. However, a non-zero ΔP_{TW} typically is observed due to slight variations in the hydraulic resistance of the top and bottom porous disks and/or slight variations in the machining of the syringes (e.g., Malusis et al. 2001; Malusis and Shackelford 2002a,b).

Once ΔP_{TW} was established, the multi-stage membrane and diffusion testing began such that the circulating liquid on the top boundary was switched to KCl solutions, and the generated pressure difference was recorded. Tap water continued as the circulating liquid across the bottom boundary. The circulation rate was set in an effort to represent "perfectly flushing" boundary conditions, such that steady-state ΔP should occur during each circulation stage (i.e., a two-day period between refilling and sampling). During the sampling/replenishment stages, the pressure difference generated during circulation was relieved partially and resulted in a momentary drop in the measured pressure difference at the beginning of each circulation stage. However, the pressure difference was re-established to the values at the end of the previous circulation stage upon recommencement of the circulation stage.

2.2.5.1 Chemico-Osmotic Pressures

In the presence of a solute-restricting membrane, chemico-osmotic flow will occur in a direction from low to high solute concentration (i.e., from high to low water (H_2O) activity). In the case of an ideal, or perfect, semipermeable membrane that restricts the migration of all solutes, the maximum chemico-osmotic pressure, π, can be estimated on the basis of the van't Hoff expression, as follows (Malusis et al. 2001):

$$\pi = RT\sum_{i=1}^{N} C_i \tag{2.2}$$

where R is the universal gas constant (8.314 $L \cdot kPa \cdot K^{-1} \cdot mol^{-1}$), T is the absolute temperature (K), C_i is the concentration (M) of solute i, and N is the total number of solute species. The van't Hoff expression is based on the assumption that the solution is relatively dilute (< 1.0 M) (Fritz 1986). For electrolyte solutions comprising a simple, fully dissociating salt (e.g., NaCl, KCl, $CaCl_2$), Eq. 2.2 can be simplified as follows (e.g., Malusis and Shackelford 2002a):

$$\pi = \nu RTC \tag{2.3}$$

where ν represents the number of moles of ions per molecule of salt (e.g., $\nu = 2$ for NaCl and KCl; $\nu = 3$ for $CaCl_2$).

For this study, values of π were calculated based on the measured concentrations of solutes in the electrolyte solutions that were circulated across the top and bottom boundaries of the specimen, as follows:

$$\pi_t = RT\sum_{i=1}^{N} C_{i,t} \tag{2.4}$$

$$\pi_b = RT\sum_{i=1}^{N} C_{i,b} \tag{2.5}$$

where π_t and π_b represent the maximum chemico-osmotic pressures at the top and bottom boundaries, respectively, and $C_{i,t}$ and $C_{i,b}$ represent the concentrations (M) of solute i in the circulation solutions at the respective boundaries. In general, the values for π_t and π_b can be based either on the concentrations of solutes in the source solutions being circulated across the boundaries of the specimen, or in terms of the averages of the solute concentrations in the circulation liquids across each boundary (e.g., Malusis et al. 2001; Malusis and Shackelford 2002a; Shackelford 2013). In the case where the source solute concentrations are used to calculated π_t and π_b, Eqs, 2.4 and 2.5 can be written specifically for the conditions imposed in this study as follows:

$$\pi_{o,t} = RT\left[\sum_{i=1}^{N} C_{o,t} + \sum_{i=1}^{N} C_{o,bio}\right] = RT\sum_{i=1}^{N} C_{o,t} + RT\sum_{i=1}^{N} C_{o,bio} \tag{2.6}$$

$$\pi_{o,b} = RT\left[\sum_{i=1}^{N} C_{o,b} + \sum_{i=1}^{N} C_{o,bio}\right] = RT\sum_{i=1}^{N} C_{o,b} + RT\sum_{i=1}^{N} C_{o,bio} \tag{2.7}$$

where $C_{o,t}$ represents the concentrations of solutes (Cl^- and K^+) in the source solutions being circulated across the top boundary of the specimen, $C_{o,b}$ represents the concentrations of solutes in the tap water (TW) being circulated across the bottom boundary of the specimen, and $C_{o,bio}$ represents the concentrations of any solutes derived from the inclusion of the biocide in the source solutions. In the case where the average of the boundary solute concentrations are used to calculate

π_t and π_b, Eqs, 2.4 and 2.5 can be written specifically for the steady-state conditions in this study as follows:

$$\pi_{ave,t} = RT\left[\sum_{i=1}^{N} C_{ave,t} + \sum_{i=1}^{N} C_{ave,bio}\right] = RT\sum_{i=1}^{N} C_{ave,t} + RT\sum_{i=1}^{N} C_{ave,bio} \tag{2.8}$$

$$\pi_{ave,b} = RT\left[\sum_{i=1}^{N} C_{ave,b} + \sum_{i=1}^{N} C_{ave,bio}\right] = RT\sum_{i=1}^{N} C_{ave,b} + RT\sum_{i=1}^{N} C_{ave,bio} \tag{2.9}$$

where the values of $C_{ave,t}$, $C_{ave,b}$, and $C_{ave,bio}$ are calculated as follows (e.g., Shackelford 2013):

$$C_{ave,t} = \frac{C_t + C_{o,t}}{2} \tag{2.10}$$

$$C_{ave,b} = \frac{C_b + C_{o,b}}{2} \tag{2.11}$$

$$C_{ave,bio} = \frac{C_{bio} + C_{o,bio}}{2} \tag{2.12}$$

where C_t, C_b, and C_{bio} represent the measured solute concentration of the circulation liquid collected as outflow from the top and bottom boundaries, respectively.

The difference in the maximum chemico-osmotic pressures across an ideal membrane, $\Delta\pi$, is defined as follows:

$$\Delta\pi = RT\sum_{i=1}^{N} \Delta C_i = \pi_b - \pi_t \tag{2.13}$$

where ΔC_i represents the concentration difference (M) across the specimen for solute i, with the positive direction designated from the top to the bottom of the specimen, i.e., in the direction of imposed concentration gradient for Cl^- and K^+. Note that, based on the assumed signed convention, the value of $\Delta\pi$ calculated in accordance with Eq. 2.13 will be negative ($\Delta\pi < 0$). Thus, the values of $\Delta\pi$ can be calculated on the basis of the source solute concentrations ($\Delta\pi_o$) or the average of the boundary solute concentrations ($\Delta\pi_{ave}$), as follows:

$$\Delta\pi_o = \left[RT\sum_{i=1}^{N} C_{o,\mathrm{b}} + RT\sum_{i=1}^{N} C_{o,bio} \right] - \left[RT\sum_{i=1}^{N} C_{o,\mathrm{t}} + RT\sum_{i=1}^{N} C_{o,bio} \right] \tag{2.14}$$

$$\Delta\pi_{ave} = \left[RT\sum_{i=1}^{N} C_{ave,\mathrm{b}} + RT\sum_{i=1}^{N} C_{ave,bio} \right] - \left[RT\sum_{i=1}^{N} C_{ave,\mathrm{t}} + RT\sum_{i=1}^{N} C_{ave,bio} \right] \tag{2.15}$$

Under a closed-system testing condition such as implemented in this study, the membrane efficiency of the specimen can be quantified by as follows (Groenevelt and Elrick 1976; Malusis et al. 2001):

$$\omega = \frac{\Delta P_{ss} - \Delta P_{TW}}{\Delta\pi} = \frac{\Delta P_e}{\Delta\pi} \tag{2.16}$$

where ΔP_{ss} (< 0) is the steady-state chemico-osmotic pressure difference (kPa) measured prior to changing the KCl concentrations of the source solution for the next stage of the test, ΔP_{TW} (< 0) is the chemico-osmotic pressure difference (kPa) measured during the initial stage of the test when tap water is circulated across both the top and bottom boundaries, and ΔP_e (< 0) is the effective or net chemico-osmotic pressure difference (kPa). The resulting values of ω based on Eqs. 2.14 and 2.15 are defined as follows:

$$\omega_o = \frac{\Delta P_e}{\Delta \pi_o} \tag{2.17}$$

$$\omega_{ave} = \frac{\Delta P_e}{\Delta \pi_{ave}} \tag{2.18}$$

As previously noted (e.g., Malusis et al. 2001; Malusis and Shackelford 2002a), values of ω_o typically are more conservative (lower) than values of ω_{ave}, because the magnitude of $\Delta\pi_o$ typically will be greater than that of $\Delta\pi_{ave}$, i.e., since $C_{ave,t} < C_{o,t}$ and $C_{ave,b} \geq C_{o,b}$, for the same measured value of ΔP_e.

2.2.5.2 Effective Diffusion Coefficients

If the specimen does not exhibit ideal membrane behavior, diffusion of solutes will occur from the higher concentration boundary at the top of the specimen to the lower concentration boundary at the bottom of the specimen due to the imposed concentration gradient (i.e., $\Delta C/L$, where L = the thickness of the specimen) across the specimen. In this case, concentrations of K^+ and Cl^- in the circulation outflow from the bottom boundary of the specimen will be greater than those in the circulation inflow at the bottom boundary ($C_b > C_{ob}$), whereas concentrations of K^+ and Cl^- in the circulation outflow from the top boundary of the specimen will be lower than those in the circulation inflow at the top of the specimen ($C_t < C_{ot}$). These boundary conditions are the same as those imposed in the through-diffusion method (also known as the steady-state or time-lag method) for determining the effective diffusion coefficient, D^*, of chemical species diffusing through porous medium (e.g., Shackelford 1991).

In the through-diffusion method, the measured concentrations of the chemical species in the circulation outflows from the bottom boundary of the specimen are continuously monitored and converted to the incremental mass of the chemical species per unit area of the specimen corresponding to the given increment in elapsed time, ΔQ_t, or:

$$\Delta Q_{t,i} = \frac{\Delta m_i}{\Delta t_i} = \frac{\Delta\left(C_b \cdot V_b\right)_i}{\Delta t_i} \tag{2.19}$$

where V_b is the volume of the circulation outflow sample corresponding to C_b, and i is the sample number. Therefore, the accumulated solute mass per unit area is represented as the sum of all of the incremental masses resulting from continuous sampling of the circulation outflows, or:

$$Q_t = \sum_{i=1}^{N} \Delta Q_{t,i} \tag{2.20}$$

where N is the total number of samples. Sampling of the circulation outflows must be continuous so that all solute mass is included in the calculations for this method. The resulting values of Q_t are plotted as a function of the cumulative elapsed time, t (= $\sum_{i=1}^{N} \Delta t_i$).

During early time Q_t-versus-t data, the test is in a transient stage, such that the Q_t-versus-t trend generally is nonlinear. However, as long as the concentrations at the boundaries remain relatively constant, diffusion through the specimen will eventually reach steady-state conditions for each solute. This steady-state stage occurs after the initial transient stage and is indicated by a straight line representing constant diffusive mass flux (Shackelford 1991).

At steady state, the charge fluxes of the anion (i.e. Cl^-) and the cation (K^+) theoretically must be the same in order to satisfy the electroneutrality requirement for simple salt solutions (e.g. the KCl solutions used in this study) diffusing through specimens where the concentration of the remaining ions in the pore fluid are much lower than that of the diffusing salts. The equivalent charge flux is the same as the equivalent molar flux for KCl with a 1:1 charge ratio; however, the atomic weights for Cl^- and K^+ are not equivalent, i.e. 35.5 g/mol versus 39.1 g/mol. Therefore, the mass flux of K^+ theoretically should be 1.1 times greater than that for Cl^- to satisfy the equivalent charge (or equivalent molar flux) requirement assuming Cl^- and K^+ are the only remaining ions in the outflow at steady state (Shackelford and Lee 2003).

Values of the effective diffusion coefficient, D^*, were determined by performing a linear regression of the steady-state portion of the Q_t-versus-t data based on the following equation (e.g. Shackelford 1991):

$$D^* = \left(\frac{\Delta Q_t}{\Delta t}\right)\left(\frac{L}{n w_A \Delta C}\right) \tag{2.21}$$

where $\Delta Q_t/\Delta t$ represents the slope of the linear regression, L is the specimen thickness, n is the specimen porosity, w_A is the atomic weight of the diffusing solute, and ΔC is the molar concentration difference of the anion (Cl^-) or cation (K^+) across the specimen. The linear portion of the data was determined via sequential linear regression where an increasing number of Q_t and t data were included in the regression until the coefficient of determination, r^2, deviated significantly from unity (Shackelford and Lee 2003). The deviation was assumed to be the distinction between the transient and steady-state stages and was designated as the time to steady-state, t_{ss}. The steady-state data were used to calculate D^* which can be defined as follows (Shackelford and Daniel 1991; Malusis and Shackelford 2002b; Shackelford and Moore 2013):

$$\mathrm{D}^* = D_o \tau_a = D_o \tau_m \tau_r = D_p \tau_r \tag{2.22}$$

where D_o is the aqueous-phase diffusion coefficient of the solute, D_p is referred to as the "pore diffusion coefficient," and τ_a is the apparent tortuosity factor representing the product of the matrix and restrictive tortuosity factors such that:

$$\tau_a = \tau_m \tau_r = \tau_m \prod_{i=1}^{N} \tau_i = \tau_m (\tau_1 \cdot \tau_2 \cdots \tau_N) \tag{2.23}$$

where the matrix tortuosity factor, τ_m ($0 \leq \tau_m \leq 1$), represents the tortuous nature of the diffusive pathways through the porous medium due to the geometry of the interconnected pores, and the restrictive tortuosity factor, τ_r ($0 \leq \tau_r \leq 1$), represents the product of additional N factors (τ_i), such as anion exclusion and increased water viscosity near the clay particle surface, that contribute to the apparent tortuosity by acting to reduce the diffusive flux of solutes through the porous medium (e.g., Kemper and Maasland 1964; Shackelford and Daniel 1991; Shackelford and Moore 2013).

2.2.6 Testing Program

Multiple-stage membrane testing was conducted in this study by sequentially increasing the molar concentration of the KCl solution (5, 10, 20, 40, and 80 mM KCl) circulated across the top boundary of the specimen while tap water was circulated across the bottom boundary. The type of salt (KCl) and range in salt concentrations (5 mM to 80 mM) were chosen based on previous membrane testing (e.g., Malusis et al. 2001; Malusis and Shackelford 2002a,b; Shackelford and Lee 2003; Kang and Shackelford 2010; Kang and Shackelford 2011; Shackelford 2013; Malusis et al. 2014), to allow for comparison of the results. Biocide was added to boundary circulation liquids (i.e., KCl solutions and tap water) to limit anaerobic biologic activity in the testing cells during the extended test durations (e.g., ~ 1 yr). Each concentration stage was performed until steady values were achieved for both the measured ΔP and the EC of the outflows at the boundaries. The measured ΔP and EC values were considered steady when the values for the last four data points were all within ± 3 % of the geometric mean of the same values.

Upon achieving a steady state at a given KCl concentration, the molar concentration was increased by a factor of two in an effort to define the trend of ω versus C_{ot}. This procedure resulted in multiple-stage membrane and diffusion test durations ranging from 132 to 370 days. At the end of each concentration stage, the concentration of anions and cations in the last four samples collected from the top and bottom of the specimen were analyzed in order to determine steady-state values of C_t and C_b via the geometric mean, respectively, and therefore determine steady-state values of D^* for Cl^- and K^+ for each concentration stage.

A duplicate test, designated as RW-2, was conducted in an effort to support the results and conclusions based on the first test (RW-1). Test RW-2 was conducted in an effort to determine if consistent trends for membrane behavior would be observed. However, the duration of test RW-2 was not as long as that for test RW-1 (i.e., 0.4 yr vs. ~ 1 yr), because the measurement of membrane behavior was the primary objective for test RW-2 (i.e., the test specimen for RW-2 was not evaluated for diffusion).

2.3 Results

2.3.1 Hydraulic Conductivity

The results of the hydraulic conductivity tests using tap water as the permeant liquid are summarized in Table 2.5 and presented in Figs. 2.10 through 2.12. All three specimens (i.e. FW-1, FW-2, and FW-3) were permeated with tap water for an additional one to two months after the termination criterion specified in ASTM D 5084 had been achieved. Thus, two values of k are reported in Table 2.5, viz., a standard value of k, or k_s, that corresponds to the time at which the standard termination criteria in ASTM D5084 were achieved, t_s, and a final value of k, or k_f, that corresponds to the final duration of permeation with tap water, t_f.

As indicated in Table 2.5, the values of both k_s and k_f for all three specimens were lower than the typical maximum allowable value of k of 10^{-9} m/s required of liners for waste containment applications when tap water is used as the permeant liquid (Daniel 1987, 1993; Benson et al. 1994, 1999; Rowe and Fraser 1995). Also, as shown in Fig. 2.13, there was no definitive trend for the k values calculated at t_s versus t_f, such that $k_s < k_f$ for FW-1 and FW-3, whereas $k_s > k_f$ for FW-2. Both of these results, i.e., the low values of k_s and k_f and the non-definitive trends in k_s versus k_f, are consistent with those reported by Tong (2015) for compacted sand-bentonite specimens containing 15 % of the same bentonite (by dry weight) when permeated with the same tap water for the same testing conditions ($\sigma' = 34.5$ kPa, $i = 30$).

In an effort to correlate the hydraulic conductivity of the compacted sand-bentonite specimens comprising 15 % bentonite (by dry weight) with the results of the membrane and diffusion testing, specimen(s) FW-1 (and FW-2) also were permeated with an 80-mM KCl solution following permeation with tap water. Specimen FW-3 was not permeated with the 80-mM KCl solution due to the relatively large volumetric change observed during the tap water permeation stage. Nonetheless, despite the abnormal volume change for the FW-3 specimen, the measured values of k for the FW-3 specimen were consistent with those for FW-1 and FW-2 specimens based on permeation with tap water.

The values of k resulting from KCl permeation, designated as k_c, are also provided in Table 2.5. Following 102 days of permeation with 80 mM KCl, the values of k_c were steady at 6.63×10^{-12} m/s and 5.35×10^{-12} m/s for FW-1 and FW-2, respectively. Following months of permeation with 80 mM KCl, values of k_c were relatively unchanged compared to values of k_f (e.g., $k_c - k_f < 1 \times 10^{-12}$ m/s). Due to the low values of k_c, chemical equilibrium in accordance with ASTM D 7100 was not achieved within the time constraints of this study. Following the collection of approximately 0.5 PVFs from FW-1 and FW-2 during the 80 mM KCl stage, the EC of the effluent, EC_f, was 610 mS/m and 631 mS/m for FW-1 and FW-2, respectively. Values of EC_f were approximately half that of the EC of the 80 mM KCl influent solution, EC_o (= 1150 mS/m).

2.3.2 Membrane Testing

The initial conditions of the two rigid-wall specimens tested for membrane behavior (i.e. RW-1 and RW-2) are provided in Table 2.6. The initial condition corresponds to the condition of the specimen after compaction whereas the final condition corresponds to the condition of the specimen after membrane testing. Hydraulic conductivity data collected during permeation for both specimens are provided in Fig. 2.14.

The k values were calculated based on the measured difference in pressure across the specimen based on under constant-flow conditions via the flow pump system described in Section 2.2.5, as follows:

$$k = \frac{Q \cdot L \cdot \gamma_w}{A \cdot \Delta u} \qquad (2.24)$$

where Q is the volumetric flow rate applied via the flow pump system (5 x 10^{-11} m^3/s to 1 x10^{-10} m^3/s), L is the specimen length (thickness) in the direction of flow (29.1 mm), A is the specimen cross-sectional area (3960 mm^2), Δu is the difference in water pressure across the specimen ($\leq$ 139 kPa (20.2 psi)), which was recorded every ten minutes via the in-line differential pressure transducer, and γ_w is the unit weight of water (9.81 kN/m^3 (62.4 lb/ft^3)). However, in order to maintain the integrity of the pressure transducers, the flow pump had to be stopped before Δu increased above the maximum values allowed by each transducer of 207 kPa (30 psi) and 159 kPa (23 psi) for tests RW-1 and RW-2, respectively. As a result, the k values reported for specimens RW-1 and RW-2 in Table 2.7 were estimated based on the steady-state trends observed for Δu shown in Fig. 2.14 that occurred prior to pressure spikes that required the flow pumps to be stopped. Therefore, the estimated values of k likely were conservative (high) because k is inversely proportional to Δu (Eq. 2.24 and Fig. 2.14), such that higher values of Δu would have resulted in lower calculated k values. Also, specimen RW-2 was permeated at a slower flow rate in an effort to avoid particle migration which occurred in specimens previously permeated in the same apparatus. The slower flow rate resulted in fewer pore volumes of flow, *PVF*, of tap water through the RW-2 specimen compared to RW-1 (e.g. 0.87 versus 1.2, respectively).

2.3.2.1 Boundary Electrical Conductivity and Solute Concentration Values

The values of electrical conductivity, *EC*, measured for samples of the circulation outflow collected from the top and bottom boundaries of specimens RW-1 and RW-2 are presented in Fig. 2.15. The *EC* of the outflows collected from the top and bottom boundaries, EC_t and EC_b, respectively, decreased during the preliminary permeation stage and the baseline circulation stage with tap water (i.e., circulation of tap water across both the top and bottom boundaries of the specimens under closed-system conditions) as soluble salts were removed from the specimen via advection and diffusion, respectively. Values for EC_t and EC_b also were measured after each sampling period during all stages of KCl circulation. Further chemical analysis of the outflow collected during KCl circulation was performed to provide additional support for the measured *EC* values. Outflow collected from the top boundary of specimens RW-1 and RW-2 and from the bottom boundary of specimen RW-2 during the last four sampling periods of each KCl circulation stage were analyzed for anion and cation concentrations via the IC and ICP, respectively, whereas every sample collected as outflow from the bottom boundary of specimen RW-1 was analyzed for anion and cation concentrations.

A summary of the measured *EC* values and KCl concentrations corresponding to the circulation inflows (source liquids) and the circulation outflows collected from the top and bottom boundaries of the specimens at steady state are provided in Table 2.8. Steady-state values of sample *EC* and solute concentrations, *C*, for the outflows collected from the top and bottom of the specimen boundaries were calculated via the average value for the outflow collected during the last four sampling periods of each KCl stage. The measured values of *EC* and *C* for the outflows are not equal to the measured values of *EC* and *C* for the inflows, and the relative difference (positive or negative) does not remain constant for all KCl circulation stages. Schematics presented in Fig. 2.16 indicate the relative direction of transport (i.e., diffusion) for ions initially in the pore fluid of the specimens (soluble metals), ions introduced via inflow at the top boundary, and ions introduced via inflow at the bottom boundary. The relative direction of transport is responsible for the discrepancy in measured values of C and EC for the inflow and outflow collected from the specimen boundaries.

Measured ion concentrations of the outflow collected from the top and bottom boundaries, C_t and C_b, respectively, for specimen RW-1 are presented in Fig. 2.17. The data presented in Fig. 2.17b are shown separately in terms of anions and cations in Figs. 2.18a, and 2.18b, respectively. Additionally, measured values of C_t and C_b for specimen RW-2 are presented in Fig. 2.19. The data presented in Fig. 2.19b are shown separately in terms of anions and cations in Figs. 2.20a, and 2.20b, respectively.

During the early stages of membrane testing where 5 mM and 10 mM KCl solutions were circulated across the top boundary of specimen RW-1, and tap water was circulated across the bottom boundary of the specimen, $EC_t > EC_{ot}$ and $EC_b > EC_{ob}$, which indicates an increase in chemical species at both boundaries relative to the concentrations of the source liquids, C_{ot} and C_{ob}. However, the concentrations for chemical species introduced into the system via the top source liquid, i.e. Cl^-, Br^-, and K^+, were greater than those for the same species in the circulation outflows from the top boundaries of the specimens ($C_{ot} > C_t$). A decrease in the outflow concentration relative to the source concentration indicates a net inward diffusion of the respective chemical species from the top boundary into the specimen. Conversely, as shown in Figs. 2.17a and 2.19a, increasing concentrations of soluble metals (e.g. Na^+, Ca^{2+}, and Mg^{2+}) were measured in the circulation outflows collected from the top boundary at relative concentrations, such that $C_t > C_{ot}$ (= 0). These increasing concentrations indicate outward diffusion from the specimen into the circulation outflows collected from the top boundary. Ions that are measured at higher concentrations in the outflow compared to the concentrations measured in the source liquid (i.e. $C_t > C_{ot}$ or $C_b > C_{ob}$) were considered accountable for any increase in the measured values of EC, such that the outward diffusion of soluble salts at the top boundary can be used to explain $EC_t > EC_{ot}$. A different trend was observed for the concentration of ions in the outflow collected from the bottom boundary during early stages, such that Cl^-, Br^-, K^+, and Na^+ were measured at relative concentrations of $C_b > C_{ob}$ (tap water), which indicates an outward diffusion of the respective ions to the bottom boundary. Ions often considered soluble metals in bentonite, e.g. Ca^{2+} and Mg^{2+}, were measured at relative concentrations of $C_{ob} > C_b$, which indicates an inward diffusion from the bottom boundary, likely due to the concentration of the respective ions in the source tap water introduced to the system via the bottom boundary.

In comparison to the trends observed for C and EC during the early stages of test RW-1, when 5 mM and 10 mM KCl solutions and tap water were circulated across the top and bottom boundaries, respectively, of specimen RW-2, $EC_{ot} > EC_t$ and $EC_b > EC_{ob}$, which indicates a decrease in chemical species at the top boundary and an increase in chemical species at the bottom boundary relative to the concentrations of the source liquids, C_{ot} and C_{ob}. Higher values of C_t for Na^+ were measured in early stages of test RW-2 compared to test RW-1, which is consistent with previous statements that specimen RW-2 was slightly less flushed of soluble metals than specimen RW-1. Although the reasoning for $EC_{ot} > EC_t$ during the early stages of test RW-2 is unknown, one proposed explanation is the higher values of C_t for Na^+, due to elevated concentrations of Na^+ in the pore fluid of specimen RW-2, could, in part, result in more compressed DDLs which would allow for greater inward diffusion of Cl^-, Br^- and K^+ ions at lower values of C_{ot} and, therefore, result in $EC_t < EC_{ot}$ at early stages (i.e., 5 mM and 10 mM KCl).

The same explanation of $EC_b > EC_{ob}$ for test RW-1 can be used for test RW-2, in that the concentration of ions in the outflow collected from the bottom boundary during early stages, such as Cl^-, Br^-, K^+, and Na^+, were measured at relative concentrations of $C_b > C_{ob}$, which indicates an outward diffusion of the respective ions to the bottom boundary resulting in $EC_b > EC_{ob}$. Additionally, relative concentrations of $C_{ob} > C_b$ were observed for Ca^{2+} and Mg^{2+} for test RW-2, which is consistent with test RW-1.

The trends in EC and C for test RW-1 and RW-2 are approximately the same at later stages. During later stages for tests RW-1 and RW-2, i.e. 20 mM through 80 mM KCl, $EC_{ot} > EC_t$, which indicates a decrease in ions at the top boundary during circulation of the source KCl solution. As C_{ot} increases for each subsequent stage of KCl circulation, the concentration gradient driving inward diffusion of Cl^- and K^+ also increases. Additionally, Ca^{2+} and Mg^{2+} are measured in increasing concentrations in C_t due, in part, to the diffusion of the respective ions through the specimen via the tap water at the bottom boundary. In such a case where de-ionized water was circulated across the bottom boundary, concentrations of Ca^{2+} and Mg^{2+} in the outflow would decrease as they were removed from the specimen as soluble metals (Bohnhoff and Shackelford 2015). The decrease in EC_t compared to EC_{ot} is due to a loss of Cl^- and K^+ ions to inward diffusion, and the outward diffusion of Ca^{2+} and Mg^{2+} ions are not sufficient to offset the effect of the inward diffusion of Cl^- and K^+ ions on values of EC_t. Additionally, the concentration of Na^+ ions in the outflow collected from both boundaries decreases as the ion is removed from the specimen as a soluble metal, see Figs. 2.17 and 2.19. The relative concentration for Na^+ ions in the outflow collected from the bottom boundary switches from $C_b > C_{ob}$ to $C_{ob} > C_b$ around day 238 for test RW-1, which indicates that diffusion of the Na^+ ion changes from outward diffusion at the bottom boundary to inward diffusion. The same trend of $EC_b > EC_{ob}$ observed in early stages persists through the later stages, however, the concentration of Na^+ is no longer large enough to have an effect on the observed $EC_b > EC_{ob}$ trend when compared to the increasing concentration of K^+ and

Cl^- in the circulation outflow collected from the bottom boundary due to diffusion through the specimen from the top boundary.

2.3.2.2 Boundary Water Pressures

The boundary water pressures measured at the top, u_{top}, and bottom, u_{bottom}, of the specimens via the in-line (gage) pressure transducers are presented in Fig. 2.21. During the initial stage of each test, when TW was circulated across both boundaries of each specimen, the values of u_{top} and u_{bottom} were approximately equal (i.e., $u_{top} \approx u_{bottom}$), because the difference in solute concentration across each specimen was zero. However, as previously noted (Malusis et al. 2001; Malusis and Shackelford 2002a; Bohnhoff 2012; Meier 2014; Sample-Lord 2015), slight differences between u_{top} and u_{bottom} can result during this stage due, in part, to slight differences in the hydraulic resistance of the porous disks located at the top and bottom of the specimen.

Upon circulation of KCl solutions across the top boundary, values of u_{top} increased relative to values of u_{bottom} for both tests, i.e. $u_{top} > u_{bottom}$. As previously discussed, when a specimen is confined in a closed-system apparatus and the specimen behaves as a semipermeable membrane, a chemico-osmotic pressure will develop along the top boundary in order to counteract the tendency for chemico-osmotic flow from the bottom to the top of the specimen due to the imposed concentration gradient. Therefore, values of u_{top} increased as the KCl solution was introduced along the top boundary. Values of u_{bottom} were negative for both tests throughout all stages of KCl circulation, which is consistent with trends for u_{bottom} previously reported in the literature (e.g., Kang and Shackelford 2010).

2.3.2.3 Maximum Chemico-Osmotic Potentials at Specimen Boundaries

Due to incomplete flushing of residual soluble salts within the pore water of the soil specimens, the use of TW, and the addition of biocide to the circulation liquids, several additional chemical species were present in the liquid at the top and bottom specimen boundaries relative to the conditions reported in previous membrane studies. Therefore, further expansion of Eqs. 2.6 through 2.9 used to calculate π was required in order to take into account the measured concentrations of these additional chemical species.

In the case where the maximum chemico-osmotic pressures at the specimen boundaries are based on the source solute concentrations, the values of π are designated as π_o. Thus, the expression of π_o for the top boundary, or $\pi_{o,t}$, based on the conditions imposed in this study can be written according to Eq. 2.6 as follows:

$$\pi_{o,t} = RT\left[C_{Cl^-} + C_{K^+}\right]_{o,t} + RT\sum_{i=1}^{N} C_{o,bio} \approx RT\nu C_{o,t,KCl} + RT\sum_{i=1}^{N} C_{o,bio} \qquad (2.25)$$

where $C_{o,t,KCl}$ represents the concentration of KCl in the source solution circulated across the top boundary. If stoichiometric balance between Cl^- and K^+ in the source solutions is assumed, then the concentration of KCl can be based on the measured concentration of Cl^-. Thus, Eq. 2.25 can be written as follows:

$$\pi_{o,t} \approx RT\nu C_{o,t,Cl^-} + RT\sum_{i=1}^{N} C_{o,bio} \qquad (2.26)$$

where C_{o,t,Cl^-} represents the measured concentration of Cl^- in the source solution. Similarly, the expression of π_o for the bottom boundary, or $\pi_{o,b}$, based on the conditions imposed in this study can be written according to Eq. 2.7 as follows:

$$\pi_{o,b} = RT\left[C_{Cl^-} + C_{F^-} + C_{NO_2^-} + C_{SO_4^{2-}} + C_{Ca^{2+}} + C_{K^+} + C_{Mg^{2+}} + C_{Na^+}\right]_{o,b} + RT\sum_{i=1}^{N} C_{o,bio} \qquad (2.27)$$

where the parameters in brackets represent the concentrations for the major solutes (Cl^-, F^-, NO_2^-, SO_4^{2-}, Ca^{2+}, K^+, Mg^{2+}, and Na^+) measured in the TW used in this study.

In the case where the average of the boundary solute concentrations were used to calculate π_t and π_b, expressed as $\pi_{ave,t}$ and $\pi_{ave,b}$, respectively, Eqs. 2.8 and 2.9 can be written for the conditions in this study as follows:

$$\pi_{ave,t} = RT\left[C_{Cl^-} + C_{F^-} + C_{NO_2^-} + C_{SO_4^{2-}} + C_{Ca^{2+}} + C_{K^+} + C_{Mg^{2+}} + C_{Na^+}\right]_{ave,\mathrm{t}} + RT\sum_{i=1}^{N} C_{ave,bio} \qquad (2.28)$$

$$\pi_{ave,b} = RT\left[C_{Cl^-} + C_{F^-} + C_{NO_2^-} + C_{SO_4^{2-}} + C_{Ca^{2+}} + C_{K^+} + C_{Mg^{2+}} + C_{Na^+}\right]_{ave,b} + RT\sum_{i=1}^{N} C_{ave,bio} \qquad (2.29)$$

where values of C_{ave} for a given solute were calculated using Eqs. 2.10 through 2.12, and the values of C_t and C_b were based on the measured concentrations of the solutes in the respective circulation outflows at steady-state. Calculated values of π based on Eqs. 2.26 through 2.29 for a given KCl testing stage are presented in Table 2.9.

In order to account for the additional solutes in the TW and biocide, Eqs. 2.14 and 2.15 were expanded as follows:

$$\left.\begin{aligned}
\Delta\pi_o &= \pi_{o,b} - \pi_{o,t} \\
&= RT\left[\left[C_{Cl^-} + C_{F^-} + C_{NO_2^-} + C_{SO_4^{2-}} + C_{Ca^{2+}} + C_{K^+} + C_{Mg^{2+}} + C_{Na^+}\right]_{o,b} + \sum_{i=1}^{N} C_{o,bio}\right] - \\
&\quad RT\left[\nu C_{o,t,Cl^-} + \sum_{i=1}^{N} C_{o,bio}\right] \\
&\approx RT\left[C_{Cl^-} + C_{F^-} + C_{NO_2^-} + C_{SO_4^{2-}} + C_{Ca^{2+}} + C_{K^+} + C_{Mg^{2+}} + C_{Na^+}\right]_{o,b} - RT\nu C_{o,t,Cl^-}
\end{aligned}\right\} \quad (2.30)$$

$$\left.\begin{aligned}
\Delta\pi_{ave} &= \pi_{ave,b} - \pi_{ave,t} \\
&= RT\left[\left[C_{Cl^-} + C_{F^-} + C_{NO_2^-} + C_{SO_4^{2-}} + C_{Ca^{2+}} + C_{K^+} + C_{Mg^{2+}} + C_{Na^+}\right]_{ave,b} + \sum_{i=1}^{N} C_{ave,bio}\right] - \\
&\quad RT\left[\left[C_{Cl^-} + C_{F^-} + C_{NO_2^-} + C_{SO_4^{2-}} + C_{Ca^{2+}} + C_{K^+} + C_{Mg^{2+}} + C_{Na^+}\right]_{ave,\mathrm{t}} + \sum_{i=1}^{N} C_{ave,bio}\right] \\
&\approx RT\left[\Delta C_{Cl^-} + \Delta C_{F^-} + \Delta C_{NO_2^-} + \Delta C_{SO_4^{2-}} + \Delta C_{Ca^{2+}} + \Delta C_{K^+} + \Delta C_{Mg^{2+}} + \Delta C_{Na^+}\right]_{ave}
\end{aligned}\right\} \quad (2.31)$$

The resulting calculated values of $\Delta\pi_o$ and $\Delta\pi_{ave}$ based on Eqs. 2.30 and 2.31 are presented in Table 2.10.

For comparison with values of $\Delta\pi$ from previous studies where DIW instead of TW was circulated across the bottom boundary (i.e., $C_{o,b} = 0$) while values of $\pi_{o,t}$ remain unchanged, Eqs. 2.27 through 2.29 may be written as follows:

$$\pi_{o,b} = RT\sum_{i=1}^{N} C_{o,bio} \quad (2.32)$$

$$\pi_{ave,t} \approx RT\nu C_{ave,t,Cl^-} + RT\sum_{i=1}^{N} C_{ave,bio} \quad (2.33)$$

$$\pi_{ave,b} \approx RT\nu\left[C_{b,Cl^-} - C_{\mathrm{o,b},Cl^-}\right] + RT\sum_{i=1}^{N} C_{o,bio} \quad (2.34)$$

where $C_{o,b}$ is zero to represent theoretical DIW circulation conditions, C_{b,Cl^-} represents the concentration of Cl^- in the collected outflow from the bottom boundary, and C_{o,b,Cl^-} was subtracted from C_{b,Cl^-} in order to represent theoretical DIW circulation conditions, such that the concentration of Cl^- ions in the bottom boundary outflow under theoretical conditions was only due to diffusion through the specimen from the top boundary. The resulting calculated values of $\Delta\pi_{o,DIW}$ and $\Delta\pi_{ave,DIW}$ based on Eqs. 2.30 through 2.34 are presented in Table 2.10

2.3.2.4 Chemico-Osmotic Pressure Differences

The measured values of the chemico-osmotic pressure differences, $-\Delta P$ (> 0) are presented in Fig. 2.22, where $-\Delta P$ was measured directly via a differential pressure transducer (DPT). The accuracy of the transducers used in the apparatus for test RW-1 was lower than that used in the apparatus for test RW-2 (1 % versus 0.25 % of the full-scale (range), which equates to ± 1 kPa versus ± 0.4 kPa, respectively), which is the reason for more scatter being apparent in the $-\Delta P$ data for test RW-1 relative to that in test RW-2. Additional scatter observed in the both sets of recorded $-\Delta P$ data can be attributed to the heterogeneous nature of soil mixtures. For example, Kang and Shackelford (2010) attributed greater scatter in measured values of $-\Delta P$ for specimens of a compacted clay amended with 5 % bentonite relative to those previously shown for specimens of a GCL containing only bentonite due to the greater complexity of the interconnected pores in the bentonite amended clay specimens resulting from the mixing of two disparate types of soil.

The values of $-\Delta P$ measured during the last four, two-day circulation cycles (i.e., eight days) for a given KCl testing stage in this study are shown in Figs. 2.23 and 2.24, which can be compared to the trend commonly reported in the literature depicted in Fig. 2.25a. The value of $-\Delta P$ recorded at the end of each two-day circulation cycle, $-\Delta P_c$, typically is considered the steady-state value of $-\Delta P$ for that cycle. However, in this study, $-\Delta P$ did not always stabilize prior to the end of the cycle, which is similar to trends previously reported for rigid-wall membrane tests with a similar circulation rate, Q, of approximately 2.3 x 10^{-10} m^3/s (Bohnhoff 2012). Therefore, two approaches for determining values of $-\Delta P_c$ for a given two-day cycle were explored, and the resulting final values of $-\Delta P_c$ are presented in Fig. 2.26. The first approach involved using the maximum measured value for each two-day cycle. The second approach involved using the central tendency in values via the geometric mean of the $-\Delta P$ data recorded during each second day of the two-day cycle. Both approaches for determining $-\Delta P_c$ were applied to the $-\Delta P$ data recorded for the tests RW-1 and RW-2 before determining the best approach given the relative data sets.

The central tendency approach applied to the second-day data recorded for test RW-1 was determined to be the most accurate method for determining $-\Delta P_c$, because the maximum values of $-\Delta P$ for each two-day cycle could not be considered a reliable representation of $-\Delta P_c$ due to the significant scatter associated with the lower accuracy of the transducers used for test RW-1. Therefore, using the maximum value of $-\Delta P$ to define $-\Delta P_c$, given the scatter in the recorded data, would result in unconservatively high values of $-\Delta P_c$.

The central tendency was estimated by the geometric mean calculated for the second-day data, which represents the geometric middle of the data such that the range (scatter) of recorded $-\Delta P$ values was normalized and did not have a dominating effect on the averaged value. This approach represented the most accurate method for estimating $-\Delta P_c$ for test RW-1 while still best reflecting the chemico-osmotic pressure difference generated across the specimen without being unconservatively high due to scatter. When the central tendency approach was applied to values of $-\Delta P$ recorded for test RW-2, the resulting values of $-\Delta P_c$ were conservatively low. However, given the higher accuracy of the transducers used for test RW-2, use of the central tendency value was not deemed necessary due to the limited scatter in these data. The maximum value of $-\Delta P$ for the RW-2 test data was on average 1.0 kPa (0.15 psi) higher than the central tendency of the second-day $-\Delta P$ data; however, the maximum value of $-\Delta P$ was considered as a more accurate representation of the chemico-osmotic pressure difference across the specimen.

The failure of $-\Delta P$ values to stabilize during the two-day cycle may have been due to the different thickness and/or the bentonite content of the specimens in this study compared to specimens tested in previous studies using approximately the same circulation rate. For example, bentonite amended clay specimens tested by Kang and Shackelford (2010) were prepared at the same thickness as the specimens in this study (i.e., 29.1 mm), but the bentonite content of the specimens tested by Kang and Shackelford (2010) was lower (5 % versus 15 %). In contrast the GCL specimens tested by Malusis and Shackelford (2002a) were thinner (10 mm), but the specimens comprised 100 % bentonite. As a result, the values of $-\Delta P_c$ derived from both methods applied to the RW-1 and RW-2 test data likely were conservatively low, i.e., given the cyclic upward trend in $-\Delta P$ during each two-day time period shown in Figs. 2.23 and 2.24, such that the resulting values of ω calculated on the basis of the values of $-\Delta P_c$ also were likely conservatively low. Values of $-\Delta P$ for a given KCl testing period were determined to be stable when there was no significant upward or downward trend in the discrete values of $-\Delta P_c$ for four consecutive pump cycles. The average value of four consecutive $-\Delta P_c$ values at the end of a given KCl testing period was defined as $-\Delta P_{ss}$. The solid and dashed lines in Figs. 2.23 and 2.24 indicate the value of $-\Delta P_{ss}$ based on the central tendency approach versus the maximum value, respectively, as discussed above.

The expected trend in the measured $-\Delta P$ data for multi-stage membrane testing is shown schematically in Fig. 2.25b, whereby an increase in $-\Delta P$ is expected in response to an increase in $C_{o,t}$ as long as membrane behavior persists (e.g., see Malusis and Shackelford 2002a). This trend is apparent in the results shown in Fig. 2.26. During higher concentration test stages, evidence of post-peak degradation in -ΔP was observed, which also is depicted in Fig. 2.25c (e.g., see Shackleford and Lee 2003). This effect is consistent with that reported by Malusis and Shackelford (2002a), and can be attributed to the progressive compression of the diffuse double layers between clay particles as a result of the increased concentration of solutes in the pore water (Fritz 1986; Malusis and Shackelford 2002a; Shackelford and Lee 2003; Shackelford et al. 2003).

2.3.2.5 Membrane Efficiency Coefficients

Values for the effective chemico-osmotic pressure difference, -ΔP_e, were calculated by subtracting the values of -ΔP_{TW} from the values of -ΔP_{ss} for each KCl testing stage, i.e. -ΔP_e = -ΔP_{ss} - (-ΔP_{TW}), to account for the non-zero pressure difference across the specimen recorded during baseline conditions. The measured values of -ΔP_{TW} for tests RW-1 and RW-2 were -0.3 kPa and 1.5 kPa, respectively. The resulting values of -ΔP_e for RW-1 and RW-2 at each KCl stage are presented in Table 2.10. These values of -ΔP_e were used in Eqs. 2.17 and 2.18 to calculate membrane efficiency coefficients, ω, for each KCl testing stage.

The values of ω for tests RW-1 and RW-2 are presented in Table 2.10 and shown as a function of $C_{o,t}$ in Figs. 2.27 and 2.28. The closeness in values of $\omega_{o,TW}$ and $\omega_{ave,TW}$ for both tests for all values of $C_{o,t}$ likely is due to the circulation of TW across the bottom boundary of the specimens in this study relative to all previous studies, which have been based on circulation of DIW across the bottom boundary of the specimen (Kemper and Rollins 1966; Malusis and Shackelford 2002a; Shackelford and Lee 2003; Yeo et al. 2005; Kang and Shackelford 2010; Mazzieri et al. 2010; Bohnhoff 2012; Dominijanni et al. 2013; Shackelford 2013; Di Emidio et al. 2015; Meier 2014; Tang et al. 2014a; Sample-Lord 2015). The use of TW as the bottom circulation liquid results in values of ΔC_o and ΔC_{ave} that were closer in magnitude relative to the differences in these values based on the use of DIW. In previous studies where DIW was circulated across the bottom boundary (see Eqs. 2.32 through 2.34), values of $\Delta\pi_o$ were always greater than values of $\Delta\pi_{ave}$, such that values of ω_o were always lower (more conservative) than values of ω_{ave}. Additionally, in previous studies, sufficiently flushing the specimens of soluble salts and the inward diffusion of chemical species from the top specimen boundary prior to and during membrane testing, respectively, resulted in $C_{o,b}$ equal to zero and $C_{o,t}$ always greater than C_t, such that $\Delta C_o > \Delta C_{ave}$ and, therefore, $\omega_{ave} > \omega_o$. However, in this study, the outward diffusion of soluble salts from the unflushed specimens during the early concentration stages (i.e., $C_{o,t}$ of 5 mM and 10 mM KCl) resulted in $\Sigma C_t > C_{o,t}$, such that $\Delta C_{ave} > \Delta C_o$ and, therefore, $\omega_o > \omega_{ave}$. For the higher concentration stages (i.e., $C_{o,t}$ of 20 mM to 80 mM KCl), the concentrations of soluble salts in the specimens had decreased due to outward diffusion, such that $\Delta C_o > \Delta C_{ave}$ and, therefore, $\omega_{ave} < \omega_o$, which is consistent with trends for ω_o and ω_{ave} previously reported in the literature (e.g., Shackelford 2013).

2.3.3 Diffusion

2.3.3.1 Boundary Outflow Concentrations

The measured concentrations of anions (Br^-, Cl^-, and SO_4^{2-}) and cations (Ca^{2+}, K^+, Na^+ and Mg^{2+}) in the circulation outflow collected from the specimen boundaries, C_t and C_b, for test RW-1 shown in Figs. 2.17 and 2.18 are a function of indigenous chemical species initially present in the pore water of the specimen and the chemical species associated with the KCl solution and tap water introduced into the system at the specimen boundaries. The predominant chemical species in the circulation outflow at the top of the specimen, $C_{t,i}$, were Cl^- and K^+, and the concentrations for these two chemical species remained relatively constant for each testing stage. However, the concentrations of the predominant chemical species in the circulation outflow at the bottom of the specimen, $C_{b,i}$, changed with each stage of a test corresponding to sequential increases in the source KCl concentration (i.e., C_{ot}) introduced as the circulation inflow at the top of the specimen. Due to the variety of chemical species in the system, the change in concentration of a given species relative to the concentration of the same chemical species in the circulation inflow solution (KCl or tap water) at the specimen boundaries, $C_{ot,i}$ and $C_{ob,i}$, was calculated for each boundary, $\Delta C_{t,i}$ and $\Delta C_{b,i}$, as follows:

$$\Delta C_{t,i} = C_{t,i} - C_{ot,i} \ ; \quad \Delta C_{b,i} = C_{b,i} - C_{ob,i} \tag{2.35}$$

Positive values of $\Delta C_{t,i}$ and $\Delta C_{t,i}$ (> 0) indicate outward diffusion of a chemical species at the specimen boundaries, whereas negative values of $\Delta C_{t,i}$ and $\Delta C_{t,i}$ (< 0) indicate inward diffusion of a chemical species at the specimen boundaries. Values of $\Delta C_{t,i}$ and $\Delta C_{b,i}$ versus time for select cation species and schematics of the test specimens indicating the relative direction of diffusion for the predominant chemical species at early and late testing stages (i.e., lower and higher values of C_{ot}) are presented in Fig. 2.29.

During the initial stage of the test (i.e., C_{ot} = 5 mM KCl), positive values of $\Delta C_{b,i}$ were calculated for the predominant anion and cation species at the bottom specimen boundary, Br^- and Na^+, respectively. Initially, the predominant anion at the bottom boundary was Br^- due, in part, to the continuous circulation of tap water which contained Br^- derived from the inclusion of the biocide. However, during the 40 mM and 80 mM KCl stages, the imposed KCl concentration gradient across the specimen was sufficiently high such that the increased diffusive flux of Cl^- resulted in Cl^- becoming the predominant anion at the bottom specimen boundary.

The magnitude of $\Delta C_{b,i}$ for Na^+ decreased during later stages (10 mM through 80 mM KCl) as the ion, which initially dominated the exchanges sites of the bentonite particles, was replaced via cation exchange with other cations in the pore water, most notably K^+, but also Ca^{2+} and Mg^{2+}. By the end of the 10 mM KCl stage, K^+ was the predominant cation exiting the bottom specimen boundary and remained the predominant cation throughout all subsequent testing stages. Additionally, negative values of $\Delta C_{b,i}$ were calculated for Na^+ by the end of the 20 mM KCl stage, and $\Delta C_{b,i}$ for Na^+ remained essentially negative for the subsequent testing stages, which indicates the direction of diffusion for Na^+ switched from outward to inward at the bottom specimen boundary at later stages. The values of $\Delta C_{b,i}$ for Ca^{2+} and Mg^{2+} also were negative for all testing stages, whereas values of $\Delta C_{t,i}$ were increasingly positive for the same cations, indicating inward diffusion of these two cations at the bottom boundary and outward diffusion at the top boundary.

2.3.3.2 Diffusive Mass Flux

Steady-state diffusion of Cl^- and K^+ was evaluated for specimen RW-1 for all testing stages in accordance with the procedure described in Section 2.2.5.2. The accumulated solute masses per unit area, Q_t, versus time for both Cl^- and K^+ are shown in Fig. 2.30. Low, background concentrations of Cl^- and K^+ (0.11 mM and 0.02 mM, respectively) were measured in the source solution (i.e., tap water) circulated continuously across the bottom boundary. Therefore, these background concentrations of Cl^- and K^+ in the tap water were subtracted from measured values of C_b prior to calculating the solute mass flux through the specimen. Failure to correct values of C_b by subtracting the baseline tap water solute concentrations would result in conservatively higher values of Q_t. The resulting values of Q_t for K^+ were slightly negative (< 0) for the first 12 days of the 5 mM KCl stage, which was due to K^+ briefly diffusing into the specimen from the bottom specimen boundary. Since the primary objective of the analysis was to quantify the diffusion of K^+ in the positive x-direction (i.e., through the specimen), the negative values of Q_t were corrected to zero. In addition, these negative values of Q_t for K^+ essentially occurred during the transient (nonlinear) portion of the data, such that the impact of these negative values on the subsequent, steady-state (linear) portion of the data, which was used to determine the D^* values reported in this study, was nil.

Due to the nature of multi-stage testing, greater diffusive mass flux of Cl^- and K^+ occurred as a result of a greater ΔC for KCl imposed across the specimen. Therefore, the magnitude of Q_t/t increased with increasing source KCl concentration, C_{ot}. The separation of Q_t and t values into net values, Q_t' and t', based on the duration of each testing stage respectively, was calculated in order to evaluate values of D^* for each concentration stage as follows (e.g. Bohnhoff and Shackelford 2015):

$$Q_t' = Q_{t,x+1} - Q_{t,x} \tag{2.36}$$

$$t' = t_{x+1} - t_x \tag{2.37}$$

where $Q_{t,x}$ and $Q_{t,x+1}$ represent the final value of Q_t from the previous stage and the value of Q_t at any given time during the current stage, respectively. Additionally, t_x and t_{x+1} represent the total elapsed time at the end of the previous stage and the elapsed time for the current stage, respectively. Essentially, the use of Q_t' and t' reset each consecutive stage to zero in terms of accumulated solute flux and time. The resulting plots of Q_t' versus t' are presented in Fig. 2.31, and values of D^* calculated based on the linear regression of the steady-state portion of the Q_t' versus t' data are presented in Table 2.11. The method of reverse fitting of values of r^2, propagated from a linear fit applied to Q_t' versus t' data, as described by Shackelford and Lee (2003), was used for steady-state determination, such that the onset of steady-state mass flux corresponds to the last data point where $r^2 \geq 0.999$ for the data set. Plots of r^2 versus number of data points for Cl^- and K^+ for test RW-1 are provided in Appendix A for each testing stage.

Values of Q_t' reached steady state more rapidly for Cl^- compared to K^+, primarily due to the exchange of K^+ for residual soluble salts (e.g., Ca^{2+}, Mg^{2+}, and Na^+) on the exchange sites and the requirement for electroneutrality in the pore water of the specimen (Bohnhoff and Shackelford 2015). However, the steady-state values of Q_t' for K^+ were greater than those for Cl^- for all testing stages, which is opposite relative to the magnitudes of Q_t' for Cl^- and K^+ reported in previous studies (e.g., Malusis and Shackelford 2002b; Bohnhoff and Shackelford 2015). Additionally, the steady-state slope of Q_t'-versus-t' data (i.e., $\Delta Q_t'/\Delta t'$) increased with increasing concentrations for both Cl^- and K^+. However, the magnitude of $\Delta Q_t'/\Delta t'$ for K^+ was greater than that for Cl^-. Lower magnitudes of $\Delta Q_t'/\Delta t'$ (i.e., shallower slopes) indicate a lower solute mass flux, likely due to the interference or exchange of Cl^- and K^+ with additional solutes in the system (e.g., Br-, Ca^{2+}, Mg^{2+}, Na^+, etc.) and the imposed ΔC across the specimen.

Values of D^* were calculated for Cl^- and K^+ via Eq. 2.21 based on values of ΔC_o and ΔC_{ave} for each testing stage, where:

$$\Delta C_{o,Cl^-} = C_{ob,Cl^-} - C_{ot,Cl^-} \ ; \ \Delta C_{o,K^+} = C_{ob,K^+} - C_{ot,Cl^-} \tag{2.38}$$

$$\Delta C_{ave,Cl^-} = \left(\frac{C_{ob,Cl^-} + C_{b,Cl^-}}{2} \right) - \left(\frac{C_{ot,Cl^-} + C_{t,Cl^-}}{2} \right); \ \Delta C_{ave,K^+} = \left(\frac{C_{ob,K^+} + C_{b,K^+}}{2} \right) - \left(\frac{C_{ot,\mathrm{Cl}^-} + C_{t,K^+}}{2} \right) \tag{2.39}$$

where $\Delta C_{o,Cl^-}$ and $\Delta C_{o,K^+}$ represent the difference in the source solute concentrations for Cl^- and K^+, respectively, at the specimen boundaries, and $\Delta C_{ave,Cl^-}$ and $\Delta C_{ave,K^+}$ represent the difference in the average solute concentrations for Cl^- and K^+, respectively, at the specimen boundaries at steady state. Note that the value of C_{ot,K^+} in Eq. 2.39 is replaced with C_{ot,Cl^-} on the assumption of stoichiometric balance between Cl^- and K^+ for source KCl solutions. The resulting values of D^*, designated as D^*_o and D^*_{ave}, are presented as a function of C_{ot} and ω in Fig. 2.32 and 2.33, respectively.

Typically, at a given C_{ot}, values of D^* for Cl^-, $D^*_{Cl^-}$, are greater than values of D^* for K^+, $D^*_{K^+}$. However, in this study, steady-state values of $D^*_{K^+}$ were higher than $D^*_{Cl^-}$. This seeming anomaly is likely due to Br^- contributing to a portion of the available negative charge based on the requirement for electroneutrality in the system, such that a lesser portion of Cl^- was required for electroneutrality during diffusion. The difference between $D^*_{Cl^-}$ and $D^*_{K^+}$ decreased with increasing values of C_{ot}, such that values of $D^*_{\mathrm{K}^+}$ increased from stages 5 mM to 10 mM KCl, as expected. However, values of $D^*_{\mathrm{K}^+}$ decreased from stages 10 mM through 80 mM KCl. The decrease in $D^*_{\mathrm{K}^+}$ with increasing values of C_{ot} (and decreasing values of ω) is likely due to the counter-diffusion of Ca^{2+}, Mg^{2+}, and Na^+ ions into the specimen from the bottom specimen boundary, shown in Fig. 2.29, which contributed a portion of the positive charge required for electroneutrality of the specimen pore fluid. Therefore, K^+ likely contributed a lesser portion of the positive charge required for electroneutrality during diffusion, such that $D^*_{\mathrm{K}^+}$ decreased with time (e.g., continued counter-diffusion of Ca^{2+}, Mg^{2+}, and Na^+).

Values of D^*_{o,Cl^-} are close to values of D^*_{ave,Cl^-} for early stages (i.e., 5 mM through 20 mM KCl), when the diffusive mass flux of Cl^- is reduced due to Br^-. However, as C_{ot} increased, the diffusive mass flux of Cl^- increased and the magnitude of ΔC_{ave} decreased relative to the magnitude of ΔC_o, such that $D^*_{ave,Cl^-} > D^*_{o,Cl^-}$. Additionally, since $\Delta C_{ave} < \Delta C_o$, values of D^*_{o,K^+} are consistently lower than values of D^*_{ave,K^+} for all stages.

2.3.3.3 Tortuosity Factors

In accordance with Eq. 2.22 (i.e., $\tau_a = D^*/D_o$), the apparent tortuosity factor, τ_a, represents the rate of solute diffusion through the porous medium relative to the rate of solute diffusion in the absence of the porous medium. Higher values of τ_a represent a less tortuous pathway for solute migration and, therefore, a greater rate of solute diffusion. Accordingly, values for τ_a were calculated in accordance with Eq. 2.22 based on diffusion of the nonreactive (i.e., nonadsorbing) tracer, Cl^-, and the value for D_o of KCl, i.e., 19.93 x 10^{-10} m^2/s, as described by Bohnhoff and Shackelford (2015). The resulting values for both $\tau_{a,o}$ and $\tau_{a,ave}$ based on the measured values of D^*_o and D^*_{ave}, respectively, are shown in Table 2.11. As indicated in Table 2.11, values of $\tau_{a,o}$ and $\tau_{a,ave}$ increased from 0.032 to 0.21 and from 0.033 to 0.130, respectively, as C_{ot} increased from 5 mM to 80 mM KCl. The increase in $\tau_{a,o}$ and $\tau_{a,ave}$ is due to the increase in D^*_o and D^*_{ave} with increasing C_{ot}, which has been attributed to the decrease in ω with increasing C_{ot} (Shackelford and Malusis 2002b; Shackelford 2014).

The apparent tortuosity factor also can be defined as the product of the matrix tortuosity factor, τ_m, and the restrictive tortuosity factor, τ_r, i.e., $\tau_a = \tau_m\tau_r$ (Shackelford and Malusis 2002b; Shackelford and Moore 2013; Shackelford 2014). The matrix tortuosity factor represents a reduction in the diffusive mass flux exclusively due to the geometry of the interconnected pores in the absence of membrane behavior (i.e., $\omega = 0$) , whereas τ_r represents any other factors (aside from pore geometry) contributing to a further reduction in the diffusive mass flux (e.g., further reduction in τ_a), such as increased viscosity near clay surfaces and anion exclusion due to membrane behavior (Shackelford and Daniel 1991; Malusis and Shackelford 2002b; Shackelford and Moore 2013). The value of τ_m is based on the ratio of the limiting value of D^* at $\omega = 0$, known as the pore diffusion coefficient D_p, relative to the value of D_o, and is considered to be unique for a given porous medium provided the specimen volume remains constant (Shackelford and Moore 2013). Values of $D_{p,o}$ and $D_{p,ave}$ corresponding to values of D^*_o and D^*_{ave}, respectively, were determined through linear extrapolation of D^* versus ω data for Cl^- as shown in Fig. 2.33a. The resulting values of $D_{p,o}$ and $D_{p,ave}$ for Cl^- were 3.4 x 10^{-10} m^2/s and 3.5 x 10^{-10} m^2/s, respectively. The linear extrapolation and, therefore, the estimated values of $D_{p,o}$ and $D_{p,ave}$, are affected, in part, by the suppression of Cl^- diffusion in earlier stages of the test (RW-1) due to the complex chemical boundary conditions, specifically the presence of Br^- derived from the inclusion of the biocide in the boundary circulation liquids. The estimated values of $D_{p,o}$ and $D_{p,ave}$ for Cl^- are considered to be conservatively high, because the extrapolated line follows the slope, $\Delta D^*/\Delta\omega$, between stages 40 mM to 80 mM KCl, which is approximately three times greater than the slope observed between previous solute stages (e.g., 20 versus 7). The increase in D^* from 40 mM to 80 mM KCl corresponds to the data presented in Fig. 2.17, where values of C_{b,Cl^-} increased to be greater than those of C_{b,Br^-}, due to the relatively high imposed KCl concentration gradient across the specimen, such that the increased diffusive flux of Cl^- resulted in Cl^- becoming the predominant anion at the bottom specimen boundary (see Fig. 2.18a).

In an effort to understand further the extent to which membrane behavior affects τ_r, values of $\tau_{r,o}$ and $\tau_{r,ave}$ were plotted as a function of values of ω_o and ω_{ave}, respectively, in Fig. 2.34. Values of $\tau_{r,o}$ and $\tau_{r,ave}$ increased (i.e., solute pathway became less restrictive) from 0.190 to 0.712 and 0.189 to 0.743, respectively, as ω_o and ω_{ave} decreased from 0.423 to 0.064 and 0.448 to 0.075, respectively, corresponding to an increase in C_{ot} from 5 mM to 80 mM KCl. The Cl^- data were fit to a nonlinear function (τ_r = -[(1-(ω-1)^2]$^{1/2}$ + 1) as opposed to the linear function (τ_r = 1 - ω) proposed by Manassero and Dominijanni (2003) based on results for GCL specimens. The applied function for τ_r intersects zero and one when ω is one and zero, respectively, because at ω = 0, sufficient compression of the DDLs likely occurred resulting in negligible ion exclusion and viscosity effects, such that the reducing contribution of τ_r to τ_a is negligible (i.e., τ_r = 1) and τ_m becomes equal to τ_a. Additionally, at ω = 1, solute diffusion is prohibited such that τ_r and, therefore τ_a, is zero. However, in contrast to the relationship τ_r = 1 - ω, which is supported by theory (Manassero and Dominijanni 2003; Dominijanni and Manassero 2012; Dominijanni et al. 2013), there is no fundamental theoretical basis for this applied nonlinear function for τ_r, which is empirical. In fact, measured values of τ_r lower than those based on the relationship τ_r = 1 – ω are directly attributable to the low measured values of D^* for Cl^- which, as previously noted, were due to the suppression of Cl^- diffusion resulting from the contribution of other ions to the electroneutrality constraint during diffusion within the pores of the bentonite at the lower stages of the test (i.e., for $C_{ot} \leq 40$ mM KCl).

2.3.3.4 Predicting Effective Diffusion Coefficients for Reactive Solutes

Values of D^* for a reactive solute (e.g., K^+ in this study) are often calculated for a given soil as the product of τ_a (= $\tau_m\tau_r$), based on the nonreactive solute (e.g., Cl^- in this study), and the free-solution diffusion coefficient of the reactive solute at infinite dilutions, D_o (Quigley et al. 1987). By analogy, values of D^*_o and D^*_{ave} for K^+ can be predicted based on τ_m (= D_p/D_o) for Cl^- and τ_r correlation (i.e., τ_r = 1 - ω) proposed by Manassero and Dominijanni (2003) in accordance with the following equation:

$$D^*_{K^+} = D_{o,K^+}\tau_{a,Cl^-} = D_{o,K^+}\left(\tau_m\tau_r\right)_{Cl^-} = D_{o,K^+}\tau_{m,Cl^-}(1-\omega) \tag{2.40}$$

where $D_{o,K}{}^+$ is the free solution diffusion coefficient for K^+ at infinite dilution, i.e., 19.96 x 10^{-10} m^2/s (Shackelford and Daniel 1991).

The resulting predicted values of D^*_o and D^*_{ave} for K^+ based on Eq. 2.40 are compared to the respective measured values in Fig. 2.35. As shown, the trend in the predicted values of D^*_o and D^*_{ave} for K^+ is not similar to that for the measured values of D^*_o and D^*_{ave} for K^+. The difference in these two trends can be attributed, in part, to the lack of compliance in measured τ_r values for Cl^- with the proposed model (i.e., $\tau_r = 1 - \omega$), which as previously described was attributed to the suppression of Cl^- diffusion in early stages (i.e., $C_{ot} \leq 40$ mM KCl) due to the complex pore water chemistry. Additionally, the continuous circulation of tap water at the bottom specimen boundary introduced additional ionic species into the system (e.g., Br^-, SO_4^{2-}, Ca^{2+}, Mg^{2+}, Na^+) which contributed to the measurement of lower values of D^*_o and D^*_{ave} for K^+ specifically at the lower values of ω and higher values of C_{ot} (i.e., $C_{ot} \geq 10$ mM KCl). In contrast, the predicted values of D^*_o and D^*_{ave} for K^+ increase systematically with decreasing values of ω and increasing C_{ot}.

Shackelford et al. (2016) also reported values of τ_r that did not comply with the linear function, i.e., $\tau_r = 1 - \omega$. For comparison, the values of $\tau_{r,o}$ and $\tau_{r,ave}$ reported by Shackelford et al. (2016) were plotted together with the results of this study in Fig. 2.36. As indicated, the results from Shackelford et al. (2016) are in good agreement with those of this study.

Shackelford et al. (2016) attributed the lower than predicted values of $\tau_{r,o}$ and $\tau_{r,ave}$ to the possibility that changes in τ_a could be attributed to the changes in τ_m instead of changes in τ_r for the relatively high source (C_{ot}) KCl concentrations used in their study of 100, 200, and 400 mM. The close agreement between the values of $\tau_{r,o}$ and $\tau_{r,ave}$ measured in this study versus those reported by Shackelford et al. (2016) shown in Fig. 2.36 do not appear to support this explanation, because the limiting values of $\tau_{r,o}$ and $\tau_{r,ave}$ measured in this study were obtained using a source KCl concentration of only 80 mM. However, the sand-bentonite specimen evaluated in this study contained only 15 % bentonite, whereas the specimen tested by Shackelford et al. (2016) was a GCL with 100 % bentonite (i.e., excluding the slight masses attributed to the geosynthetic components of the GCL). Thus, the similar trends in values of $\tau_{r,o}$ and $\tau_{r,ave}$ reported in this study relative to those reported in the study by Shackelford et al. (2016), despite the use of lower KCl concentrations in this study, may be attributable to the lower chemical resistance of the sand-bentonite specimen evaluated in this study due to the significantly lower bentonite content (i.e., 15 % vs. 100 %).

Another possible explanation describing the different trends in the values of $\tau_{r,o}$ and $\tau_{r,ave}$ shown in Fig. 2.36 is the difference in the chemistries of the pore waters of the various specimens. For example, previous results reported by Malusis et al. (2014) based on diffusion of KCl through a GCL specimen were shown to be in general agreement with the relationship $\tau_r = 1 - \omega$. However, DIW was used as the circulating water during the test, and the GCL was flushed (leached) of soluble salts prior to testing via prolonged permeation with DIW at a relatively high hydraulic gradient, such that the pore water chemistry within the bentonite of the GCL likely was relatively dilute. In contrast, neither the GCL specimen tested by Shackelford et al. (2016), nor the compacted sand-bentonite specimen evaluated in this study was flushed of soluble salts prior to diffusion testing. Thus, the pore water chemistry in both of the latter specimens likely was far more complex than that for the specimen evaluated by Malusis et al. (2014). As previously noted, the complex chemical conditions imposed in the present study likely resulted in lower measured D^* values for Cl^-, resulting in lower values of τ_r. The consistent trends in in the values of $\tau_{r,o}$ and $\tau_{r,ave}$

shown in Fig. 2.36 between these two studies suggest that similar conditions may have existed in the test conducted by Shackelford et al. (2016), such that the reason for the lower values of in the values of $\tau_{r,o}$ and $\tau_{r,ave}$ determined in both studies relative to the theoretical relationship given by $\tau_r = 1 - \omega$ may be the relative lack of control on the pore-water and boundary chemistry associated with the unflushed specimens.

2.4 Comparison of Tests RW-1 and RW-2

The initial conditions for specimens RW-1 and RW-2 were in good agreement with one another, as shown in Table 2.7 and 2.12. The *EC* values of the outflow collected at the end of the saturation stage for tests RW-1 and RW-2 were 381 and 172 mS/m respectively. The lower value of *EC* for test RW-2 versus RW-1 measured at the end of saturation suggested that the soluble salts in the pore water of specimen RW-2 were lower (more flushed) than in specimen RW-1. However, the *EC* values of the outflow collected at the end of the baseline circulation stage for test RW-1 and RW-2 were 22 and 28 mS/m, respectively. Additionally, the concentration of Na^+ in the outflow collected at the end of the baseline circulation stage was higher for test RW-2 compared to RW-1 (i.e., 2.0 versus 1.2 mM). Higher values of C_t and C_b for Na^+ were also measured in early stages of test RW-2 compared to test RW-1 (e.g., C_{t,Na^+} = 3.2 mM versus 1.9 mM for test RW-2 versus RW-1 for C_{ot} of 5 mM KCl), see Figs. 2.17a and 2.19a. Therefore, the value of *EC* of the effluent collected from test RW-2 following specimen saturation is likely not representative of the conditions of the pore fluid. The unlikely low measured value of *EC* for the effluent collected from test RW-2 at the end of saturation has been attributed, in part, to the periodic removal of air bubbles by flushing tap water across the top specimen boundary during the saturation stage.

Additionally, the effect of the KCl stage duration on final values of ω was compared for tests RW-1 and RW-2. Values of $-\Delta P$ for test RW-1 corresponding to the shorter KCl stage duration of test RW-2 for a given KCl stage were used to calculate alternate values of ω. Values of $-\Delta P$ for RW-1 based on the shorter duration were, on average, 90 % of the final value of $-\Delta P_{ss}$. This resulted in values of ω that were, on average, 10% lower than the final values of ω for test RW-1 (e.g., for C_{ot} of 10 mM KCl, $\omega_o = 0.24$ versus 0.26). Despite the slight increase in values of ω when KCl stages were continued for longer durations, shorter test durations are considered conservative for calculating values of ω so long as values of $-\Delta P$ and EC_b are steady and there isn't significant post-peak degradation (primarily observed at higher values of C_{ot}).

Overall, the values of ω were slightly lower for test RW-2 compared to test RW-1. Lower values of ω for test RW-2 are explained by the higher initial concentration of residual soluble salts in specimen RW-2 compared to specimen RW-1 at the start of KCl circulation. Additionally, with increasing C_{ot}, values of C_t and C_b for major species (i.e., Br^-, Cl^-, SO_4^{2-}, Ca^{2+}, K^+, Mg^{2+}, Na^+) for test RW-2 became closer to values of C_t and C_b for test RW-1, respectively. Ultimately, following the 5 mM KCl stage, the difference between values of ω for tests RW-1 and RW-2 was low (i.e., ≤ 0.025).

2.5 Comparisons of Membrane Behavior for Different Bentonite-Based Liners

2.5.1 Compacted Sand-Bentonite Mixtures

Barbour and Fredlund (1989) performed membrane testing on two sand-bentonite specimens comprising 20 % bentonite and 80 % Ottawa sand consolidated at 200 kPa with a value of n for both specimens of approximately 0.44. The resulting values of ω reported by Barbour and Fredlund (1989) were measured based on osmotic consolidation (open system) testing, and ranged from 0.00065 to 0.40 for solutions containing NaCl at concentrations of 4 M and 8 mM, respectively. As shown in Fig. 2.37, these values of ω are similar to those reported in this study within the same range of values of C_{ot} and $C_{o,ave}$ (= $C_{ot}/2$). Although values of ω have been shown to generally increase with decreasing values of n, as expected, values of ω also have been shown to generally increase with increasing *BC* (Shackelford 2013) Therefore, the higher *BC* of specimens tested by Barbour and Fredlund (1989) likely contributed, in part, to the similar values of ω despite lower values of n relative to the specimens tested in this study (i.e., 0.44 versus 0.34).

Additionally, Saindon and Whitworth (2005) tested compacted sand-bentonite specimens comprising from 12 % to 100 % bentonite mixed with simulated fine-grained sand (i.e., glass beads with d = 0.20 mm). However, the results from this study have not been included in Fig. 2.37 for several reasons. First, despite the use of an extremely dilute, 1 mM NaCl solution for measurement of ω (referred to as a reflection coefficient, σ), the values of ω reported by Saindon and Whitworth (2005) were relatively low, ranging from 0.03 to 0.04 for specimens containing from 12 % to 50 % bentonite, respectively. One reason for difference in the values of ω reported by Saindon and Whitworth (2005) versus those reported in this study may be the method of measurement, as Saindon and Whitworth (2005) used an open-system testing method (hyperfiltration) versus the closed-system testing method used in this study.

Also, the compaction energy applied to the specimens tested by Saindon and Whitworth (2005) was 60 % of that applied to the specimens compacted for this study (i.e., 345 kN-m/m^3 versus 587 kN-m/m^3). Tang et al. (2014b) reported that a 20 % reduction in compaction energy resulted in a 30 % decrease in membrane behavior for specimens tested under similar conditions for low values of C_{ot} ($\leq$ 50 mM KCl). Therefore, the low values of ω reported by Saindon and Whitworth (2005) also can be attributed to the lower compaction energy applied to their specimens compared to the compaction energy applied to specimens tested in this study.

2.5.2 Geosynthetic Clay Liners (GCLs)

Values of ω_o and ω_{ave} reported in the literature for GCLs (Malusis and Shackelford 2002a; Kang and Shackelford 2011; Meier et al. 2014) are compared to the values of ω_o and ω_{ave} measured in this study for compacted sand-bentonite specimens in Figs. 2.38a and 2.39a, respectively. As indicated in these figures, the values of ω_o and ω_{ave} for the specimens tested in this study are generally within the range of values previously reported for GCLs when exposed to KCl solutions with varying concentrations. However, values of ω for some of the GCL specimens are lower than those for the specimens tested in this study for the same value of C_{ot} or $C_{o,ave}$. The differences in measured values of ω can be attributed, in part, to differences in specimen *BC*, porosity, and early-stage boundary conditions. For example, as previously noted, specimens comprising greater percentages of bentonite, such as GCLs, typically exhibit greater membrane behavior, i.e., higher values of ω (Shackelford 2012, 2013; Shackelford and Moore 2013). Therefore, a possible explanation for the higher values of ω for compacted sand-bentonite specimens evaluated in this study relative to those measured for some GCL specimens is the higher porosity of GCLs (e.g., n = 0.80 versus 0.34).

Additionally, the salt concentration that the specimen is exposed to in the early stages of membrane testing may have influenced the sustainability of observed membrane behavior. This effect is analogous to the first exposure or prehydration effect that has been studied extensively with respect to bentonite based specimens, whereby the final hydraulic conductivity of a specimen at steady state, k_f, has been shown to be affected by whether or not the specimen was prehydrated via exposure to water prior to being permeated with chemical solutions, with prehydrated specimens generally resulting in lower values of k_f relative to non-prehydrated specimens (e.g., Creek and Shackelford 1992; Lo et al. 1994; Shackelford 1994; Lee and Shackelford 2005). For example, Shackelford (1994) showed results indicating that the value of k_f for a compacted sand-bentonite mixture comprising 16 % bentonite permeated directly with a saturated $CaCl_2$ solution was 135 times greater than the value of k_f for an identical specimen that was first prehydrated by permeation with water prior to being permeated with same $CaCl_2$ solution, i.e., 2.3×10^{-7} m/s vs. 1.7×10^{-9} m/s (see also Lee and Shackelford 2005).

If this prehydration or first exposure effect is extended to the measurement of membrane behavior, then the lower the initial salt concentration, the greater the amount of initial swelling associated with the bentonite portion of the specimen, and the higher the salt concentrations required to effectively destroy any observed membrane behavior. For example, the values for ω_o in this study of 0.16 and 0.14 for RW-1 and RW-2, respectively, based on circulation of a 20 mM KCl solution (= C_{ot}) are approximately 1.6 times greater than the value for ω_o of 0.096 reported by Meier et al. (2014) for a GCL specimen subjected to the same salt solution (i.e., C_{ot} = 20 mM KCl) following exposure to only a 5 mM KCl solution. Although this difference in ω values may be considered relatively minor compared to the aforementioned difference in k_f values based on the study by Shackelford (2014), values of k for bentonite based specimens exposed to chemical solutions can range over several orders of magnitude (e.g., Shackelford 1994; Shackelford et al. 2000), whereas values of ω are restricted to a much narrower range (i.e., $0 \leq \omega \leq 1$).

2.5.3 Compacted Clay Liners (CCLs)

Values of ω_o and ω_{ave} reported in the literature for bentonite amended CCLs (Kang and Shackelford 2010; Tang et al. 2014a) are compared to values of ω_o and ω_{ave} measured in this study for compacted sand-bentonite specimens in Figs. 2.38b and 2.39b, respectively. The values of ω_o and ω_{ave} for the specimens tested in this study are within the range of values previously reported for bentonite amended CCLs when exposed to KCl solutions of varying concentrations. However, as previously noted, differences in measured membrane behavior can be attributed, in part, to differences in specimen porosity and *BC*. Therefore, variations in the specimen porosity likely contribute to differences in measured values of ω (e.g., for C_{ot} = 10 mM KCl and 15% *BC*, ω_o of 0.21 versus 0.26 for n = 0.47 and 0.34, respectively). Additionally, the bentonite amended CCL tested by Kang and Shackelford (2010) comprising 5 % Na-bentonite was highly sensitive to increasing salt concentrations (e.g., ω_o = 0.03 for C_{ot} = 20 mM KCl compared to ω_o = 0.76 for C_{ot} = 3.9 mM KCl). In comparison, the bentonite amended CCL specimens tested by Tang et al. (2014a) comprising a range of *BC*s (i.e., 5 % to 20 %) did not exhibit the same sensitivity. However, some values of ω_{ave} reported by Tang et al. (2014a) were greater than unity (see Fig. 2.39b), which is fundamentally impossible.

2.5.4 Compacted Natural Bentonites

Values of ω_o and ω_{ave} reported in the literature for compacted bentonite specimens (Kemper and Rollins 1966; Kemper and Quirk 1972; Dominijanni et al. 2013; Di Emidio et al. 2015) are compared to the values of ω_o and ω_{ave} measured in this study for compacted sand-bentonite specimens in Figs. 2.38c and 2.39c. The values of ω_o and ω_{ave} for the specimens tested in this study are within the range of values previously reported for compacted natural Na-bentonite specimens when exposed to salt solutions of varying molar concentrations. However, differences in measured membrane behavior can be attributed, in part, to differences in bentonite preparation, porosity, and boundary salt solutions. Unlike in this study, the bentonite in previous studies was saturated with Na^+ ions in an effort to remove excess salts from the clay surfaces (i.e., homo-ionized) prior to testing. Additionally, values of n for the compacted bentonite specimens ranged from 0.72 to 0.91

compared to the *n* of 0.34 for specimens evaluated in this study. Furthermore, Malusis and Shackelford (2002a) showed that values of ω increase for specimens exposed to solutions comprising solutes with larger hydrated radii for the same average salt concentration and similar values of *n*, because ions with larger hydrated radii are more restricted from transport through specimens with similar pore sizes (MacKay 1946). The relative size of the hydrated radii is provided by the well-known lyotropic series for monovalent ions as $Na^+ > K^+ > Cs^+$. Therefore, the use of NaCl rather than KCl or CsCl is expected to result in higher values of ω, which is apparent in Fig. 2.30c for specimens with similar values of *n*. Additionally, a specimen with an *n* of 0.91 and exposed to NaCl by Kemper and Quirk (1972) exhibited lower values of ω relative to a specimen exposed to the same molar concentration of CsCl with an *n* of 0.84. Therefore, as expected, higher values of *n* may compensate for the effect the hydrated radii size due to the overall higher volume of pores.

Additionally, the use of salt solutions comprising multivalent cations, such as $CaCl_2$, has been shown to reduce membrane behavior due to the higher charge density of the multivalent cation solutions compared to monovalent cation solutions of the same molar concentration (Kemper and Rollins 1966). Therefore, the relatively low values of ω for low values of C_{ot} and $C_{o,ave}$ (≤ 5 mM $CaCl_2$) reported by Di Emidio et al. (2015) are likely due to diffusion of Ca^{2+} ions and the concomitant increase in pore sizes due to compression of DDLs (e.g., see Shackelford and Lee 2003).

Note that the results of Keijzer et al. (1999) and Keijzer and Loch (2001) were not included in Figs. 2.38c and 2.39c due to the low values of ω (≤ 0.003) reported in these studies. Shackelford and Lee (2003) indicated that measurement of ω in systems with open boundary conditions that allow boundary solute concentrations to equilibrate over time may have an impact on the measured values of ω, since such that the potential osmotic pressure difference across the specimen, $\Delta\pi$, will approach zero over time.

2.5.5 Compacted Polymerized Bentonites

Values of ω_o and ω_{ave} reported for specimens comprising polymerized bentonites (Bohnhoff and Shackelford 2013; Di Emidio et al. 2015) are compared to those for the compacted sand-bentonite specimens tested in this study in Figs. 2.38d and 2.39d, respectively. Values of ω_o and ω_{ave} for the specimens tested in this study are within the same range of values previously reported for polymerized bentonite specimens when exposed to salt solutions of varying molar concentrations. However, differences in measured membrane behavior can be attributed, in part, to differences in the bentonite properties and boundary salt species. Additionally, the bentonite-polymer composite (BPC), also referred to as bentonite-polymer nanocomposite (BPN), specimens tested in rigid-wall cells by Bohnhoff and Shackelford (2013) exhibited values of ω_o and ω_{ave} approximately 2.5 times greater than values for the sand-bentonite specimens for similar KCl concentrations. Bohnhoff and Shackelford (2013) reported that their BPC specimens exhibited greater membrane behavior compared to GCLs under similar testing conditions due to greater swell and clogging of interconnected pores from excess polymer present in the BPC specimens (Bohnhoff and Shackelford 2013). Also, as previously noted, the lower values of ω reported by Di Emidio et al. (2015) compared to those reported by Bohnhoff and Shackelford (2013) and those measured in this study are likely due to the use of $CaCl_2$ and the resulting compression of DDLs due to diffusion of Ca^{2+} ions into the specimen.

2.5.6 *Summary of Comparisons with Bentonite-Based Barriers*

Overall, values of ω_o and ω_{ave} for compacted sand-bentonite specimens comprising 15 % bentonite tested in this study are in good agreement with values reported in the literature for other bentonite-based engineered barriers based on similar testing conditions. Furthermore, values of ω_o and ω_{ave} measured in this study were in the same range as specimens comprising up to 100 % bentonite. Therefore, the bentonite in the specimens tested in this study can be considered to have dominated the void spaces, such that values of ω are comparable to 100 % bentonite specimens. Additionally, the relative size of the pores has been proven to affect membrane behavior (Shackelford 2013) Therefore, the relatively low porosity of the specimens tested in this study (i.e., n = 0.34) likely also contributed to the magnitude of ω values. Additional membrane testing is recommended to determine the sustainability of membrane behavior at higher salt concentrations (i.e., C_{ot} > 80 mM KCl) for compacted sand-bentonite specimens comprising 15 % bentonite as well as to determine the overall membrane behavior of compacted sand-bentonite mixtures with variable *BC*s and different types of bentonite, such as polymer modified bentonites.

2.6 Comparisons of Diffusion Behaviors for Different Bentonite-Based Barriers

2.6.1 *Compacted Sand-Bentonite Mixtures*

Gillham et al. (1984) and Cotton et al. (1998) performed diffusion testing on compacted sand-bentonite and compacted sand-attapulgite specimens, respectively, and the resulting values of D^* are compared to those measured for Cl^- in this study in Fig. 2.40. Gillham et al. (1984) performed diffusion testing on bentonite specimens comprising 5 % to 50 % Na-bentonite with both nonreactive (i.e., tritium (HTO), Cl^-) and reactive (i.e., ^{85}Sr) ion species. As expected, values of D^* for HTO (i.e., tritium) were the highest (i.e., 8 to 11 x 10^{-10} m^2/s), compared to the other ion species, for all *BCs*. Values of D^* reported by the authors for Cl^- were similar to, but approximately 2 x 10^{-10} m^2/s lower than those for HTO over the tested range of *BCs*. Additionally, values of D^* for $^{85}\mathrm{Sr}$ were more than one order of magnitude lower than those reported for HTO and Cl^-. In this study, values of D^* increased with increasing C_{ot}. The value of D^* for C_{ot} of 5 mM KCl was more similar in magnitude to those reported for the reactive $^{85}\mathrm{Sr}$ cation in Gillham et al. (1984) (e.g., ~1 x10^{-10} m^2/s). For C_{ot} of 80 mM KCl, the value of D^* measured in this study was still lower than those reported for Cl^- in Gillham et al. (1984) for all values of *BC* (i.e., 2.6 x10^{-10} m^2/s versus 7.0 x10^{-10} m^2/s). The values of D^* measured for Cl^- in this study have been attributed to suppressed diffusion of Cl^- at early stages (i.e., $\leq$ 40 mM KCl) due, in part, to the complex chemical conditions imposed in this study. Therefore, the complex chemical conditions imposed in this study result in values of D^* that are more similar to those measured for a reactive cation (i.e., $^{85}\mathrm{Sr}$) than Cl^- for a similar compacted sand-bentonite specimen comprising 15 % bentonite.

2.6.2 Geosynthetic Clay Liners (GCLs)

Values of D^* for chloride ions reported in the literature for GCLs (Shackelford and Lee 2003; Malusis et al. 2014; Shackelford et al. 2016) are compared to the values of D^* measured in this study for the compacted sand-bentonite specimen RW-1 in Fig. 2.41a. Values of D^* for the reported GCLs ranged from 4.3 x10^{-11} m^2/s to 2.8 x10^{-10} m^2/s, compared to the range of 6.6 x 10^{-11} m^2/s to 2.6 x10^{-10} m^2/s for D^* values measured in this study. Therefore, values of D^* for the specimen tested in this study are within the same range of values previously reported for GCLs when exposed to varying concentrations of salt solutions.

2.6.3 Compacted Clay Liners (CCLs)

Values of D^* for chloride ions reported in the literature for CCLs (Crooks and Quigley 1894; Shackelford et al. 1989; Shackelford and Daniel 1991; Rowe and Badv 1996; De Soto et al. 2012) are compared to the values of D^* measured in this study for the compacted sand-bentonite specimen RW-1 in Fig. 2.41b. Values of D^* for the reported CCLs ranged from 1.5 x 10^{-11} m^2/s to 4.4 x10^{-9} m^2/s, compared to the range of 6.6 x 10^{-11} m^2/s to 2.6 x10^{-10} m^2/s for D^* values measured in this study. The CCL specimens in the literature comprised natural clay with values of cation exchange capacity, CEC, ranging from 5 to 42 meq/100g. Additionally, values of n ranged from 0.29 to 0.59. Therefore, the seemingly indiscriminate trend in values of D^* for the CCLs reported in the literature is likely due, in part, to the variability among the clay and specimen properties. However, values of D^* measured in this study are within the same range as those reported for CCLs when exposed to varying concentrations of salt solutions.

2.6.4 Compacted Natural Sodium Bentonites

Values of D^* for chloride ions reported in the literature for compacted Na-bentonite specimens (Rosanne et al. 2003; Dominijanni et al. 2013; Di Emidio et al. 2015) are compared to the values of D^* measured in this study for the compacted sand-bentonite specimen RW-1 in Fig. 2.41c. Values of D^* for the compacted Na-bentonite specimens ranged from 4.0 x10^{-11} m^2/s to 9 x10^{-10} m^2/s, compared to the range of 6.6 x 10^{-11} m^2/s to 2.6 x10^{-10} m^2/s for D^* values measured in this study. Values of n for the Na-bentonite specimens were higher than the porosity of the specimen in this study (i.e., from 0.46 to 0.81 versus 0.34). However, at a given C_{ot}, values of D^* were generally higher for the Na-bentonite specimens compared to the sand-bentonite specimen in this study. Therefore, despite the higher porosities, the higher values of D^* of the Na-bentonite specimens are likely due, in part, to the greater *BC* (i.e., 100 % versus 15 %).

2.6.5 Compacted Polymerized Bentonites

Values of D^* for chloride ions reported in the literature for compacted polymerized bentonite specimens (Mazzieri et al. 2010; Bohnhoff and Shackelford 2015; Di Emidio et al. 2015) are compared to the values of D^* measured in this study for the compacted sand-bentonite specimen RW-1 in Fig. 2.41d. Values of D^* for the compacted polymerized bentonite specimens ranged from 3.7 x10^{-11} m^2/s to 2.9 x10^{-10} m^2/s, compared to the range of 6.6 x 10^{-11} m^2/s to 2.6 x10^{-10} m^2/s for D^* values measured in this study. Values of *n* for the compacted polymerized bentonite specimens were significantly greater than in this study (i.e., 0.72 to 0.95 compared to 0.34). Values of D^* decreased with decreasing values of *n* for specimens tested by Bohnhoff and Shackelford (2015). However, despite the low value of *n* for the specimen tested in this study, values of D^* were still within the same range as those reported for polymerized bentonites when exposed to varying concentrations of salt solutions.

2.7 Conclusions

Based on the research objectives and results of experimental testing presented in this study, two primary conclusions can be made. First, the results of duplicate tests (designated as RW-1 and RW-2) performed using specimens of a compacted sand-bentonite (SB) mixture comprising 15 % bentonite indicated that both specimens exhibited virtually the same magnitude of membrane behavior, with measured values of the membrane efficiency coefficients, ω, ranging from0.395 ± 0.053 to 0.063 ± 0.012 when exposed to KCl solutions with source concentrations, C_{ot}, ranging from 5 mM KCl to 80 mM KCl, respectively. The testing conditions imposed in this study were complicated by not flushing the specimens of soluble salts via permeation with de-ionized water (DIW) prior to membrane testing, using tap water instead of DIW as the bottom boundary circulation liquid, and adding a biocide to the circulating liquids to control biological activity. Nonetheless, the values of ω measured in this study were in general agreement with those measured in previous studies for other bentonite-based barriers, such as geosynthetic clay liners (GCLs), compacted clay liners (CCLs), compacted natural bentonites, and compacted polymerized bentonites, when exposed to a similar range of concentrations of the same or similar salts. Therefore, despite more unfavorable testing conditions, the extent and magnitude of the membrane behavior for the compacted SB mixture evaluated in this study was consistent with that previously observed for other bentonite-based barrier materials.

Second, the relative trends for the effective diffusion coefficients, D^*, measured for the primary chemical species in the system (i.e., Cl^- and K^+) for one of the two specimens evaluated in this study (RW-1) were somewhat atypical. The presence of additional anions such as Br^-, derived from the inclusion of the biocide in the boundary circulation liquids, and SO_4^{2-}, introduced to the system via the bottom circulation liquid (i.e., tap water), likely fulfilled a portion of the electroneutrality requirement that otherwise would have been fulfilled primarily by Cl^- in a more simplified chemical system. During the earlier stages of testing when electrolyte solutions with relatively low concentrations of KCl were circulated across the top specimen boundary (i.e., $C_{ot} \leq$ 40 mM KCl), values of D^* for Cl^- were lower (e.g., suppressed) relative to those for K^+ (e.g., 6.62 $\times 10^{-11}$ m^2/s versus 3.35 $\times 10^{-10}$ m^2/s), This relative difference in the D^* values for Cl^- versus those for K^+ is atypical, because K^+ is the more reactive species with typically lower values of D^*, especially for diffusion occurring through clays with negatively charged particle surfaces (e.g., bentonite). This suppression of D^* values for Cl^- at early testing stages was attributed, in part, to the presence of additional anions, primarily Br^- and SO_4^{2-}, in the system. Additionally, values of D^* for K^+ decreased from 4.93 x10^{-10} m^2/s to 2.38 x 10^{-10} m^2/s as C_{ot} increased from 10 mM to 80 mM KCl, which also was atypical because values of D^* increase with increasing C_{ot} due to the compression of DDLs and the concomitant increase in relative pore sizes. This decrease in the D^* of K^+ with increasing C_{ot} of KCl was attributed to the diffusion of Ca^{2+}, Mg^{2+}, and Na^+ that were continuously introduced to the system via the bottom circulation liquid (i.e., tap water) upward through the specimen, such that a portion of the electroneutrality requirement ordinarily filled by the downward diffusing K^+ was instead occupied by the upward diffusing Ca^{2+}, Mg^{2+}, and Na^+, thereby inhibiting the diffusion of K^+ through the specimen. Both of these atypical trends were attributed to the more complex chemical conditions imposed in this study relative to most previous studies involving the evaluation of similar behavior. This explanation was supported by the measured concentrations of chemical species in the outflows collected from the bottom specimen boundary, C_b. At the beginning of the 40 mM KCl stage, values of C_{b,Cl^-} increased for the first time to be greater than those of C_{b,Br^-}, presumably due to the relatively high imposed KCl concentration gradient across the specimen, such that the increased diffusive flux of Cl^- resulted in Cl^- becoming the predominant anion at the bottom specimen boundary. Chloride is often used as a tracer in order to estimate unique soil properties such as tortuosity. However, the results of this study indicate the presence of additional anions in the system could reduce the effectiveness of Cl^- as a tracer at low values of C_{ot} (i.e., $\leq$ 40 mM KCl).Despite the suppression of D^* for Cl^- and K^+ due to the presence of additional chemical species in the system, values of D^* for Cl^- were in good agreement with those reported for other bentonite-based barriers when exposed to similar or the same salts at similar ranges of concentrations.

Table 2.1. Chemical properties of tap water used in this study.

Chemical Property	Value	
pH	7.0	
Electrical Conductivity, *EC* (mS/m)	14.6	
Anion Concentrations [a] (mg/L (mM)):	Cl^-	3.7 (0.10)
	F^-	0.7 (0.04)
	HCO_3^-	24.4 (0.40)
	SO_4^{2-}	11.7 (0.12)
Cation Concentrations [b] (mg/L(mM)):	Ca^{2+}	16.1 (0.40)
	Mg^{2+}	2.3 (0.095)
	Na^+	3.5 (0.15)
	K^+	0.7 (0.018)

[a] Based on ion chromatography analysis performed by the Soil, Water and Plant Testing Laboratory, CSU, Fort Collins, CO.

[b] Based on inductively coupled plasma-atomic emission spectrometry analysis performed by the Soil, Water and Plant Testing Laboratory, CSU, Fort Collins, CO.

Table 2.2. Properties of source KCl solutions used in this study.

Concentrations (mM)		Electrical Conductivity, EC^a (mS/m)	pH[a]
Target	Measured		
5	5.02	76.3	4.5
10	10.2	151	4.6
20	20.4	286	4.8
40	42.2	593	4.5
80	82.1	1152	4.6

[a]Values of *EC* and pH were measured for KCl source solutions following the addition of 500 ppm biocide.

Table 2.3. Mineralogical composition and physical and chemical properties of soil used in this and previous studies.

Property	Standard	Natural Gel Wyo-Ben Product			Sand
		Yeo (2005)	Hong (2012)	This study (2015)	
Specific Gravity, G_s	ASTM D 854	2.72	2.67	2.81	2.66
Liquid Limit, *LL*	ASTM D 4318	497	511	426	--
Plasticity Index, *PI*	ASTM D 4318	454	457	393	--
Classification	ASTM D 2487	CH	CH	CH	SP
Principal Minerals (%)	a				
Montmorillonite		65	69	70	--
Cristobalite		18	14	--	--
Quartz		6	12	9	--
Plagioclase feldspar		5	2	15	--
Calcite		2	3	1	--
Other		4	--	5	--
CEC (cmol_c/kg)	b	86.1	83.4	86.8	--
Bound Cations (cmol_c/kg)	b				
Ca^{2+}		4.4	4.9	34.4	--
Mg^{2+}		8.1	8.8	12.0	--
Na^{+}		77.5	73.4	39.0	--
K^{+}		0.99	1.1	0.7	--
Sum		90.99	88.2	86.1	--
Soluble Salts (mg/kg)	b				
Ca^{2+}		47	46.1	91.5	--
Mg^{2+}		14.1	15.3	14.9	--
Na^{+}		2097	2042	4183.1	--
K^{+}		61.2	58.4	183.4	--
Soil pH	ASTM D 4972	7.9	8.1	9.7[c]	--

[a] Based on X-ray diffraction analysis performed my Mineralogy Inc., Tulsa, OK.

[b] Procedures described in Shackelford and Redmond (1995).

[c] Determined with DIW.

Table 2.4. Measured gravimetric water contents of hydrated sand-bentonite mixtures (following the 48-h curing period) and the corresponding specimens compacted from the respective mixture. The average decrease in water content was 0.67 % ± 0.13%.

Specimen ID	Water Content, *w* (%)		-Δ*w (%)*
	Mixture	Specimen	
1	13.20	12.61	0.59
2	13.20	12.50	0.70
3	13.30	12.56	0.74
4	13.30	12.37	0.93
5	13.50	12.93	0.57
6	13.50	12.97	0.53
7	13.50	12.76	0.74
8	13.50	12.75	0.75
9	13.17	12.60	0.57

Table 2.5. Results of triplicate flexible-wall hydraulic conductivity tests conducted on compacted sand-bentonite specimens containing 15 % bentonite (by dry weight).

Permeant Liquid	Category	Termination Criteria	Parameter Designation	Test Specimen Designation		
				FW-1	FW-2	FW-3
Tap Water	Duration of Permeation, t or PVF[a]	Standard	t_s (d)	93.7	67.9	33.9
			PVF_s	0.38	0.27	0.10
		Final	t_f (d)	157.7	127.9	65.9
			PVF_f	0.70	0.50	0.20
	Hydraulic Conductivity, k (m/s)	Standard	k_s	6.34 x10^{-12}	5.29 x10^{-12}	5.14 x10^{-12}
		Final	k_f	6.82 x10^{-12}	4.80 x10^{-12}	5.38 x10^{-12}
	Volumetric Flow Ratio, Q_{out}/Q_{in}	Standard	$(Q_{out}/Q_{in})_s$	1.00	0.82	0.80
		Final	$(Q_{out}/Q_{in})_f$	1.09	0.8	0.85
80 mM KCl	Duration of Permeation	N/A	t_c (d)	101.9	101.9	--
			PVF_c	0.58	0.43	--
	Hydraulic Conductivity, k (m/s)	N/A	k_c	6.63 x 10^{-12}	5.35 x 10^{-12}	--
	Volumetric Flow Ratio, Q_{out}/Q_{in}	N/A	$(Q_{out}/Q_{in})_c$	1.07	0.97	--

[a] t = time; PVF = pore volumes of flow

Table 2.6. Initial properties of compacted sand-bentonite specimens (RW-1 and RW-2) containing 15 % bentonite (by dry weight) tested for membrane behavior in rigid-wall cells.

Parameter Designation	Value(s)	
	RW-1	RW-2
Measured Volume, V_t (x 10^{-4} m^3)	1.13	1.11
Dry Unit Weight, γ_d (kN/m^3 (lb/ft^3))	17.2 (109.5)	17.5 (111.4)
Water Content, w (%)	12.8	12.5
Porosity, n	0.34	0.34
Void Ratio, e	0.53	0.50
Saturation, S (%)	65.0	66.5

Table 2.7. Results of the saturation/permeation stage for specimens RW-1 and RW-2 with tap water as the permeant liquid.

Parameter		Value(s)	
		RW-1	RW-2
Duration of Saturation Stage[a]	*t* (d)	41	102
	PVF	1.2	0.87
Estimated Steady-State Pressure Difference, $-\Delta u$ (kPa (psi))		105 (15.2)	139 (20.2)
Estimated Hydraulic Conductivity, k (x 10^{-11} m/s)		2.7	0.26
Electrical Conductivity of Effluent at the end of Saturation, EC_s (mS/m) @ 25 ^{o}C		381.0	172.4

[a] *t* = time; *PVF* = pore volumes of flow

Table 2.8. Values for the sum of concentrations (C_{sum}) for the major solutes in this study (i.e., Cl^-, F^-, NO_2^-, SO_4^{2-}, Ca^{2+}, K^+, Mg^{2+}, and Na^+) and electrical conductivity (*EC*) for the liquids at the boundaries of specimens RW-1 and RW-2 for multi-stage membrane behavior testing using KCl as the source liquid.

Target KCl Source Concen-tration, C_{ot} (mM)	Boundary Location	Inflow				Outflow			
		RW-1		RW-2		RW-1		RW-2	
		C_{sum} (mM)	*EC* (mS/m) @ 25 °C	C_{sum} (mM)	*EC* (mS/m)	C_{sum} (mM)	*EC* (mS/m)	C_{sum} (mM)	*EC* (mS/m)
5	Top	9.32	76.3	10.37	81.9	11.32	82.5	12.19	81.5
	Bottom	1.64	17.4	2.56	19.8	3.16	22.4	3.87	26.6
10	Top	18.49	150.6	19.48	152.8	19.93	151.9	18.35	147.1
	Bottom	1.57	15.9	2.70	20.1	3.32	26.6	3.23	29.65
20	Top	35.80	286.5	36.96	285.6	36.83	280.3	35.67	274.7
	Bottom	1.64	19.7	2.06	22.1	4.32	34.6	4.18	36.5
40	Top	76.47	595	76.26	591	71.38	566	72.27	554
	Bottom	1.80	20.4	2.15	22.6	6.03	50.0	6.31	57.1
80	Top	148.2	1156	151.9	1147	138.8	1083	140.7	1069
	Bottom	1.63	22.7	2.30	27.5	9.62	82.4	10.31	91.2

Table 2.9. Summary of the calculated values of maximum chemico-osmotic pressure for tests RW-1 and RW-2 based on tap water as the bottom circulating liquid.

Test Designation	Target KCL Source Concentration, C_{ot} (mM)	Maximum Chemico-osmotic Pressure, π, and Pressure Difference, $\Delta\pi$ (kPa)					
		$\pi_{o,t}$[1]	$\pi_{o,b}$[2]	$\pi_{ave,t}$[3]	$\pi_{ave,b}$[4]	$-\Delta\pi_o$	$-\Delta\pi_{ave}$
RW-1	5	26.3	4.09	26.4	5.41	22.2	21.0
	10	51.0	3.66	47.4	5.31	47.3	42.1
	20	98.2	4.11	89.0	6.56	94.1	82.4
	40	207	4.39	181	8.88	203	172
	80	403.4	4.00	353.0	13.76	399	339
RW-2	5	27.6	6.27	32.3	7.88	21.4	24.4
	10	54.0	6.61	49.0	7.33	47.4	41.6
	20	106.5	5.03	91.3	7.88	101	83.4
	40	209.7	5.26	184.3	10.37	204	174
	80	404.9	5.64	360.8	15.40	399	345

[1] $\pi_{o,t}$ = chemico-osmotic potential calculated for the top boundary based on C_{o,t,Cl^-} (Eq. 2.25).

[2] $\pi_{o,b}$ = chemico-osmotic potential calculated for the bottom boundary based on $\Sigma C_{o,b}$ (Eq. 2.26).

[3] $\pi_{ave,t}$ = chemico-osmotic potential calculated for the top boundary based on $\Sigma C_{ave,t}$ (Eq. 2.27).

[4] $\pi_{ave,b}$ = chemico-osmotic potential calculated for the bottom boundary based on $\Sigma C_{ave,b}$ (Eq. 2.28).

Table 2.10. Summary of results of membrane testing for tests RW-1 and RW-2.

Test Designation	KCl Stage	$-\Delta P_e$[1] (kPa)	$-\Delta\pi$ (kPa)				ω			
			$-\Delta\pi_{o,TW}$[2]	$-\Delta\pi_{o,DIW}$[3]	$-\Delta\pi_{ave,TW}$[4]	$-\Delta\pi_{ave,DIW}$[5]	$\omega_{o,TW}$[6]	$\omega_{o,DIW}$[7]	$\omega_{ave,TW}$[8]	$\omega_{ave,DIW}$[9]
RW-1	5 mM	9.40	22.2	24.6	21.0	23.5	0.423	0.383	0.448	0.401
	10 mM	12.2	47.3	49.7	42.1	47.1	0.258	0.246	0.290	0.259
	20 mM	15.3	94.1	96.5	82.4	94.4	0.163	0.159	0.186	0.162
	40 mM	20.7	203	206	172	193	0.102	0.101	0.120	0.107
	80 mM	25.4	399	402	339	374	0.064	0.063	0.075	0.068
RW-2	5 mM	8.40	21.4	24.1	24.4	23.1	0.391	0.347	0.342	0.362
	10 mM	11.6	47.4	50.0	41.6	47.7	0.244	0.231	0.277	0.242
	20 mM	14.3	101	104	83.4	98.2	0.141	0.138	0.171	0.145
	40 mM	16.5	204	207	174	197	0.081	0.080	0.095	0.084
	80 mM	17.7	399	402	345	380	0.044	0.044	0.051	0.047

[1] $-\Delta P_e$ = the effective chemico-osmotic pressure difference at steady state ($-\Delta P_e = -\Delta P_{ss} - (-\Delta P_{TW})$), where $-\Delta P_{TW}$ (> 0) for RW-1 and $-\Delta P_{TW}$ (< 0) for RW-2.

[2] $-\Delta\pi_{o,TW}$ = chemico-osmotic potential difference based on $-\Delta C_o$ where C_{ob} = TW.

[3] $-\Delta\pi_{o,DIW}$ = chemico-osmotic potential difference based on $-\Delta C_o$ where C_{ob} = DIW.

[4] $-\Delta\pi_{ave,TW}$ = chemico-osmotic potential difference based on $-\Delta C_{ave}$ where C_{ob} = TW.

[5] $-\Delta\pi_{ave,DIW}$ = chemico-osmotic potential difference based on $-\Delta C_{ave}$ where C_{ob} = DIW.

[6] $\omega_{o,TW}$ = membrane efficiency coefficient based on $-\Delta\pi_{o,TW}$.

[7] $\omega_{o,DIW}$ = membrane efficiency coefficient based on $-\Delta\pi_{o,DIW}$.

[8] $\omega_{ave,TW}$ = membrane efficiency coefficient based on $-\Delta\pi_{ave,TW}$.

[9] $\omega_{ave,DIW}$ = membrane efficiency coefficient based on $-\Delta\pi_{ave,DIW}$.

Table 2.11. Effective diffusion coefficients and tortuosity factors based on ΔC_o and ΔC_{ave} for test RW-1.

Chemical Species	Target KCl Source Concentration, C_{ot} (mM)	Osmotic Efficiency Coefficients ω		Diffusive Mass Flux, $\Delta Q_t'/\Delta t'$ (mM/m^2-d)	Time Lag, t_L (d)	Effective Diffusion Coefficient, D^* (x 10^{-10}) (m^2/s)		Apparent Tortuosity Factor, τ_a		Restrictive Tortuosity Factor, τ_r		Matrix Tortuosity Factor, τ_m	
		ω_o	ω_{ave}			D^*_o	D^*_{ave}	$\tau_{a,o}$	$\tau_{a,ave}$	$\tau_{r,o}$	$\tau_{r,ave}$	$\tau_{m,o}$	$\tau_{m,ave}$
Cl^-	5	0.423	0.448	0.32	11.83	0.645	0.662	0.032	0.033	0.190	0.189	0.171	0.176
	10	0.258	0.290	1.02	6.29	0.991	1.03	0.050	0.052	0.291	0.295		
	20	0.163	0.186	3.00	3.25	1.50	1.52	0.075	0.076	0.441	0.434		
	40	0.102	0.120	8.07	2.99	1.88	2.00	0.094	0.100	0.553	0.571		
	80	0.064	0.075	20	4.45	2.42	2.6	0.121	0.130	0.712	0.743		
K^+	5	0.423	0.448	1.27	48.8	2.48	3.35	0.124	0.168	0.729	0.958	0.075	0.085
	10	0.258	0.290	4.16	24.2	4.01	4.93	0.201	0.247	1.179	1.409		
	20	0.163	0.186	6.10	3.05	3.02	3.71	0.152	0.186	0.888	1.059		
	40	0.102	0.120	10	1.65	2.32	2.82	0.116	0.141	0.682	0.805		
	80	0.064	0.075	17	3.71	2.02	2.38	0.101	0.119	0.594	0.680		

Table 2.12. Comparison of membrane testing results for tests RW-1 and RW-2.

Test Designation	Testing Stage	Circulation Stage Duration, $t_{c\ (d)}$	Steady-state EC_b[a] (mS/m)	$-\Delta P_e$[b] (kPa)	ω_o[c]	ω_{ave}[d]
RW-1	Saturation	46	381.0	--	--	--
	Baseline	29	22.01	0.00	--	--
	5 mM KCl	86	22.55	9.40	0.423	0.448
	10 mM KCl	92	26.32	12.2	0.258	0.290
	20 mM KCl	88	34.60	15.3	0.163	0.186
	40 mM KCl	58	49.90	20.7	0.102	0.120
	80 mM KCl	46	82.40	25.4	0.064	0.075
RW-2	Saturation	104	172.4	--	--	--
	Baseline	30	28.03	0.00	--	--
	5 mM KCl	42	26.72	8.35	0.391	0.342
	10 mM KCl	30	29.65	11.6	0.244	0.277
	20 mM KCl	20	36.50	14.3	0.141	0.171
	40 mM KCl	20	57.10	16.5	0.081	0.095
	80 mM KCl	20	91.20	17.7	0.044	0.051

[a] EC_b = the electrical conductivity of the outflow collected from the bottom specimen boundary.

[b] $-\Delta P_e$ = the effective pressure difference across the specimen at steady state ($-\Delta P_e = -\Delta P_{ss} - (-\Delta P_{TW})$, where $-\Delta P_{TW}$ (> 0) for RW-1 and $-\Delta P_{TW}$ (< 0) for RW-2.

[c] ω_o = the chemico-osmotic efficiency coefficient based on $-\Delta\pi_{o,TW}$.

[d] ω_{ave} = the chemico-osmotic efficiency coefficient based on $-\Delta\pi_{ave,TW}$.

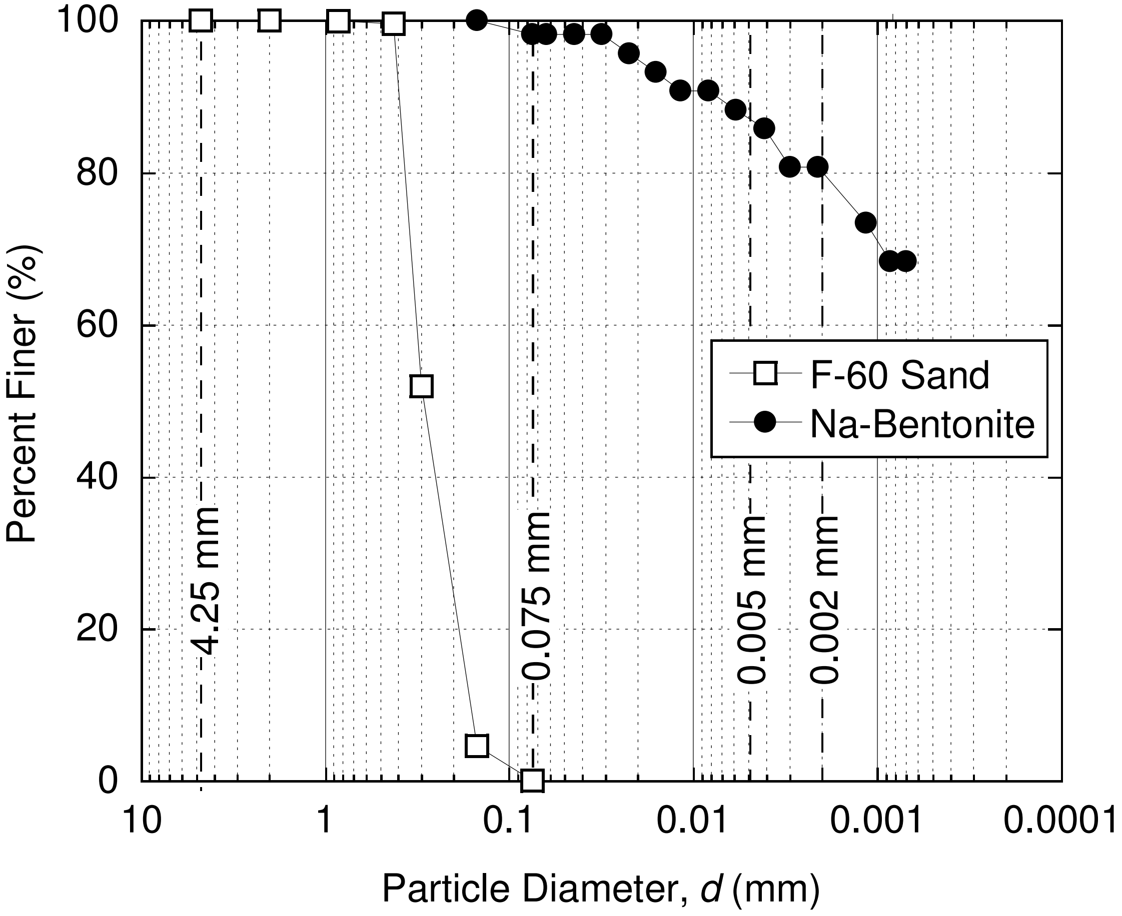

Figure 2.1. Particle-size distributions of the soil used in this study.

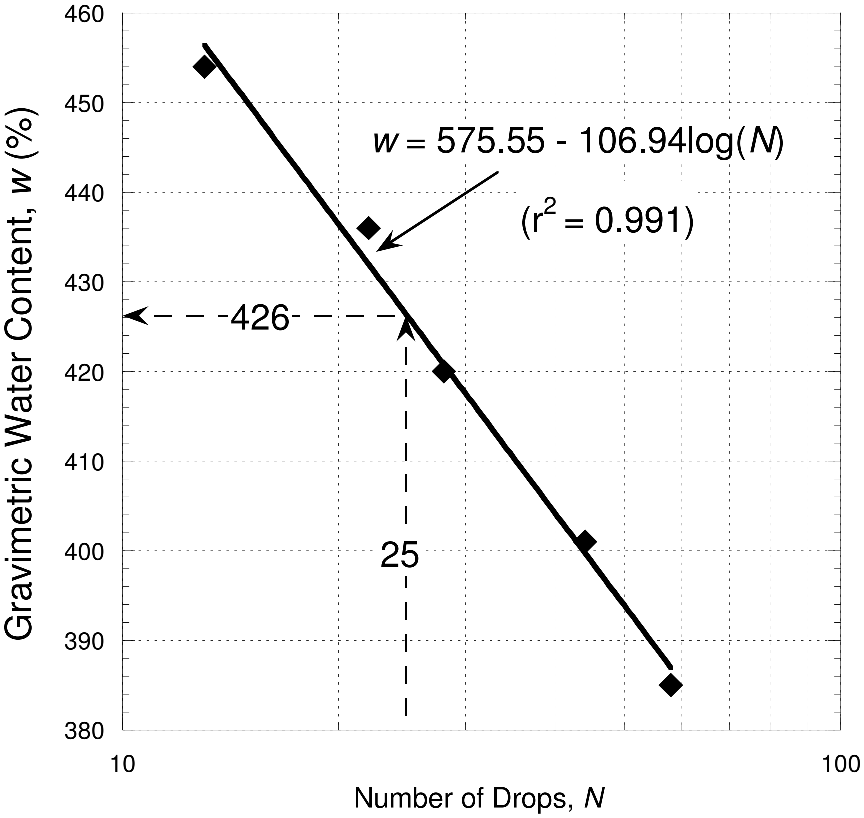

Figure 2.2. Flow curve for determination of the liquid limit, *LL* (= 426), of powdered bentonite with DIW as the mixing liquid.

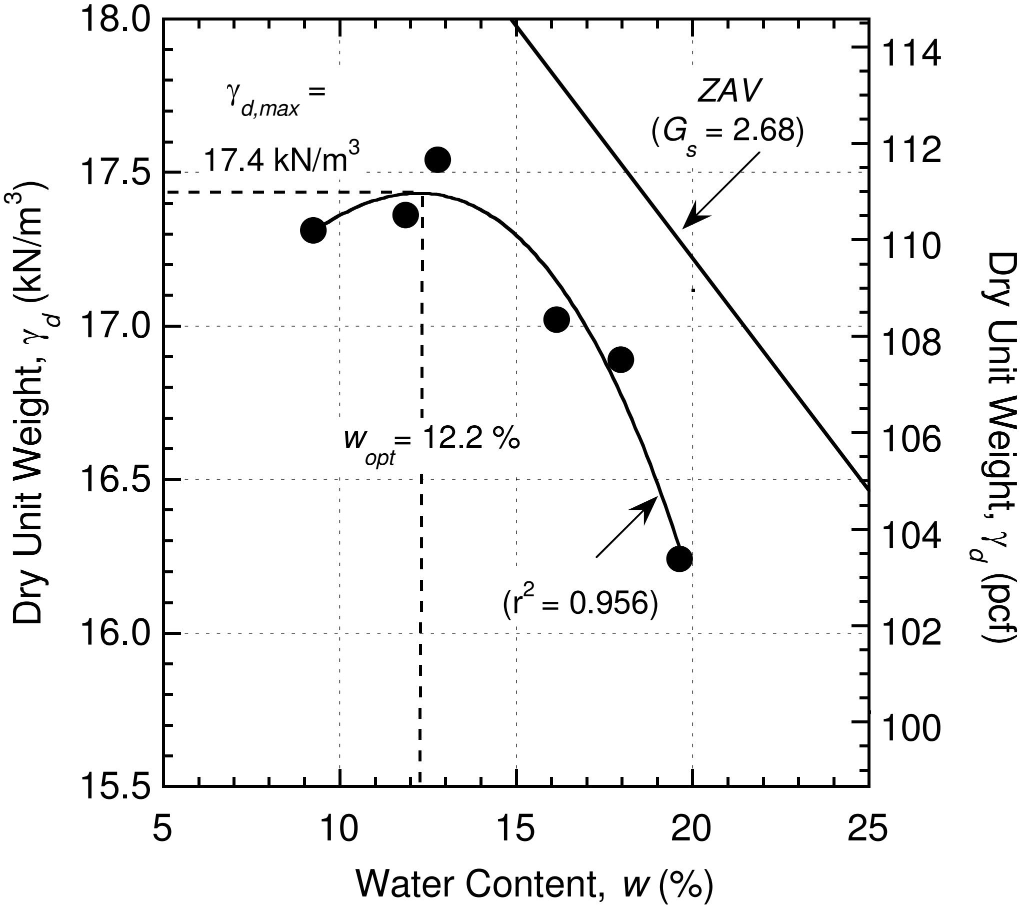

Figure 2.3. The 3rd-order polynomial fit used to determine $\gamma_{d,max}$ and w_{opt} from the compaction curve for 15 % sand-bentonite specimens compacted in the quarter-size mold.

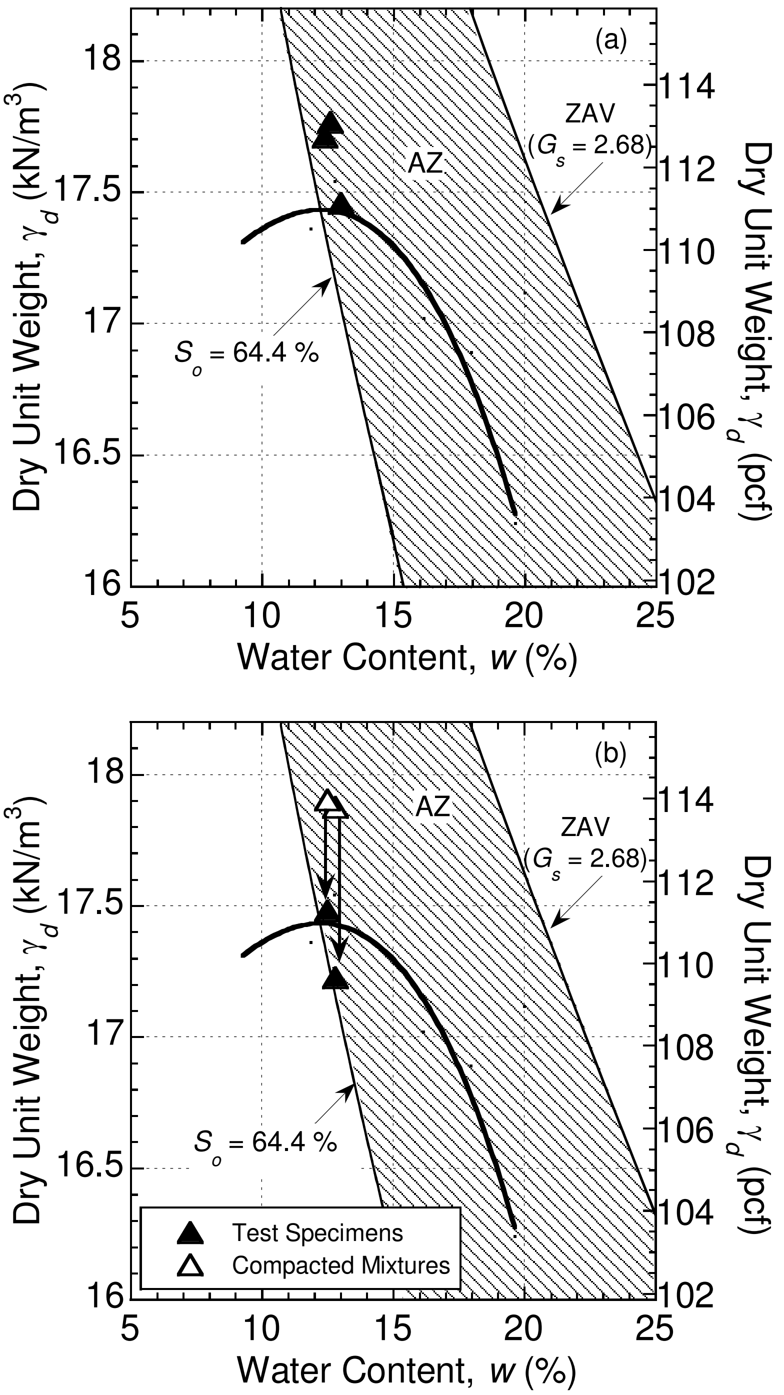

Figure 2.4. Compacted 15 % sand-bentonite test specimens and the respective acceptable zone (AZ) for (a) hydraulic conductivity testing, and (b) membrane and diffusion testing (ZAV = zero air voids curve.

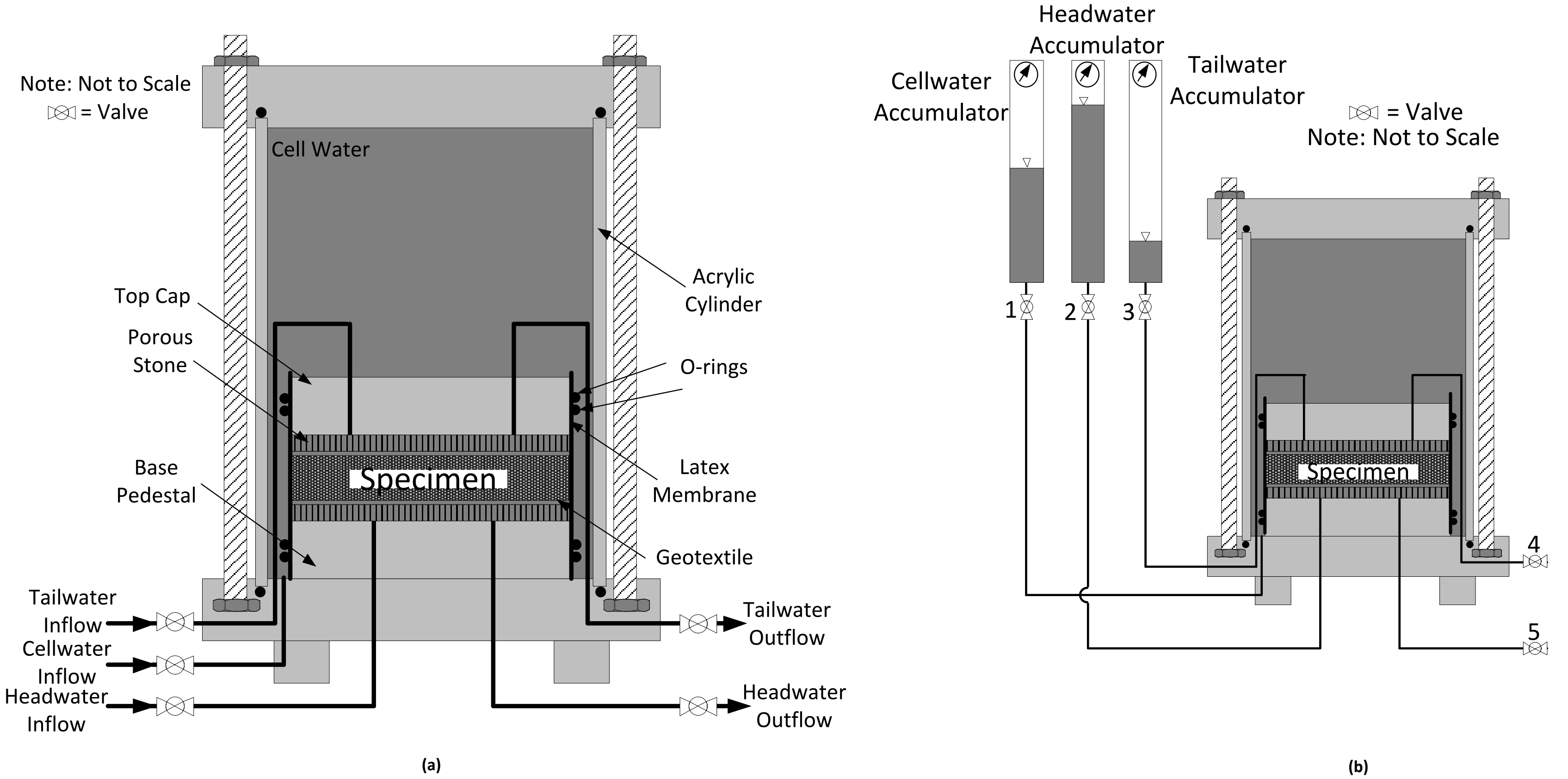

Figure 2.5. Schematics of the (a) flexible-wall permeameter and (b) hydraulic conductivity testing apparatus with a flexible-wall permeameter.

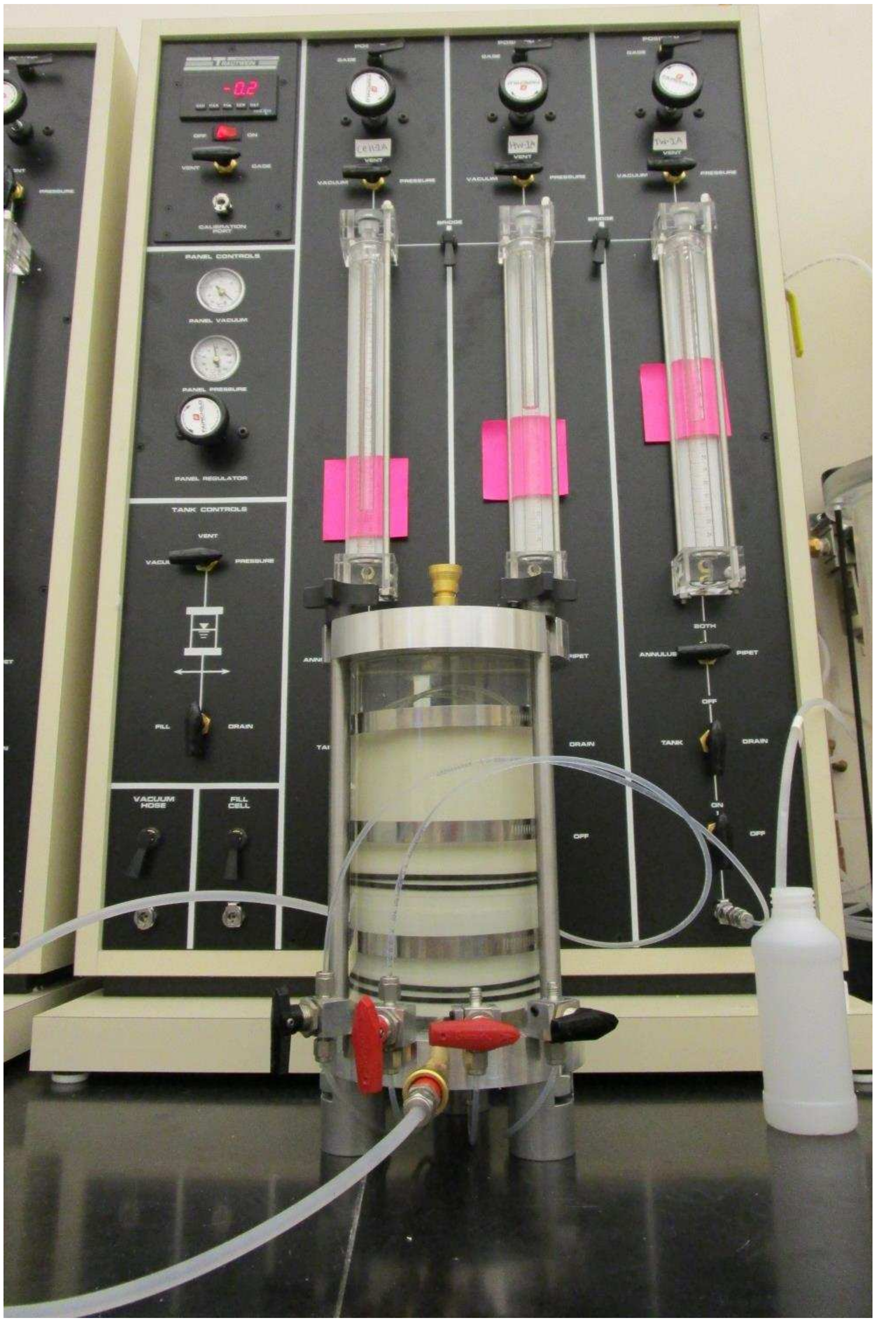

Figure 2.6. Image of the hydraulic conductivity testing apparatus comprised of the panel board and a flexible-wall permeameter.

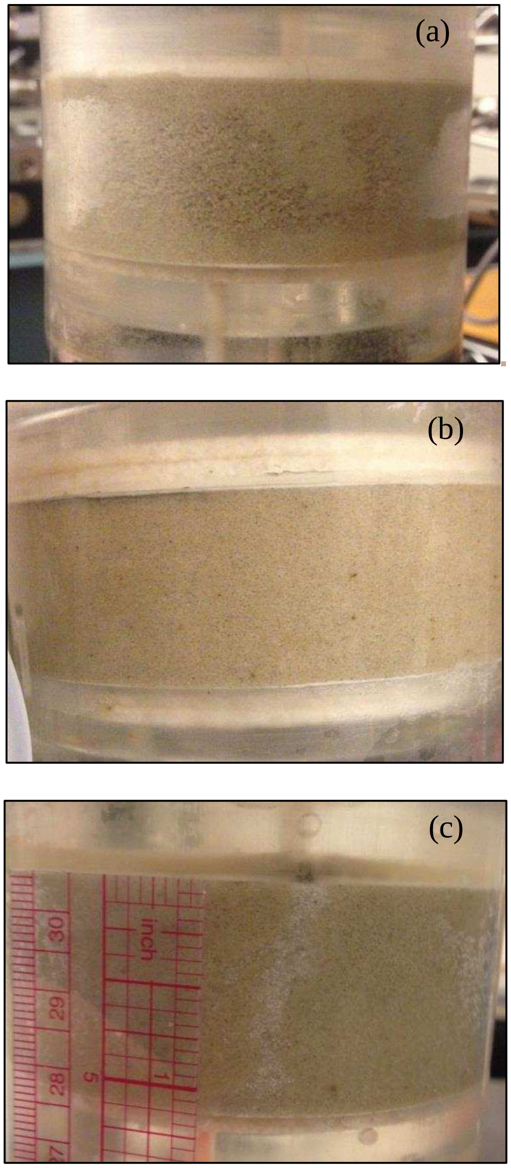

Figure 2.7. Images of 15 % sand-bentonite specimens in the rigid-wall cell following (a) initial placement in cell, (b) complete saturation (good side-wall contact) and (c) specimen failure due to side-wall leakage and/or particle migration.

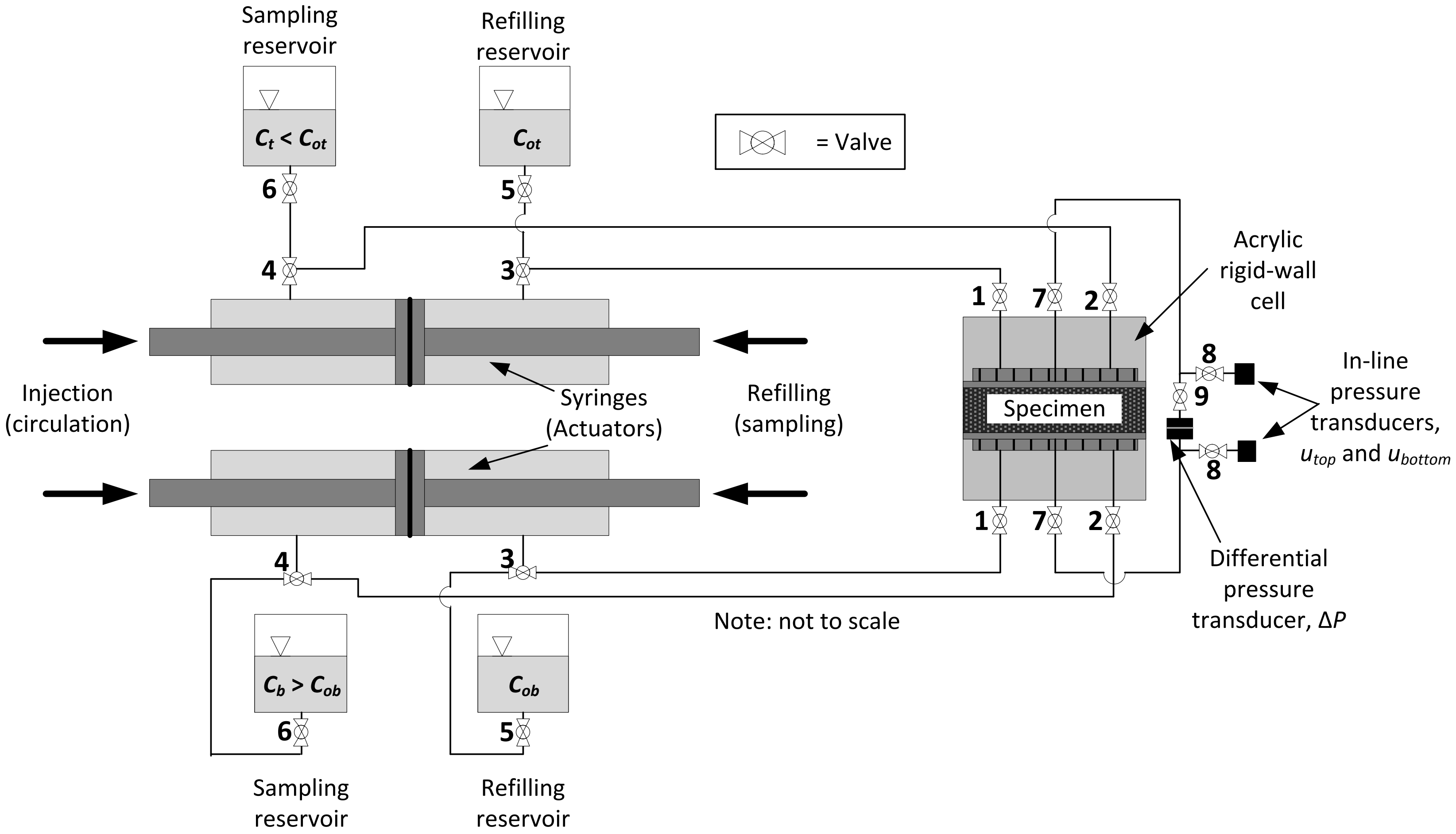

Figure 2.8. Schematic of the rigid-wall membrane testing apparatus (after Bohnhoff 2012).

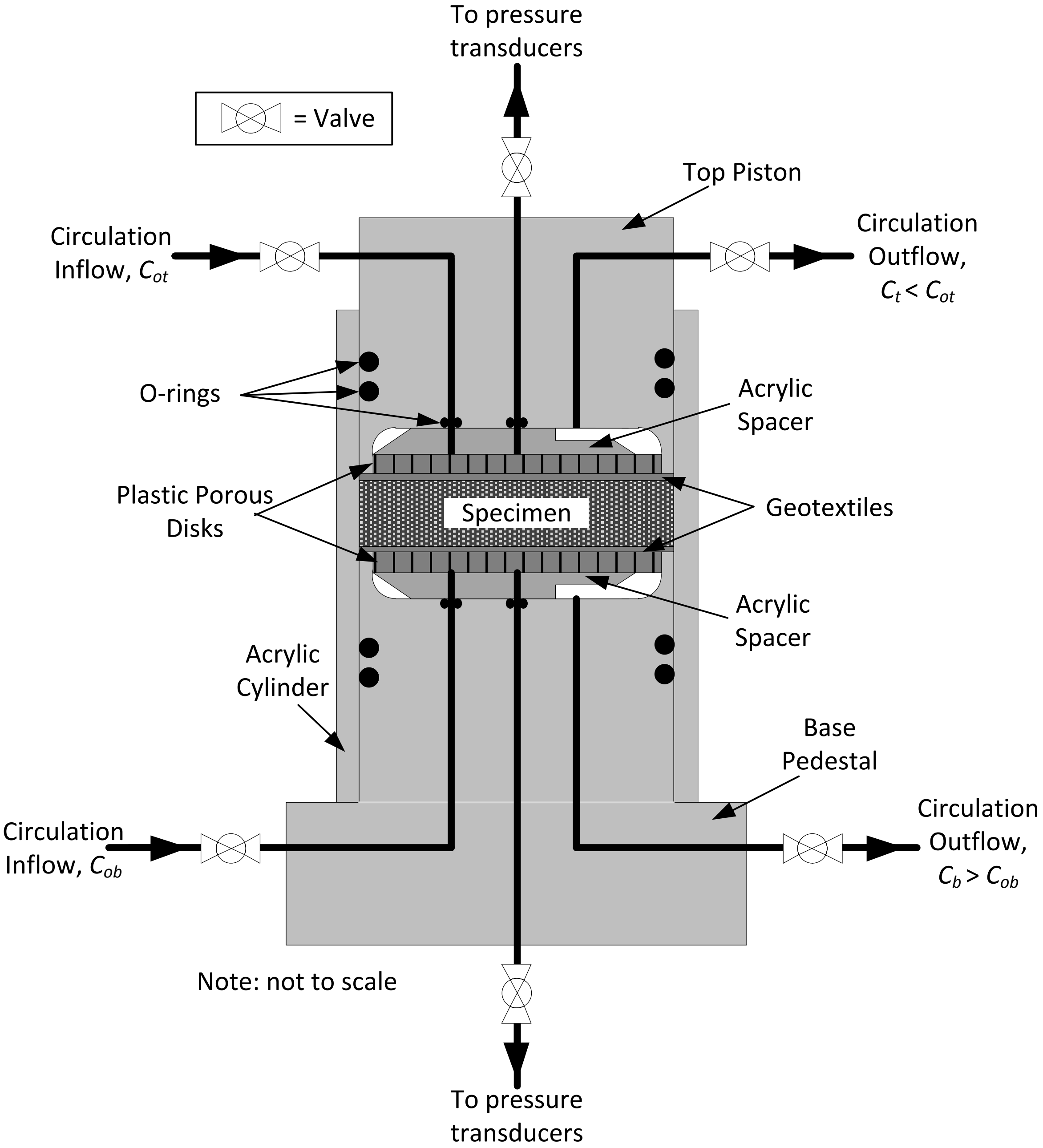

Figure 2.9. Schematic of the rigid-wall membrane testing cell (after Bohnhoff 2012).

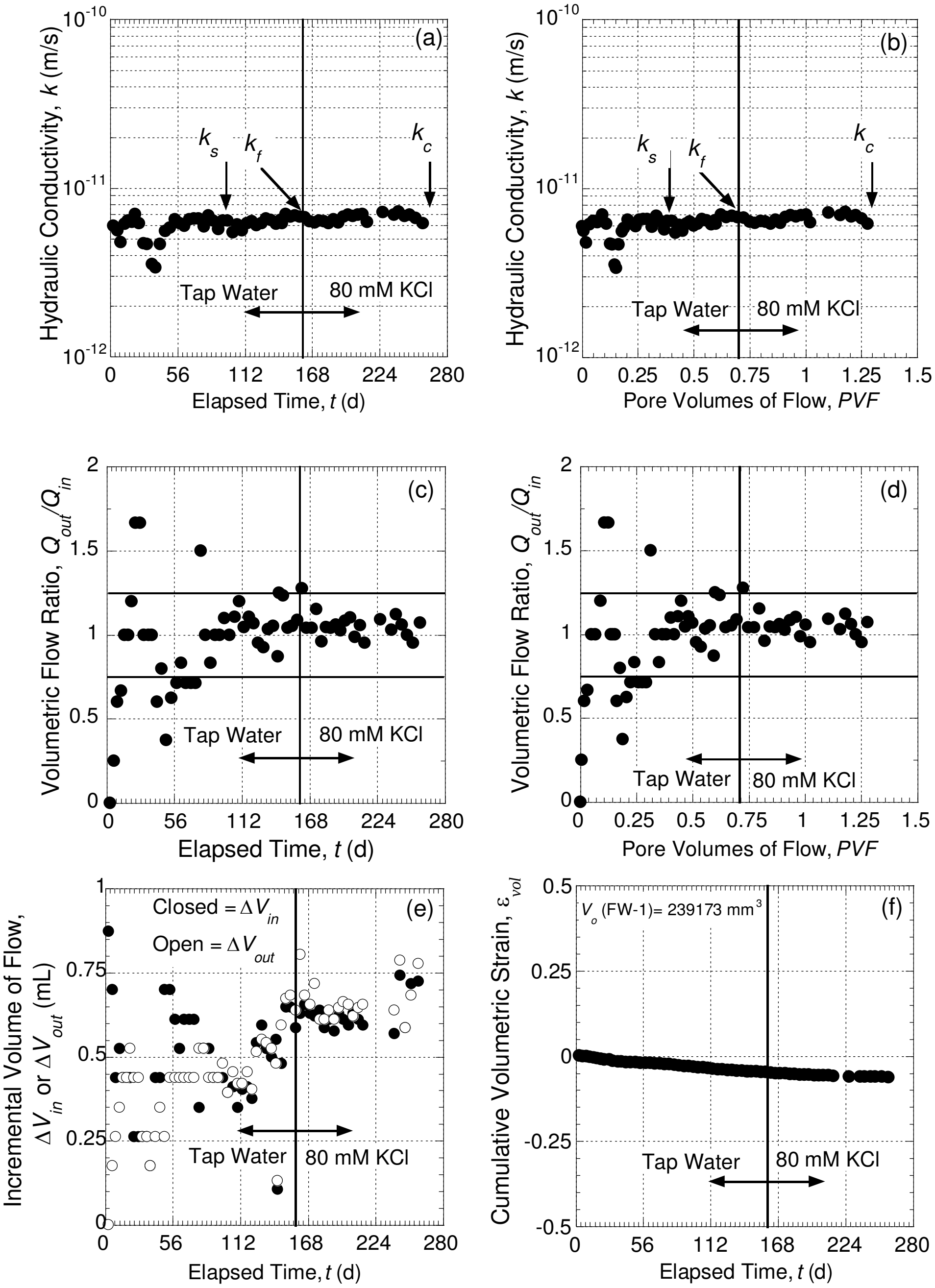

Figure 2.10. Hydraulic conductivity test results for test FW-1: (a) k versus t; (b) k versus PVF; (c) Q_{out}/Q_{in} versus t; (d) Q_{out}/Q_{in} versus PVF; (e) ΔV_{in} or ΔV_{out} versus t; (f) ε_{vol} versus t. (Note: arrows designate values corresponding to the standard termination criteria; V_o designates initial volume of specimen).

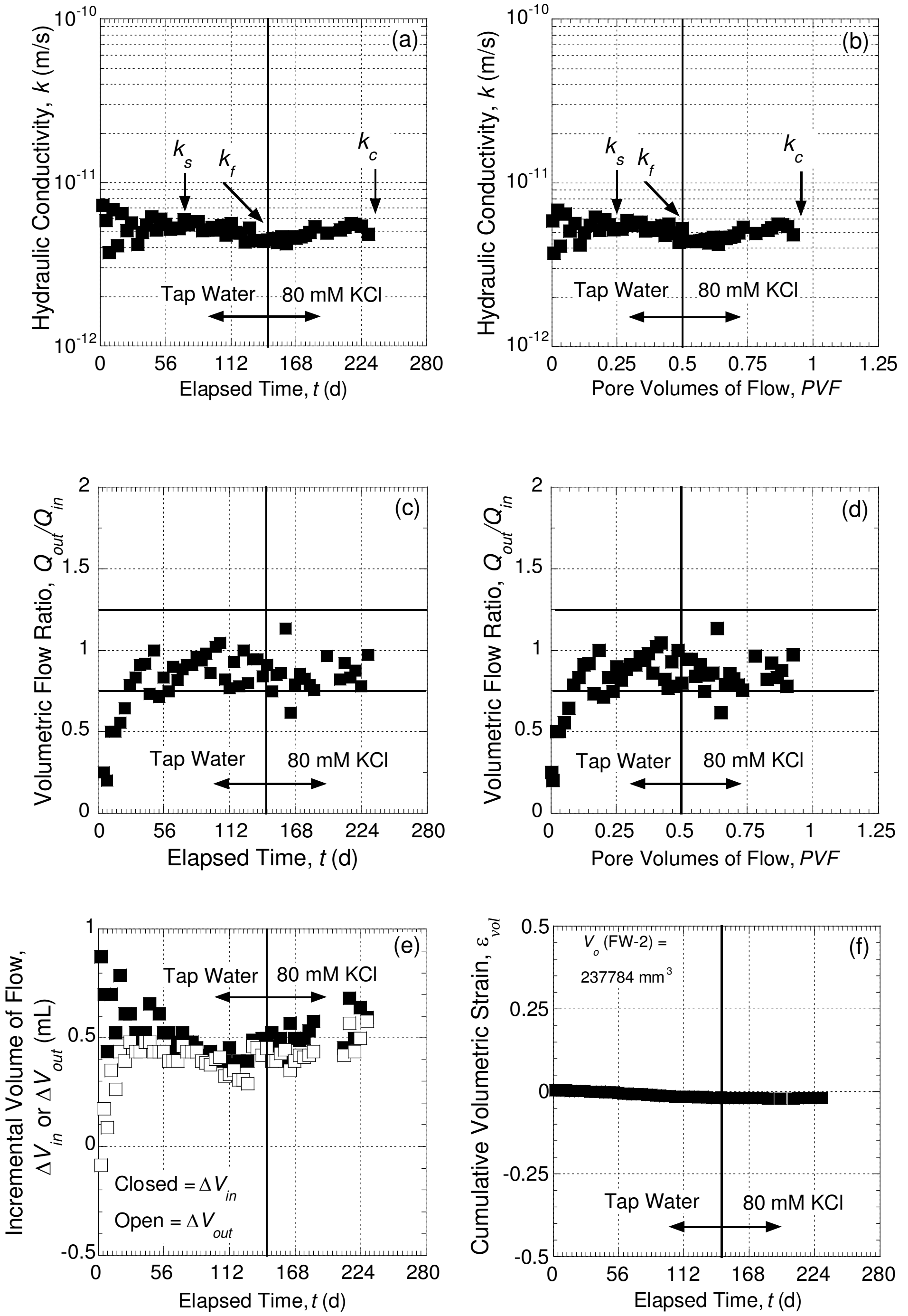

Figure 2.11. Hydraulic conductivity test results for test FW-2: (a) *k* versus *t*; (b) *k* versus *PVF*; (c) Q_{out}/Q_{in} versus *t*; (d) Q_{out}/Q_{in} versus *PVF*; (e) ΔV_{in} or ΔV_{out} versus t; (f) ε_{vol} versus t. (Note: arrows designate values corresponding to the standard termination criteria; V_o designates initial volume of specimen).

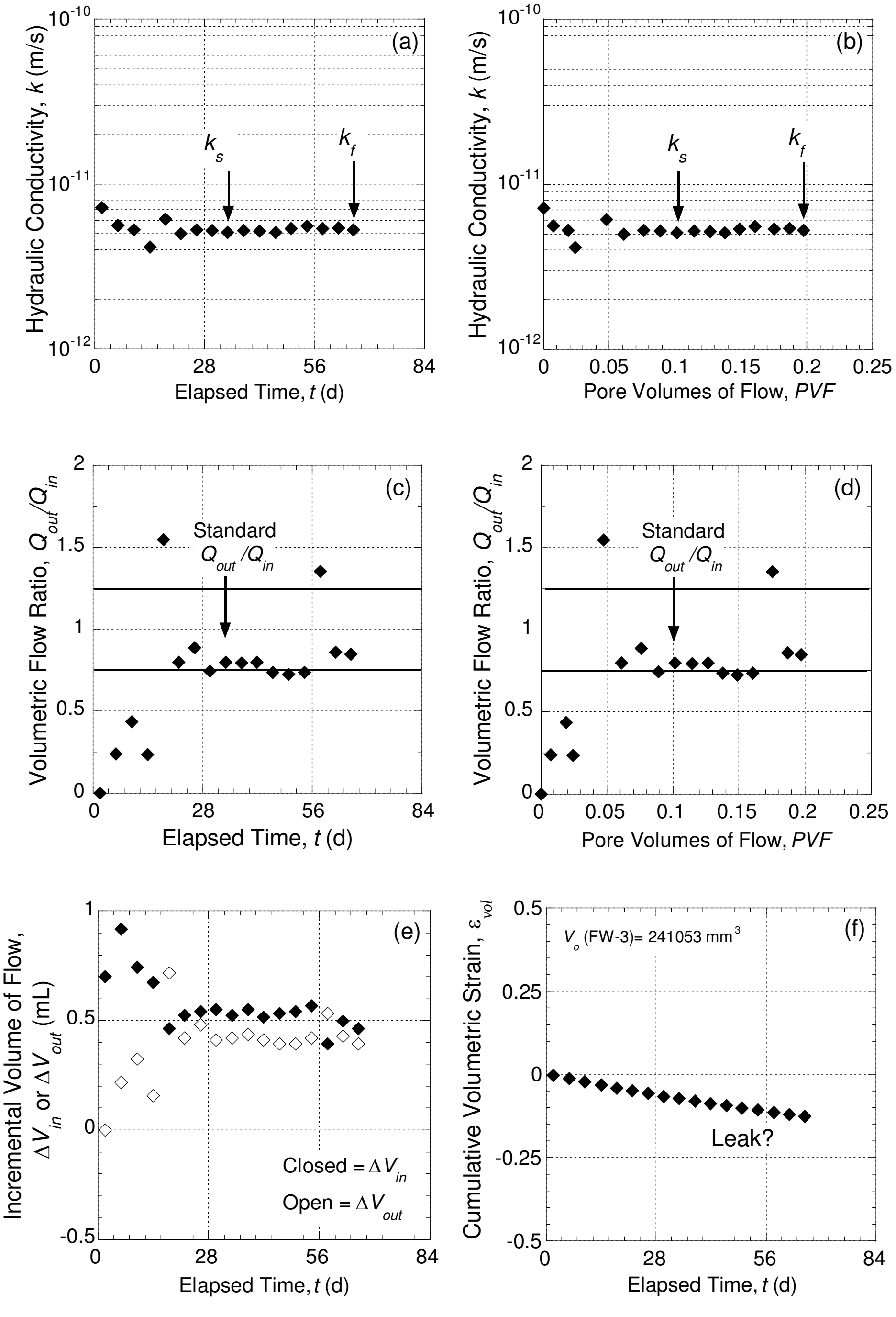

Figure 2.12. Hydraulic conductivity test results for test FW-3: (a) k versus t; (b) k versus PVF; (c) Q_{out}/Q_{in} versus t; (d) Q_{out}/Q_{in} versus PVF; (e) ΔV_{in} or ΔV_{out} versus t; (f) ε_{vol} versus t. (Note: arrows designate values corresponding to the standard termination criteria; V_o designates initial volume of specimen).

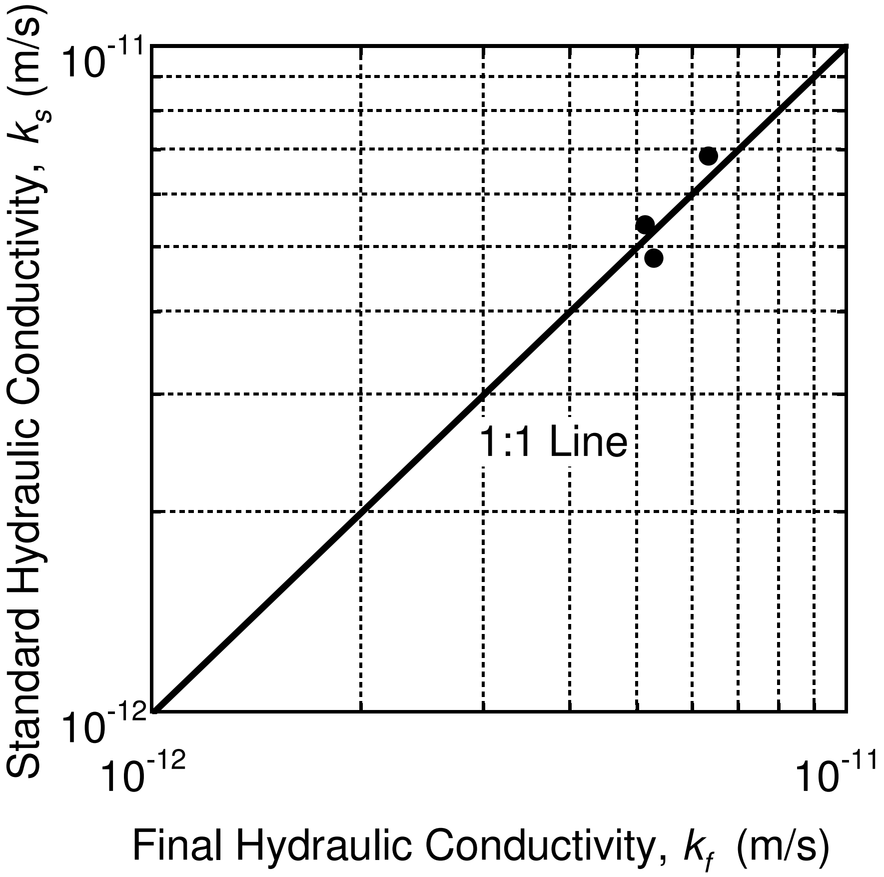

Figure 2.13. The relative values of *k* based on the standard determination criterion in ASTM D 5084 and the final measured value for specimens permeated with tap water in flexible-wall cells.

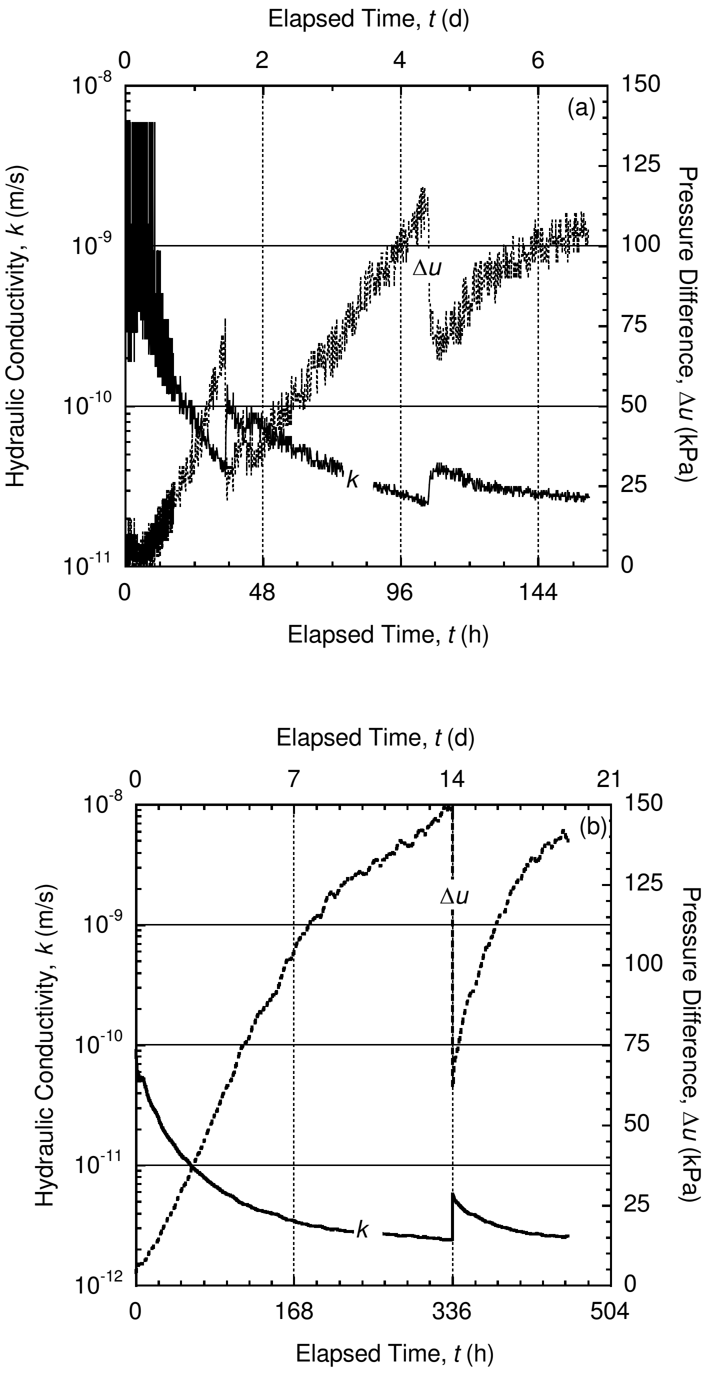

Figure 2.14. Hydraulic conductivity trends during the constant-flow saturation stage with tap water as the permeant liquid: (a) RW-1; (b) RW-2.

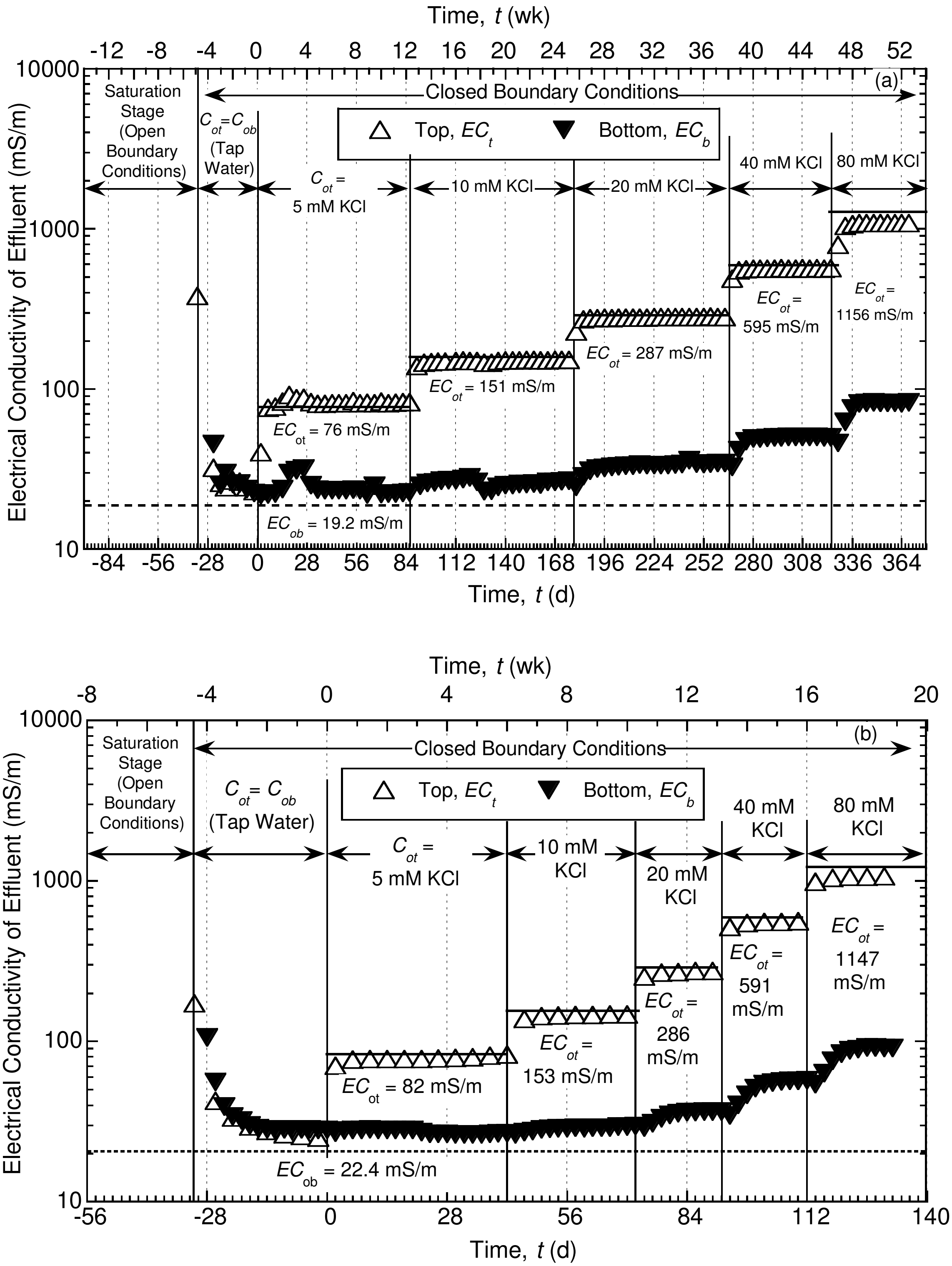

Figure 2.15. Measured electrical conductivity values of the circulation liquid collected from the top and bottom boundaries of compacted sand-bentonite specimen: (a) RW-1; (b) RW-2.

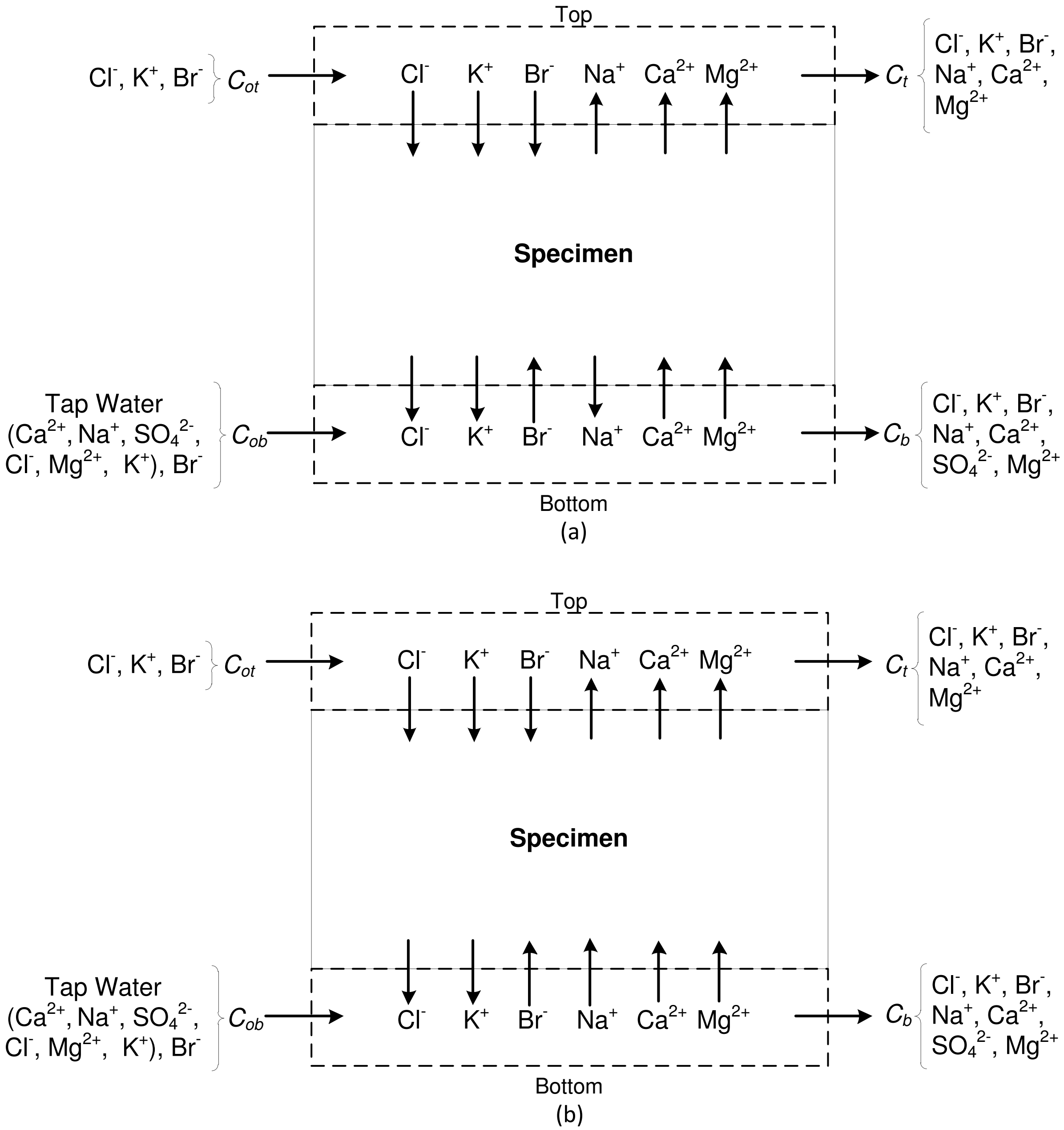

Figure 2.16. Schematic of the major chemical species in the system and the primary direction of transport: (a) at early stages (5 mM through 20 mM KCl); (b) at late stages (40 mM and 80 mM KCl).

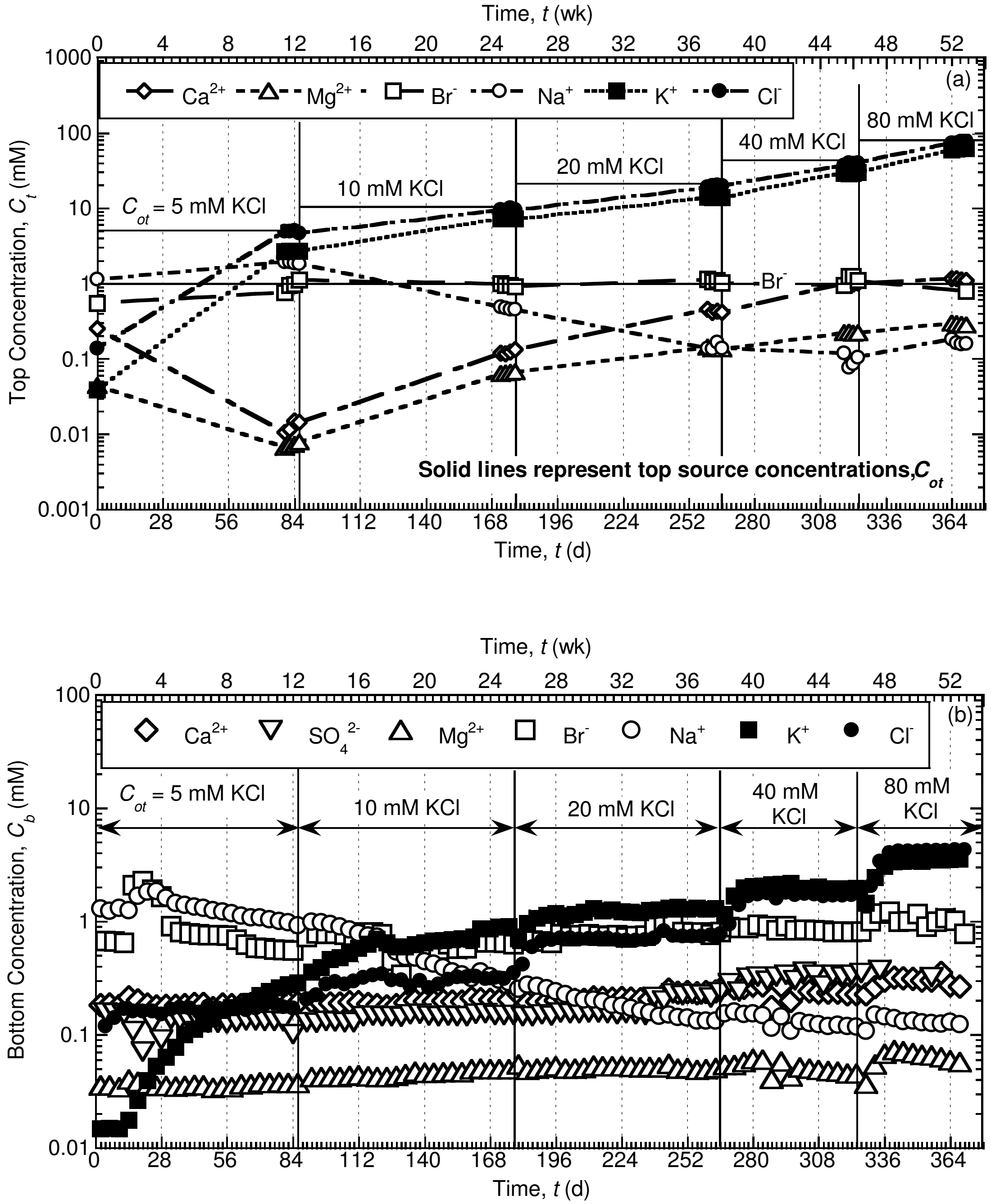

Figure 2.17. Measured concentrations of dominant chemical species in the circulation outflows for specimen RW-1: (a) concentrations in the top circulation outflow, C_t; (b) concentrations in the bottom circulation outflows, C_b.

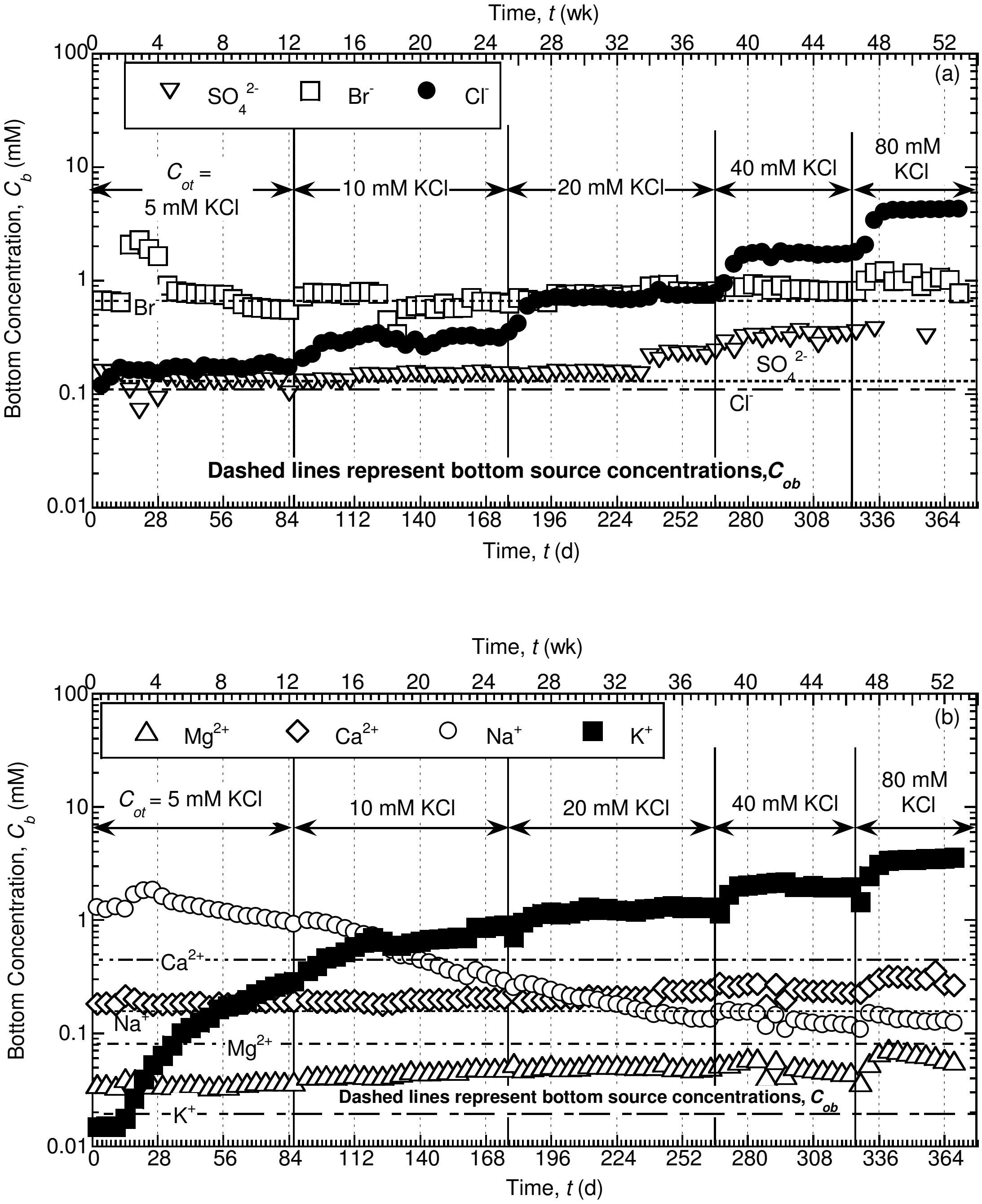

Figure 2.18. Measured concentrations of dominant chemical species in the circulation outflows from the bottom of specimen RW-1: (a) anion concentrations; (b) cation concentrations.

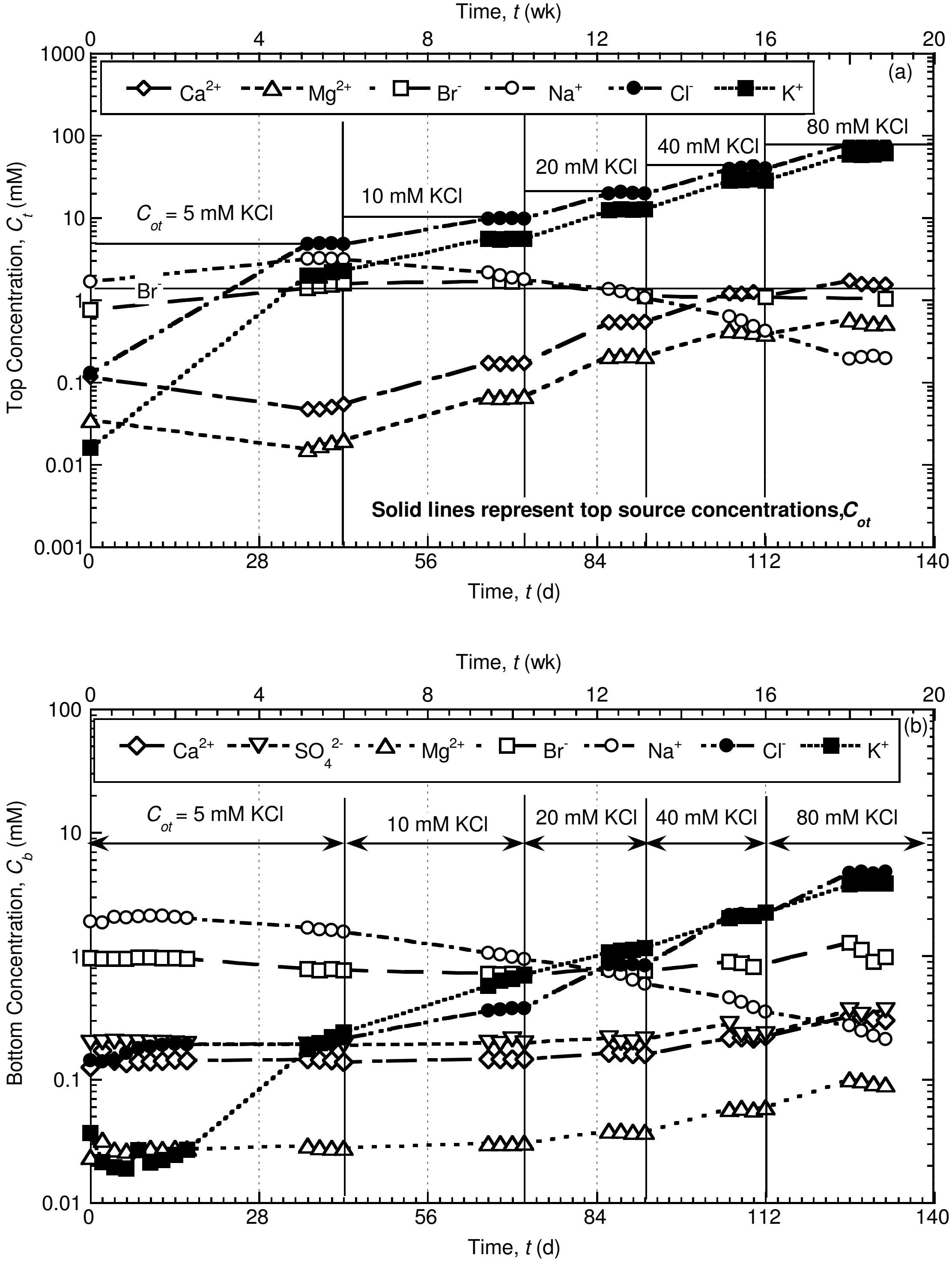

Figure 2.19. Measured concentrations of dominant chemical species in the circulation outflows for specimen RW-2: (a) concentrations in the top circulation outflow, C_t; (b) concentrations in the bottom circulation outflows, C_b.

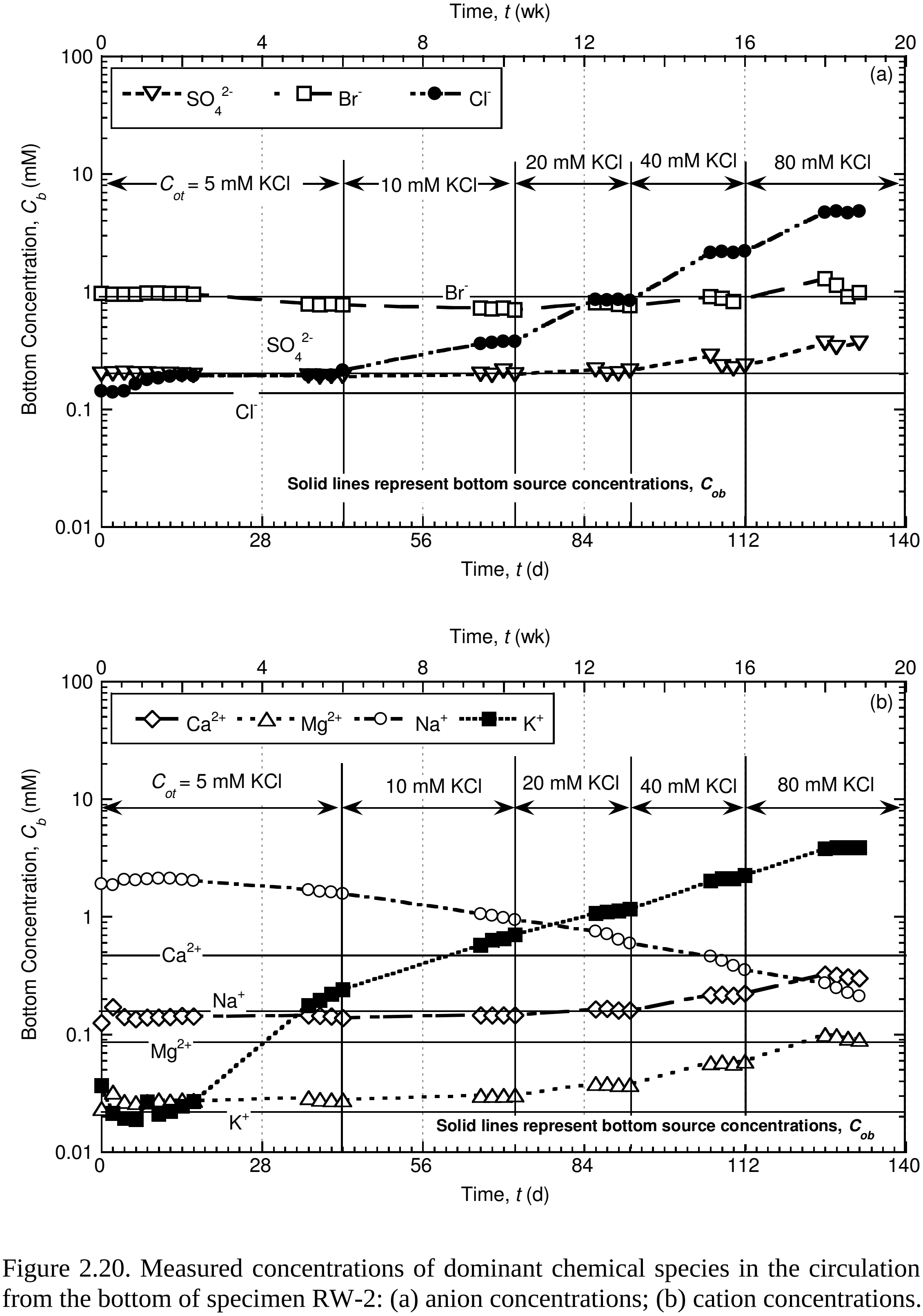

Figure 2.20. Measured concentrations of dominant chemical species in the circulation outflows from the bottom of specimen RW-2: (a) anion concentrations; (b) cation concentrations.

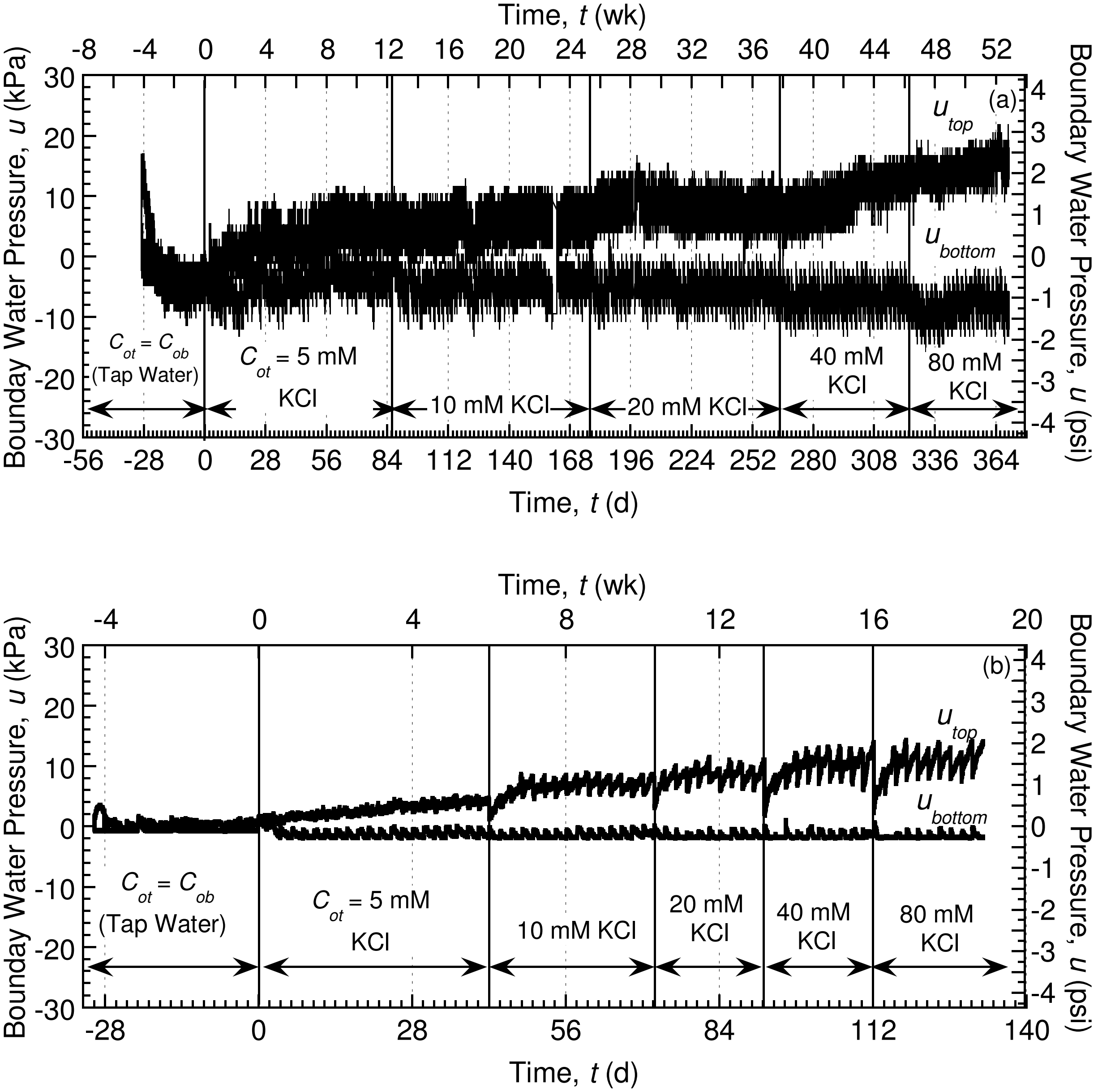

Figure 2.21. Boundary water pressures measured via in-line gage transducers: (a) RW-1; (b) RW-2.

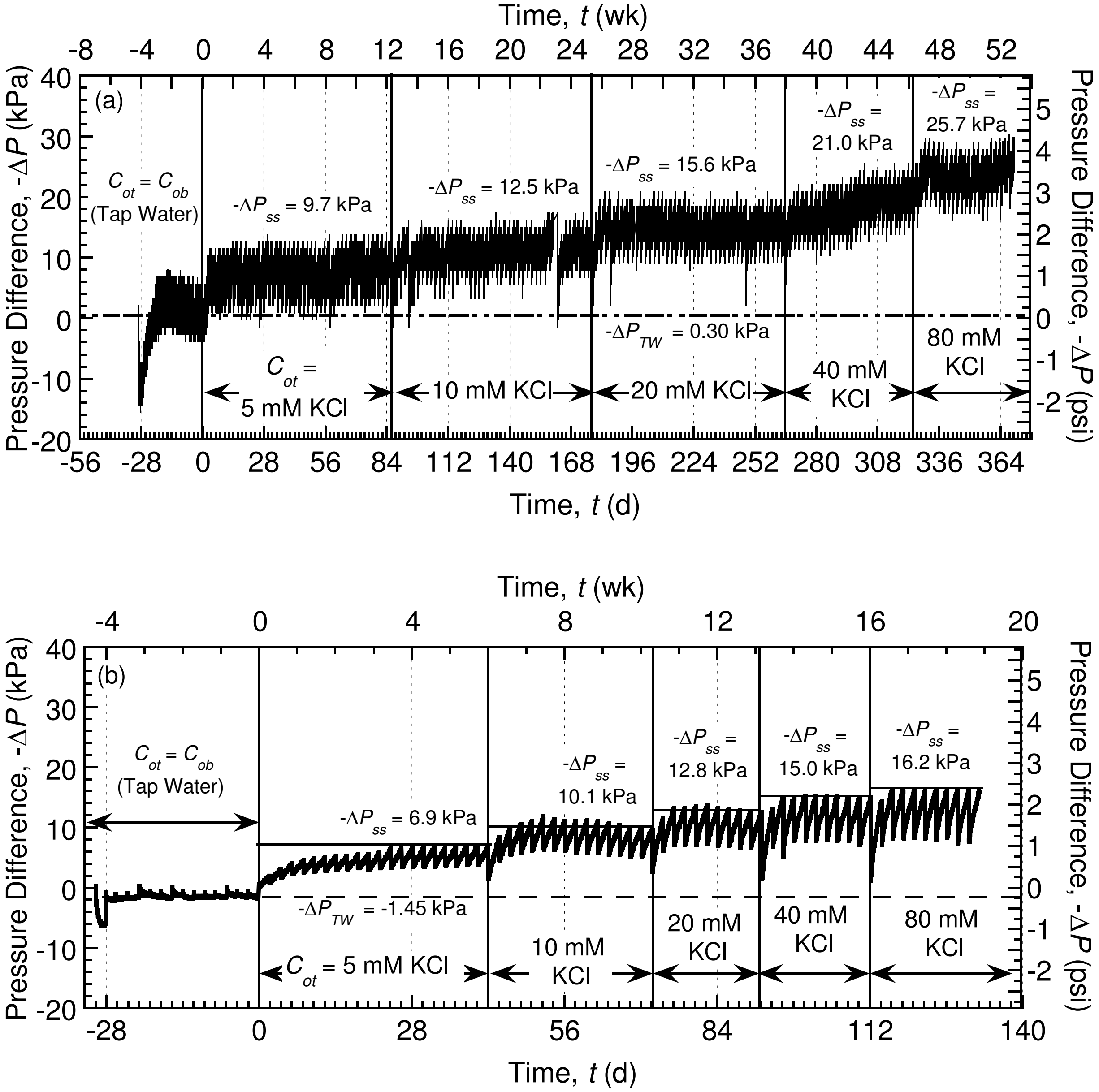

Figure 2.22. Chemico-osmotic pressure differences across the specimen measured via a differential pressure transducer: (a) RW-1; (b) RW-2.

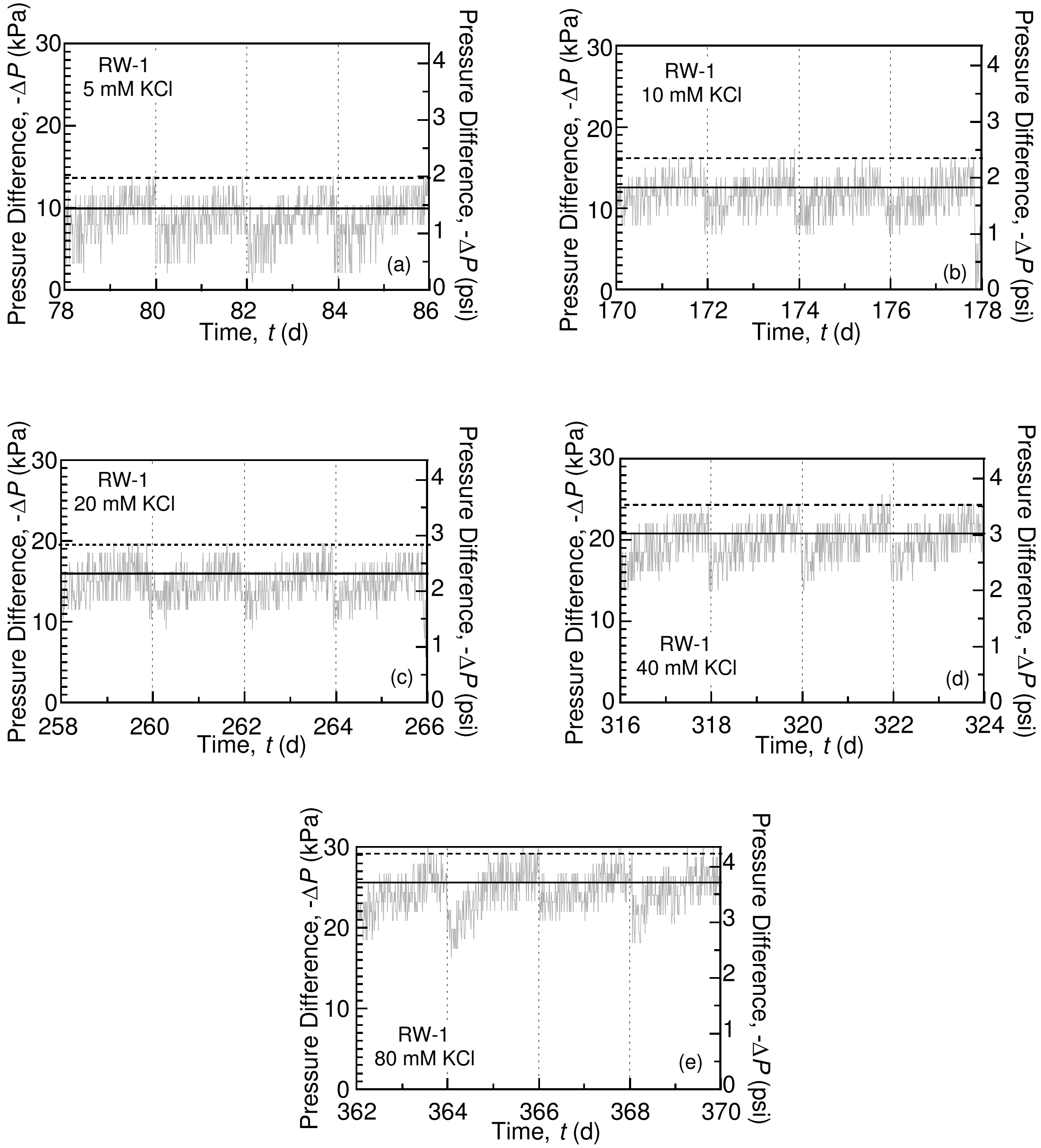

Figure 2.23. Chemico-osmotic pressure differences across specimen RW-1 at the end of each KCl testing period where the dashed and solid lines indicate the value of -ΔP_{ss} via the maximum value and the central tendency approach, respectively: (a) 5 mM KCl; (b) 10 mM KCl; (c) 20 mM KCl; (d) 40 mM KCl; (e) 80 mM KCl.

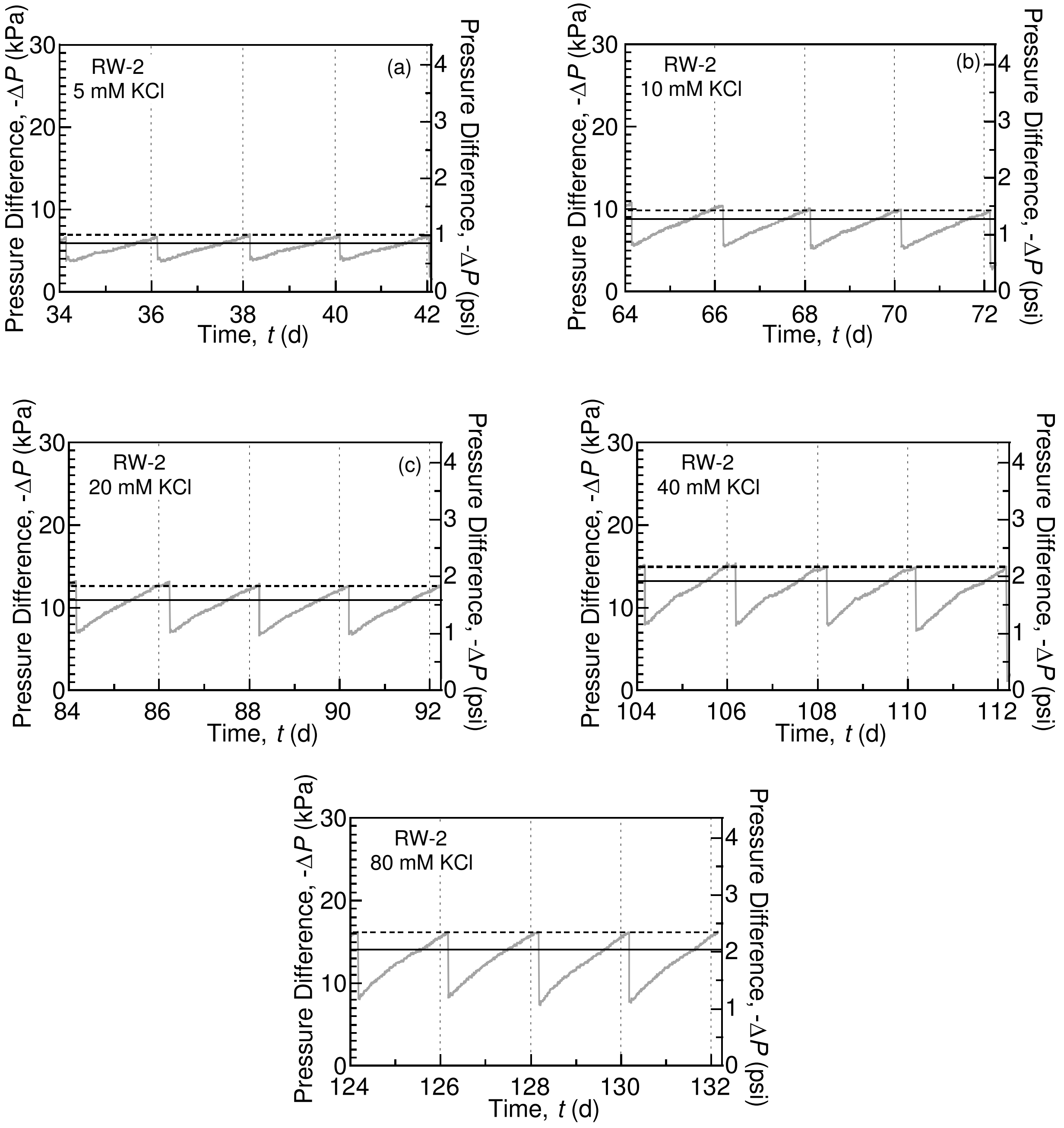

Figure 2.24. Chemico-osmotic pressure differences across specimen RW-2 at the end of each KCl testing period where the dashed and solid lines indicate the value of -ΔP_{ss} via the maximum value and the central tendency approach, respectively: (a) 5 mM KCl; (b) 10 mM KCl; (c) 20 mM KCl; (d) 40 mM KCl; (e) 80 mM KCl.

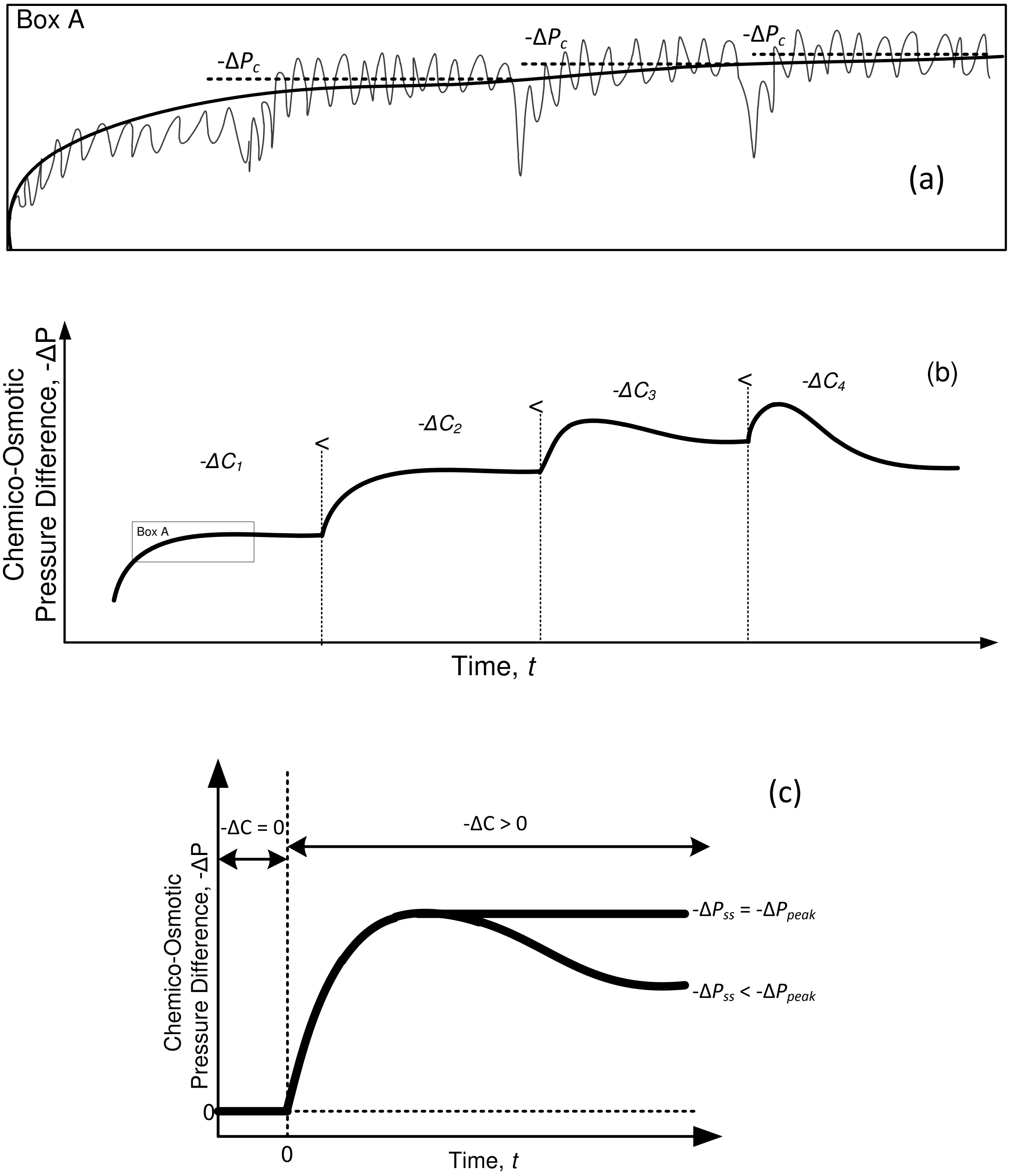

Figure 2.25. Schematics of expected trends for chemico-osmotic pressure differences: (a) zoomed-in portion showing continuous record of -Δ*P*; (b) evolution for multi-stage testing with increasing values of $C_{o,t}$; (c) single concentration stage with or without post-peak degradation.

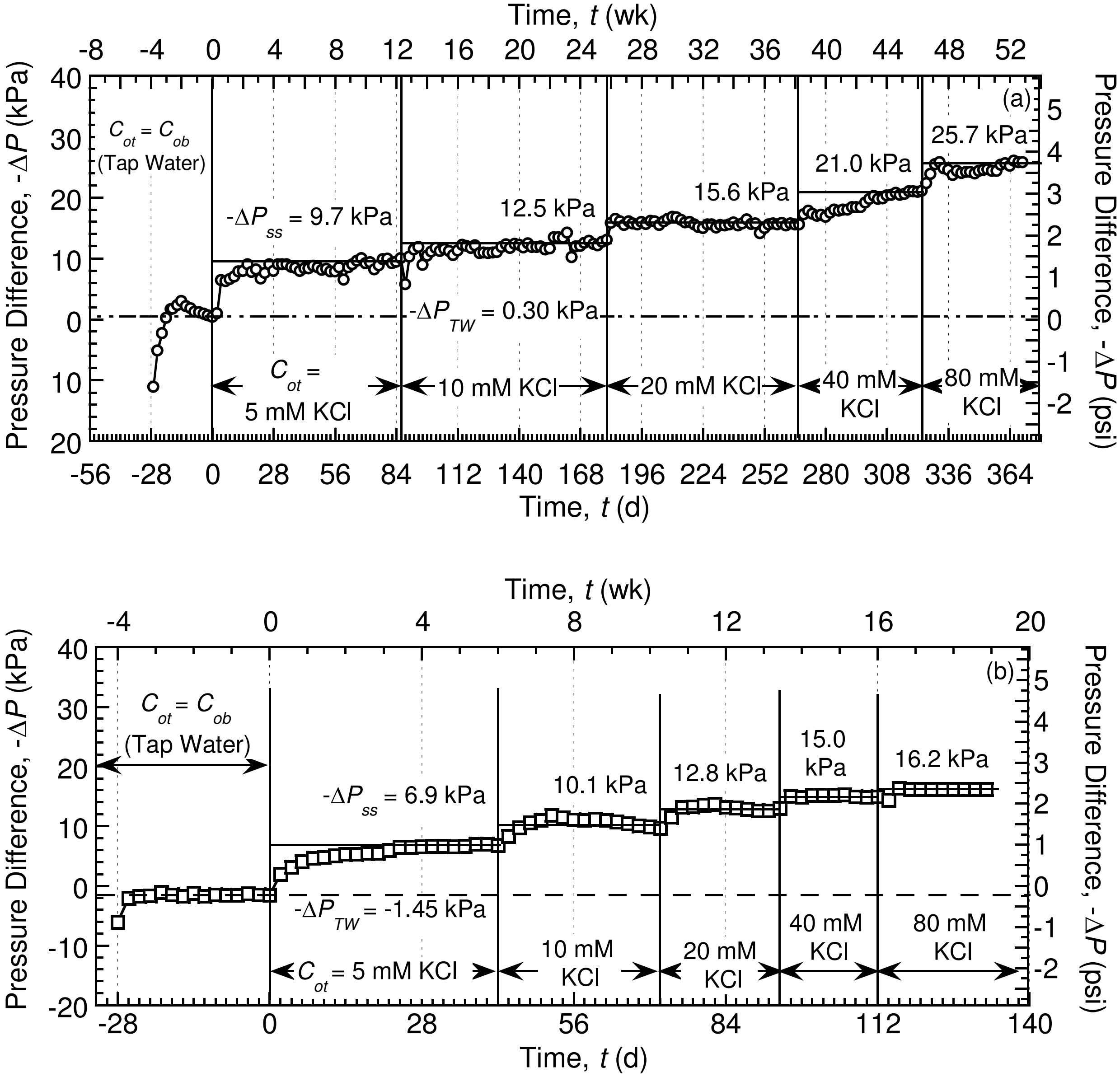

Figure 2.26. The final chemico-osmotic pressure difference generated across the specimen for every two-day pump cycle: (a) RW-1; (b) RW-2.

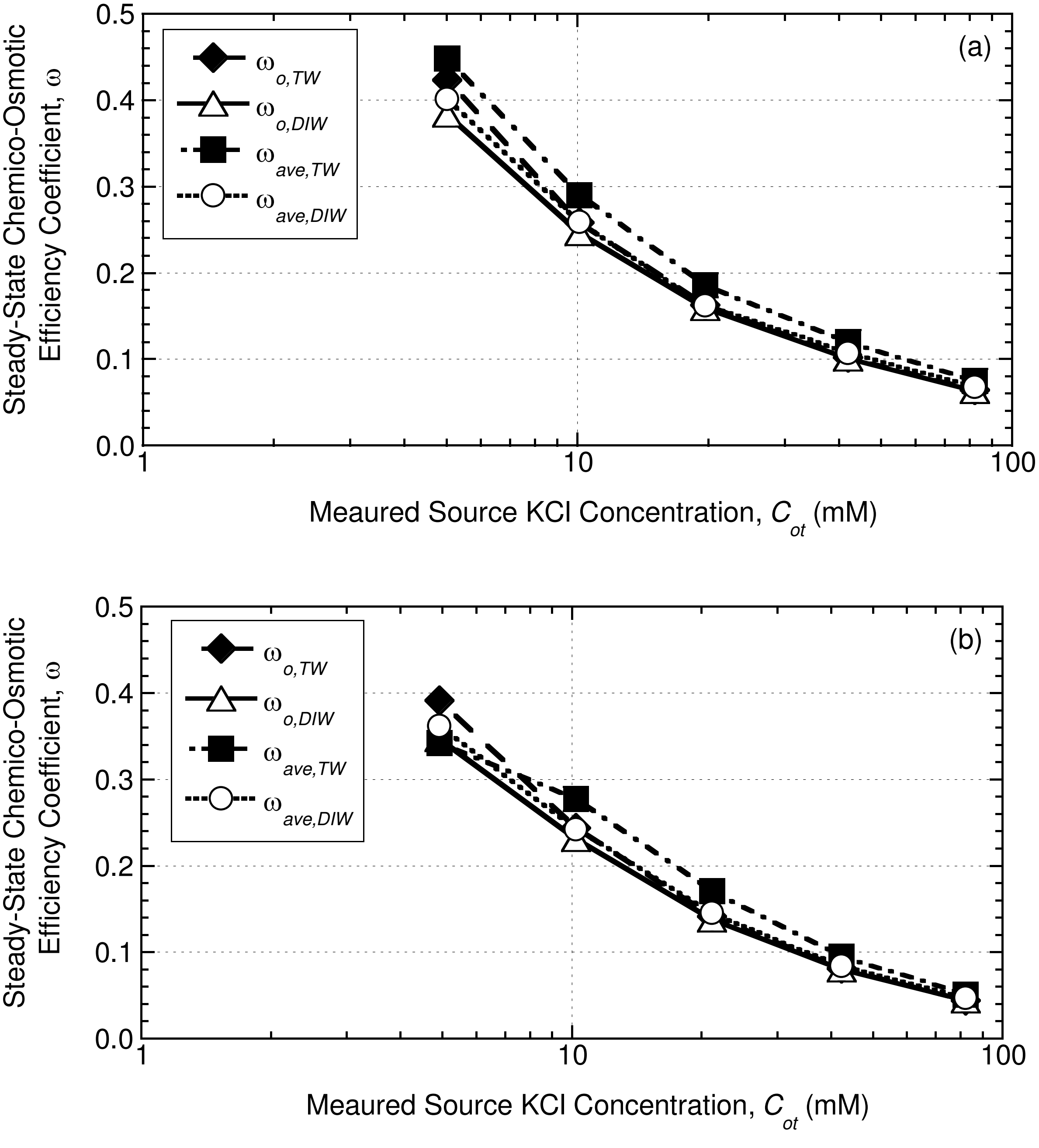

Figure 2.27. Chemico-osmotic efficiency coefficients calculated based on different methods of calculating -Δπ and therefore ω: (a) RW-1; (b) RW-2.

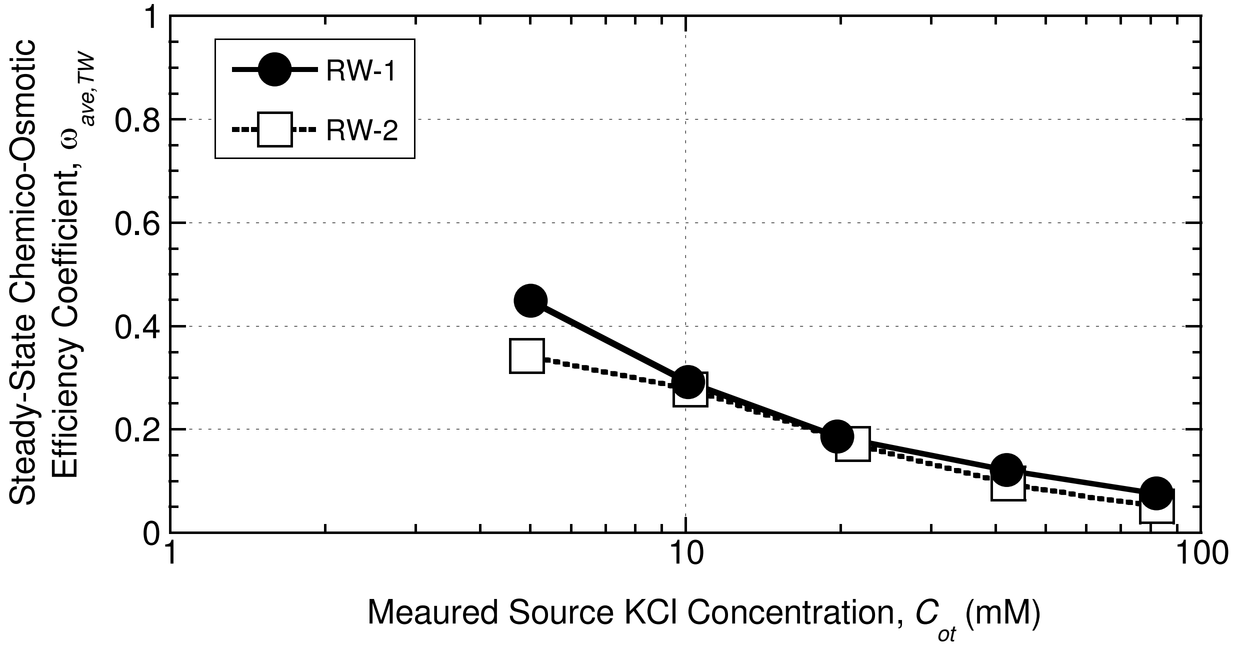

Figure 2.28. Chemico-osmotic efficiency coefficients based on -ΔC_{ave} and the imposed testing conditions (i.e., tap water circulated across the bottom boundary) for RW-1 and RW-2 tests.

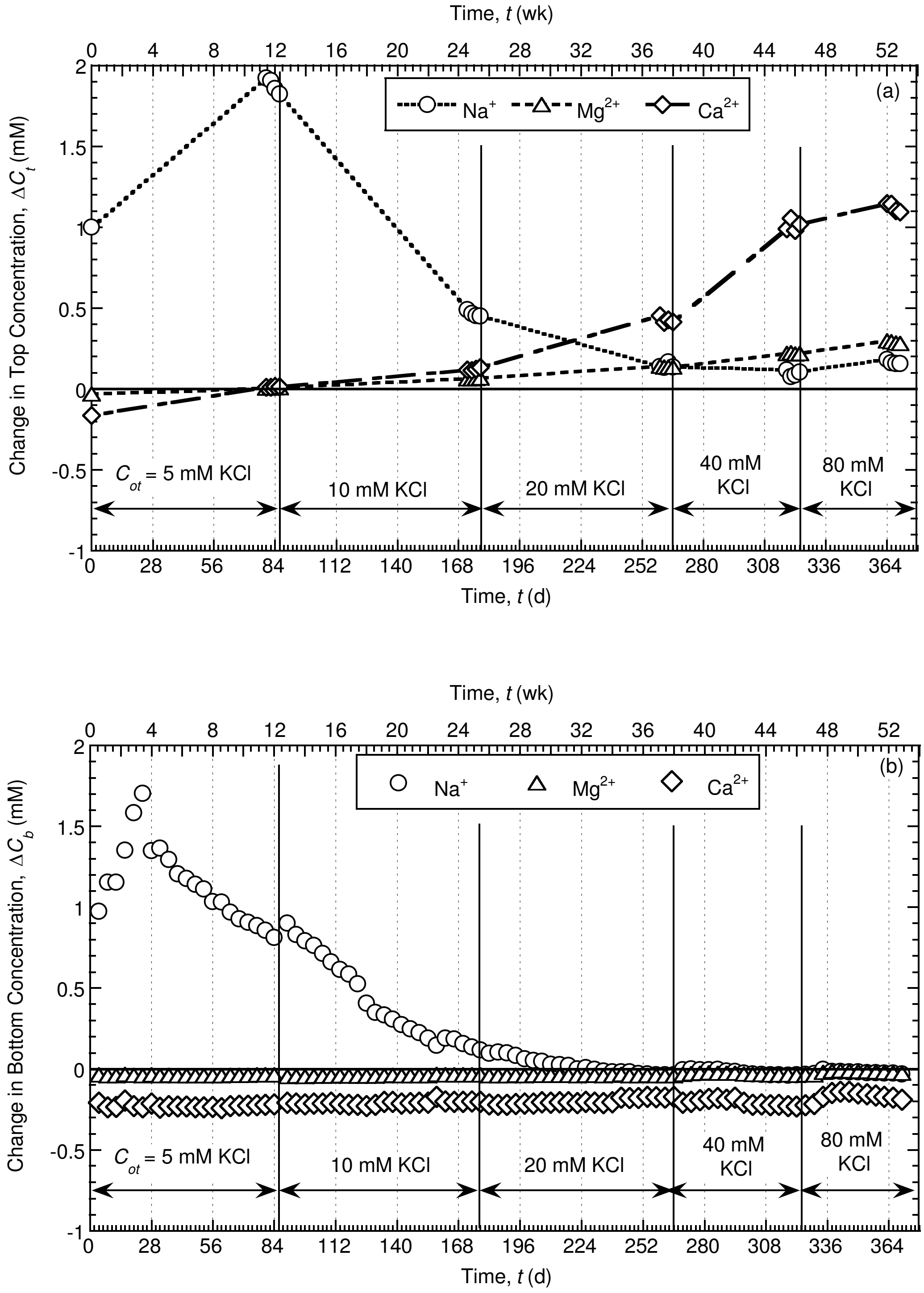

Figure 2.29. The change in concentration, calculated via Eq. 2.34, relative to the inflow (source) for predominant cation species (excluding K^+) measured in the outflow collected from the specimen boundaries: (a) top specimen boundary; (b) bottom specimen boundary.

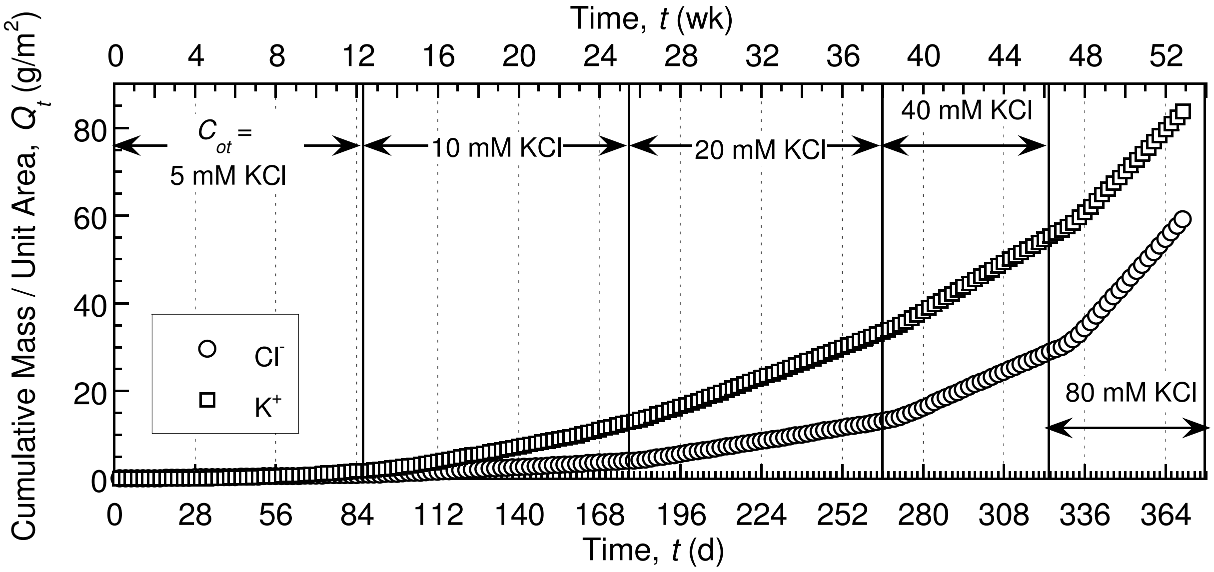

Figure 2.30. Cumulative mass data for chloride (Cl^-) and potassium (K^+) diffusing through specimen RW-1 for multiple-stage KCl concentration testing.

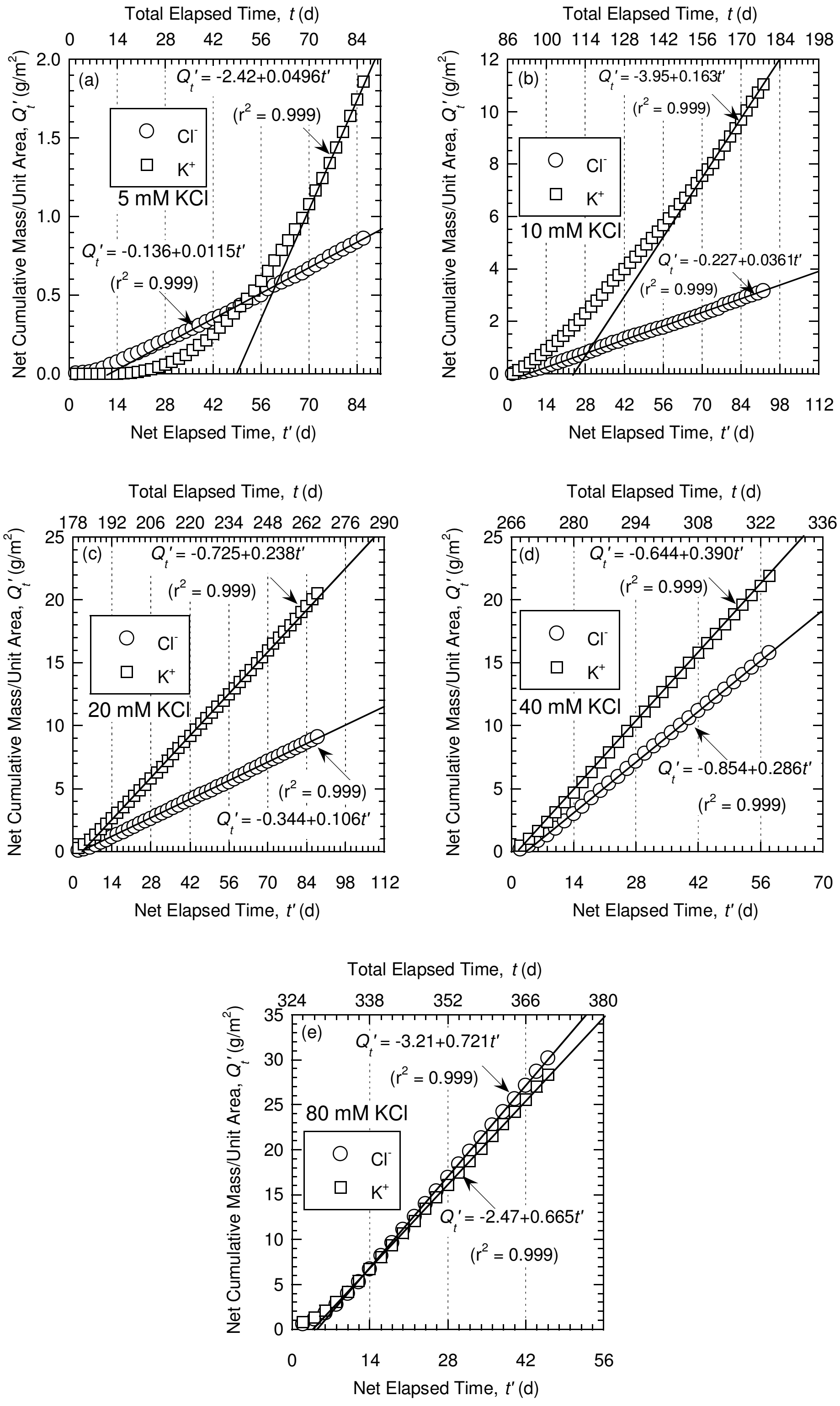

Figure 2.31. Net values of cumulative mass data with steady-state linear regressions for Cl^- and K^+: (a) 5 mM KCl; (b) 10 mM KCl; (c) 20mM KCl; (d) 40 mM KCl; (e) 80 mM KCl.

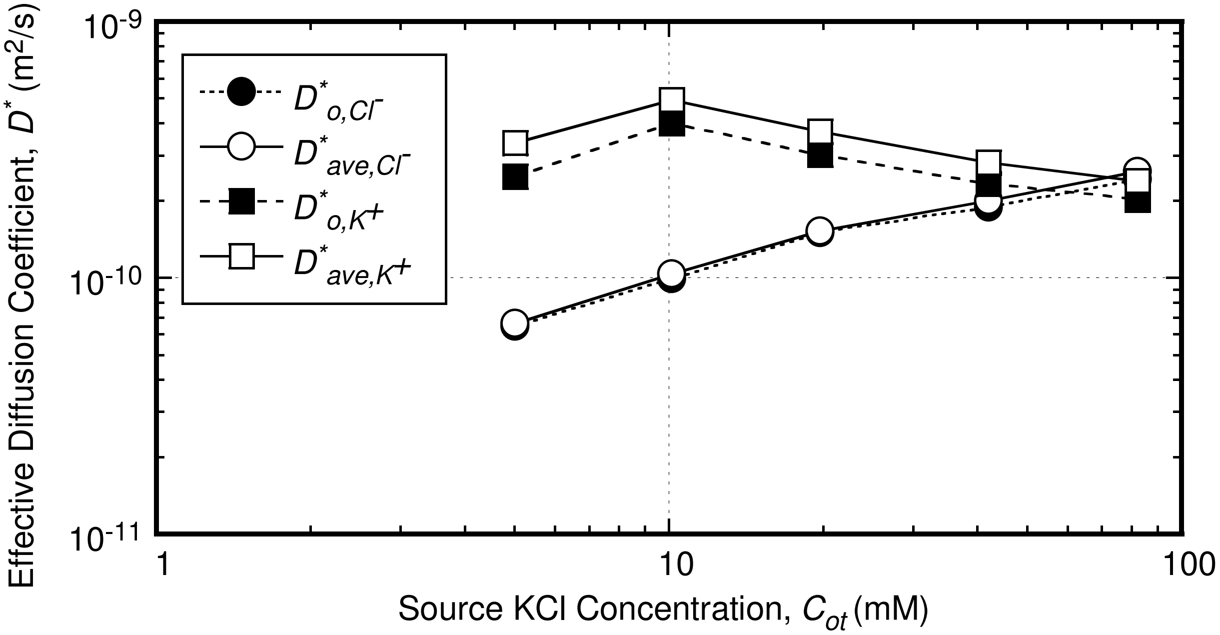

Figure 2.32. Effective diffusion coefficients for Cl^- and K^+ based on ΔC_o and ΔC_{ave}.

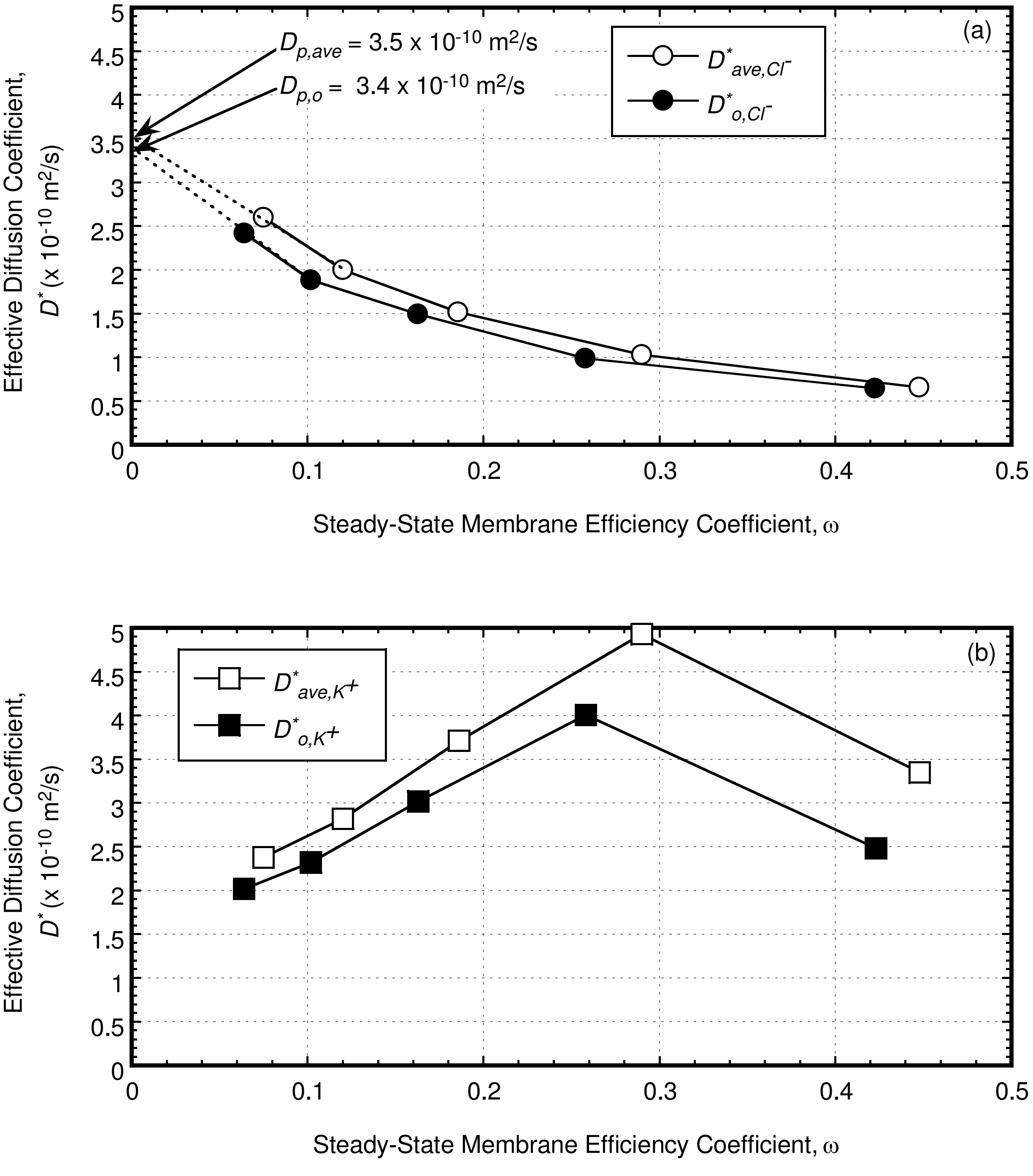

Figure 2.33. Effective diffusion coefficients as a function of the steady-state membrane efficiency coefficients based on ΔC_o and ΔC_{ave}: (a) Cl^- data; (b) K^+ data.

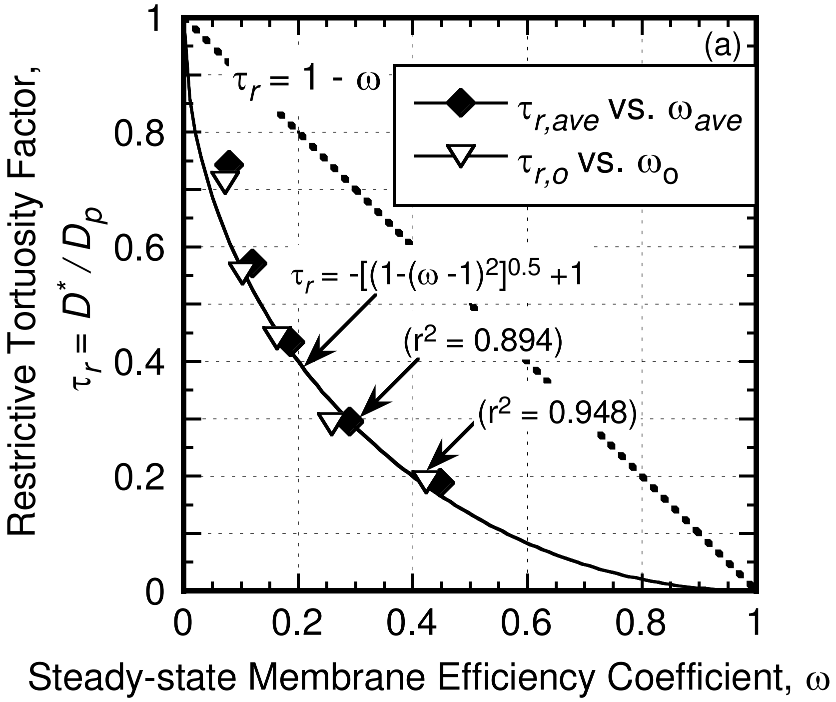

Figure 2.34. Restrictive tortuosity factors based on the measured effective diffusion coefficients (D^*) and pore diffusion coefficients (D_p) for chloride, Cl^-.

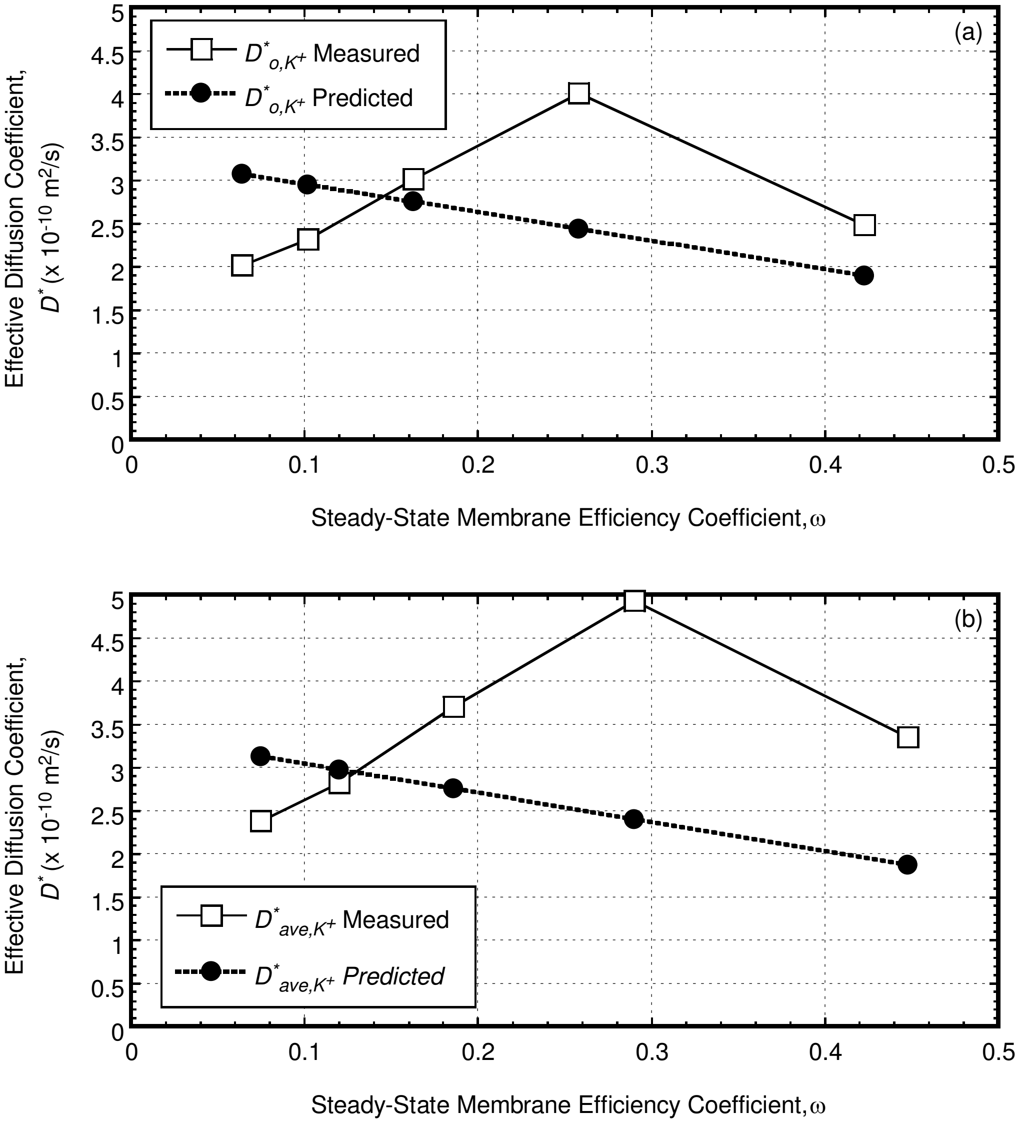

Figure 2.35. Measured and predicted effective diffusion coefficients, D^*, for potassium, K^+.

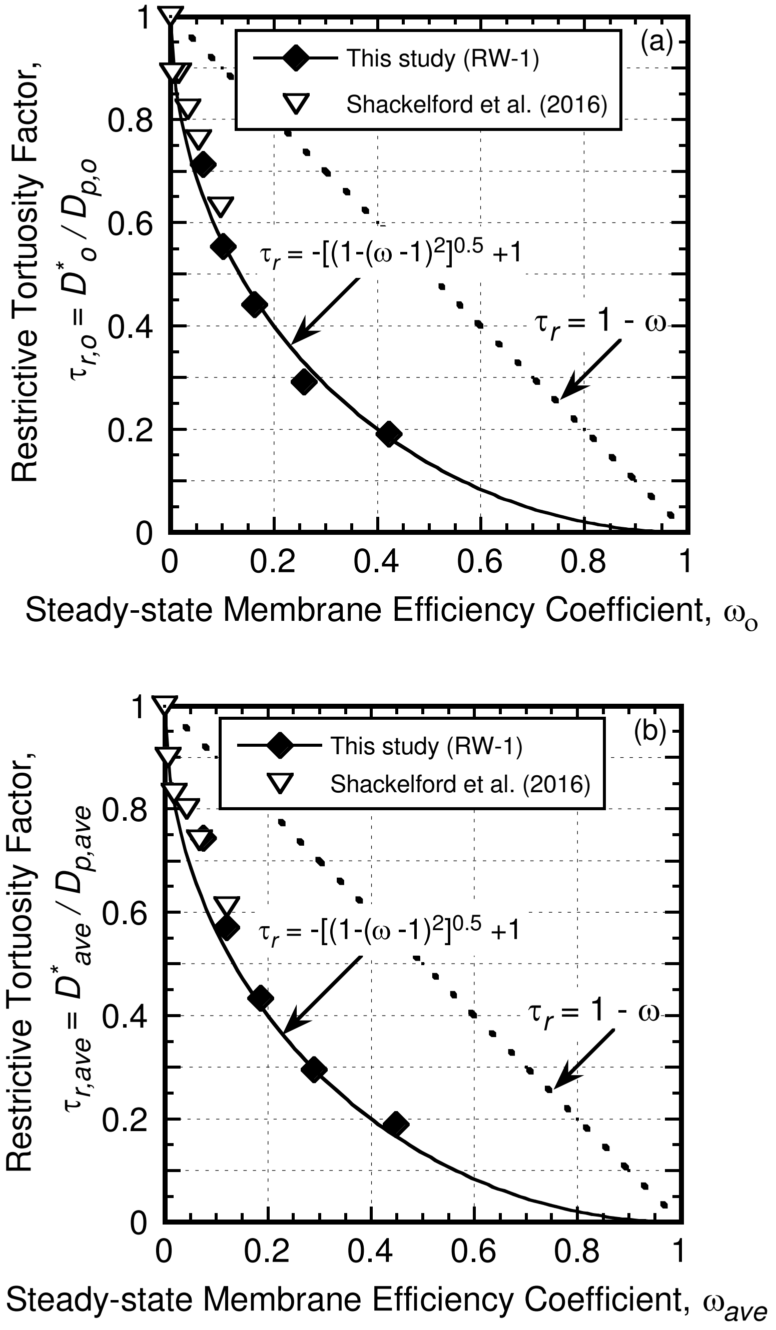

Figure 2.36. Comparison of restrictive tortuosity factors based on the measured effective diffusion coefficients (D^*) and pore diffusion coefficients (D_p) for chloride, Cl^- for this study and Shackelford at al. (2016): (a) based on ΔC_o; (b) based on ΔC_{ave}.

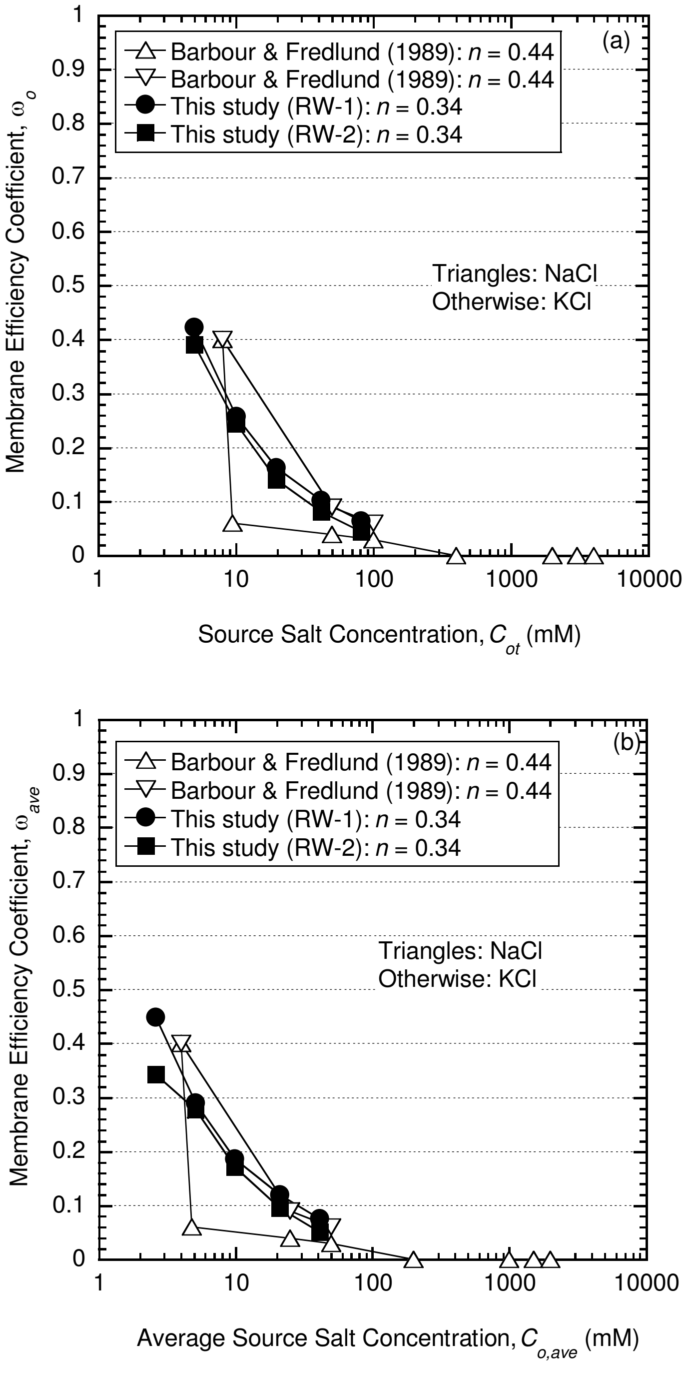

Figure 2.37. Steady-state membrane efficiency coefficients for compacted sand-bentonite specimens at difference porosities, *n*, as a function of the source salt concentration: (a) values based on the source boundary concentrations; (b) values based on the average source boundary concentrations.

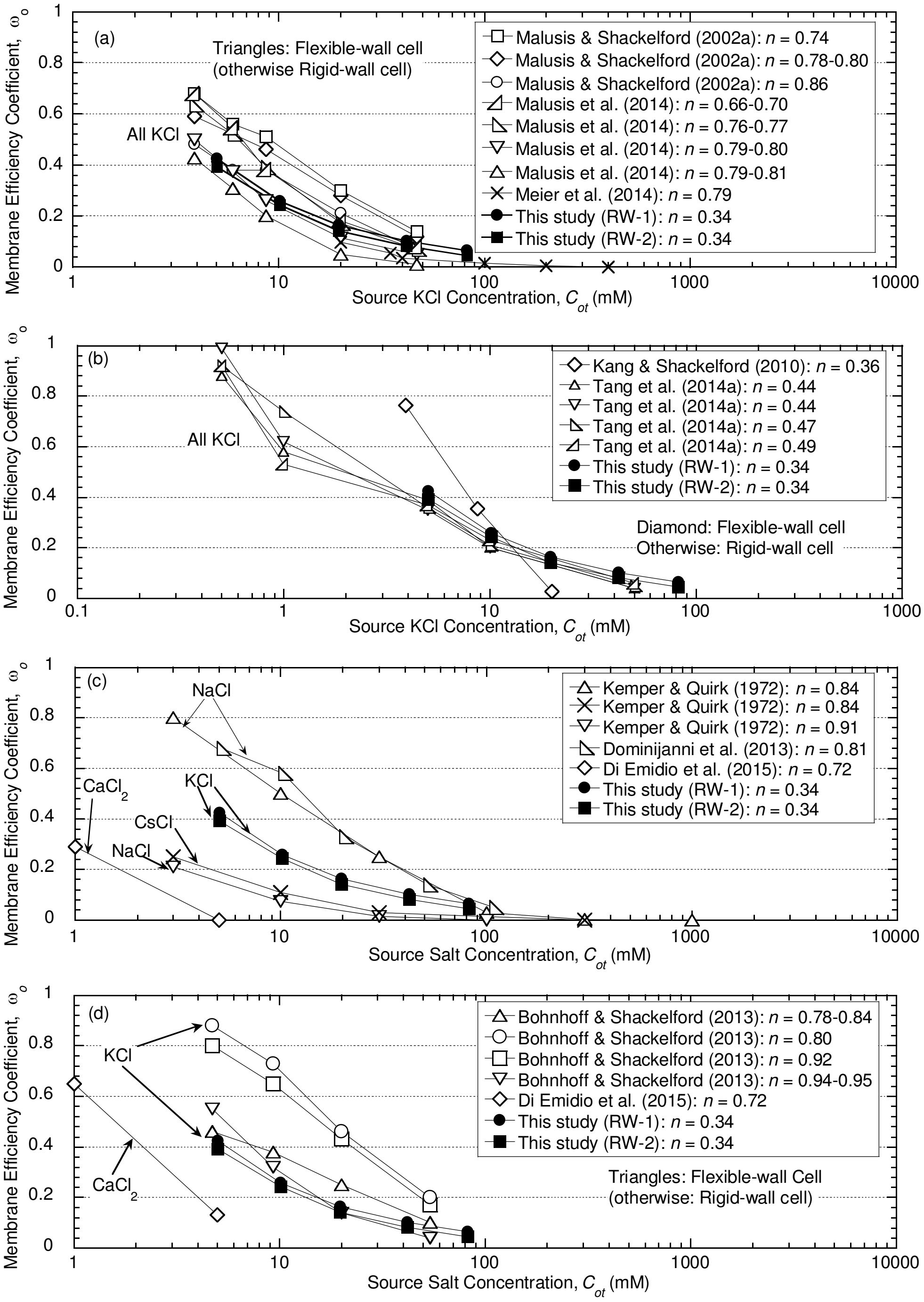

Figure 2.38. Steady-state membrane efficiency coefficients based on the average source boundary concentrations, ω_o, for specimens at difference porosities (n) as a function of the initial (measured) salt concentration at the top boundary, C_{ot}: (a) GCLs; (b) CCLs; (c) pure bentonite; (d) polymer-enhanced bentonite.

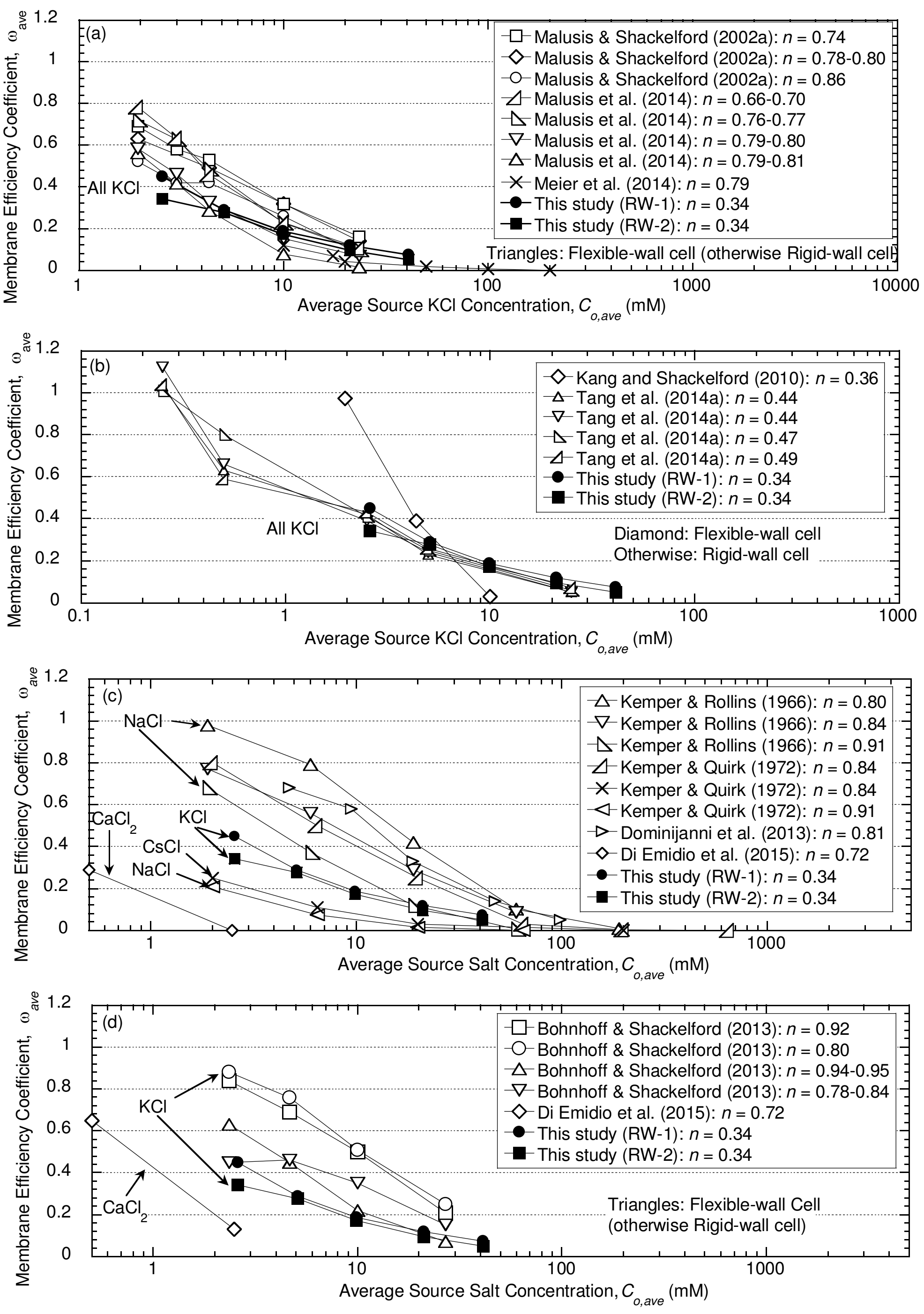

Figure 2.39. Steady-state membrane efficiency coefficients based on the average boundary concentrations, ω_{ave}, for specimens at difference porosities, n, as a function of the average (measured) source boundary concentrations, $C_{o,ave}$ (= $[C_{ot} + C_{ob}]/2$): (a) GCLs; (b) CCLs; (c) pure bentonite; (d) polymer-enhanced bentonite.

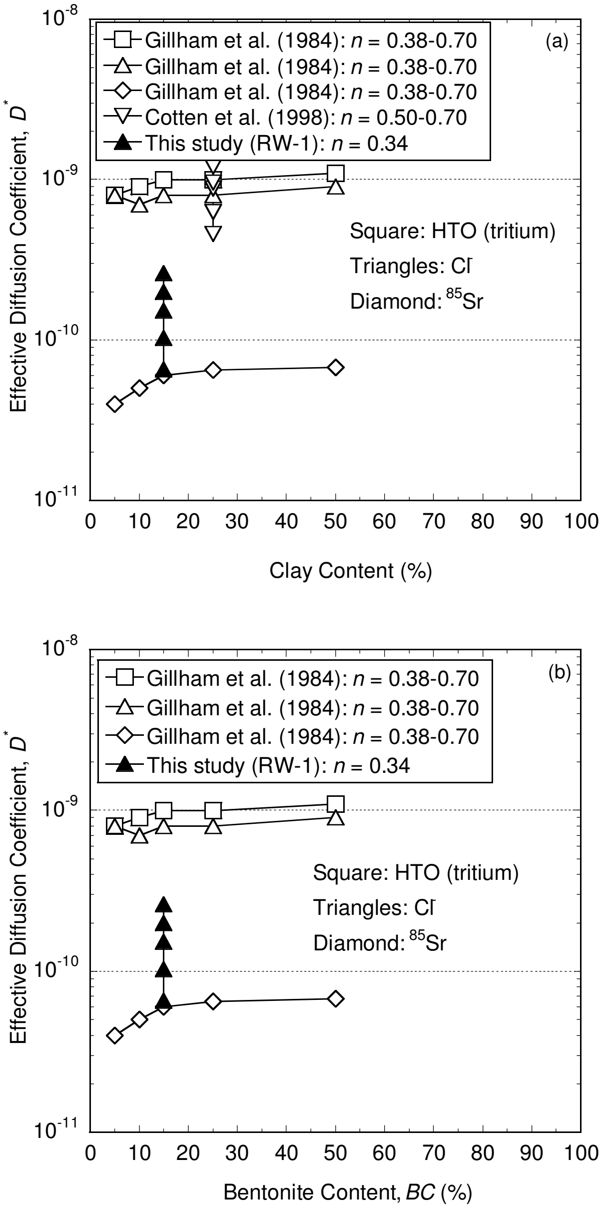

Figure 2.40. Representative effective diffusion coefficients for different chemical species: (a) compacted sand-clay mixtures; (b) compacted sand-bentonite mixtures.

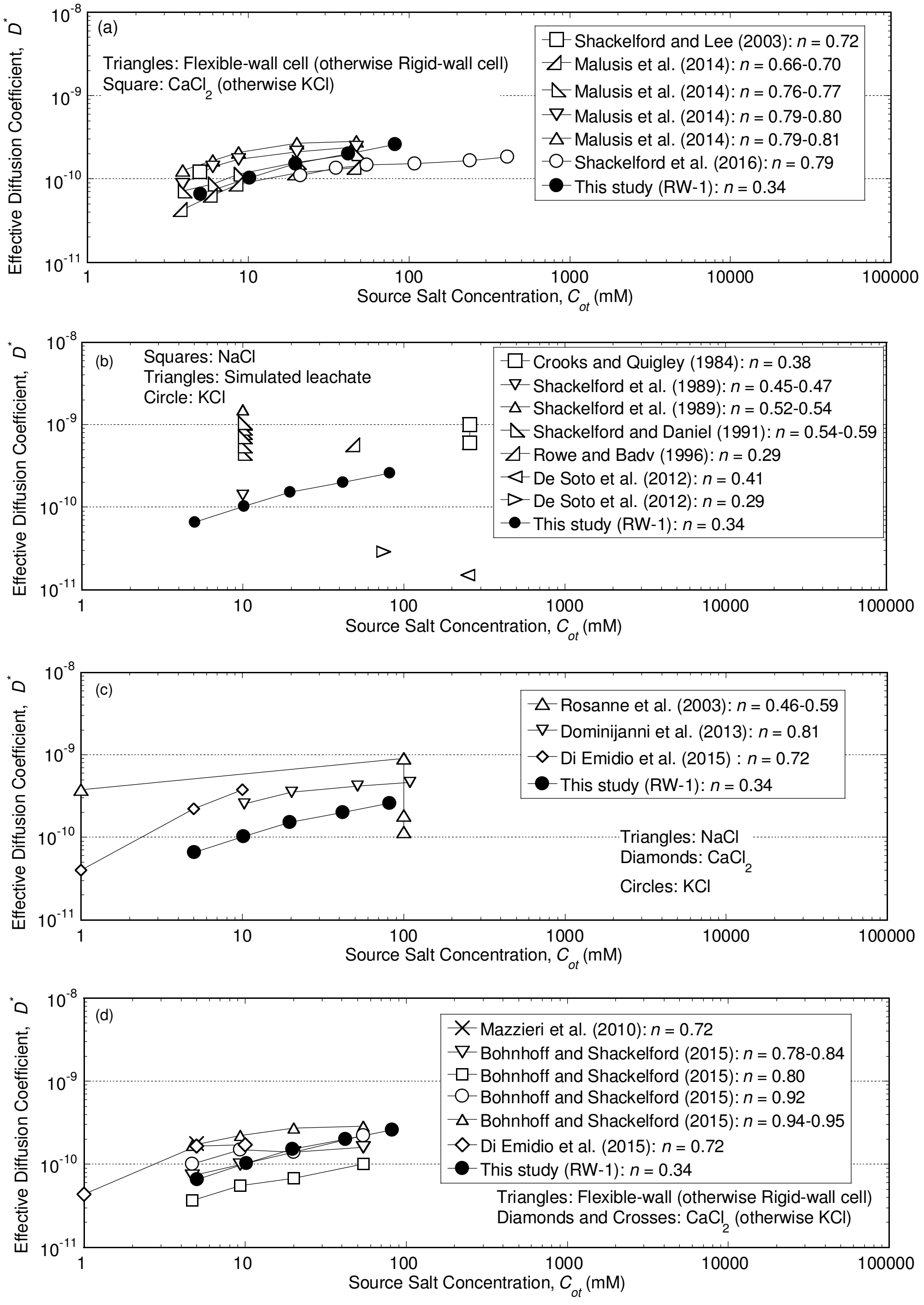

Figure 2.41. Representative effective diffusion coefficients for chloride based on different bentonite based barriers: (a) GCLs; (b) CCLs; (c) compacted bentonite; (d) polymerized bentonite.

REFERENCES

Alther, G.R., 1987. "The Qualifications of Bentonite as a Soil Sealant." *Engineering Geology*, 23(3/4), 177-191.

ASTM D422-63, 2007: Standard Test Method for Particle-Size Analysis of Soils, *Annual Book of ASTM Standards*, ASTM International, West Conshohocken, PA.

ASTM D4972-01, 2007: Standard Test Methods for pH of Soils, *Annual Book of ASTM Standards*, ASTM International, West Conshohocken, PA.

ASTM D854-10, 2010: Standard Test Methods for Specific Gravity of Soil Solids by Water Pycnometer, *Annual Book of ASTM Standards*, ASTM International, West Conshohocken, PA.

ASTM D4318-10, 2010: Standard Test Methods for Liquid Limit, Plastic Limit, and Plasticity Index of Soils, *Annual Book of ASTM Standards*, ASTM International, West Conshohocken, PA.

ASTM D5084-10, 2010: Standard Test Methods for Measurement of Hydraulic Conductivity of Saturated Porous Materials Using a Flexible Wall Permeameter, *Annual Book of ASTM Standards,* ASTM International, West Conshohocken, PA.

ASTM D7100-11, 2012: Standard Test Method for Hydraulic Conductivity Compatibility Testing of Soils with Aqueous Solutions, *Annual Book of ASTM Standards*, ASTM International, West Conshohocken, PA.

ASTM D7503-10, 2010: Standard Method for Measuring the Exchange Complex and Cation Exchange Capacity of Inorganic Fine-Grained Soils, *Annual Book of ASTM Standards*, ASTM International, West Conshohocken, PA.

ASTM D2487-11, 2011: Standard Practice for Classification of Soils for Engineering Purposes (Unified Soil Classification System), *Annual Book of ASTM Standards*, ASTM International, West Conshohocken, PA.

ASTM D698-12, 2012: Standard Test Methods for Laboratory Compaction Characteristics of Soil Using Standard Effort (12400 ft-lbf/ft3 (600 kN-m/m3)), *Annual Book of ASTM Standards*, ASTM International, West Conshohocken, PA.

Barbour, S., and Fredlund, D., 1989. "Mechanisms of Osmotic Flow and Volume Change in Clay Soils." *Canadian Geotechnical Journal*, 26(4), 551-562.

Benson, C.H., Zhai, H., and Wang, X., 1994. "Estimating Hydraulic Conductivity of Compacted Clay Liners." *Journal of Geotechnical Engineering*, 120(2), 366–387.

Benson, C.H., Daniel, D.E., and Boutwell, G.P. 1999. "Field Performance of Compacted Clay Liners." *Journal of Geotechnical and Geoenvironmental Engineering*, 125(5), 390-403.

Bohnhoff, G., 2012. *Membrane Behavior, Diffusion, and Compatibility of a Polymerized Bentonite for Containment Barrier Applications*. PhD Dissertation, Colorado State University, Fort Collins, CO.

Bohnhoff, G.L., and Shackelford, C.D., 2013. "Improving Membrane Performance via Bentonite Polymer Nanocomposite." Applied Clay Science, 86, 83-98.

Bohnhoff, G.L., and Shackelford, C.D., 2015. "Salt Diffusion through a Bentonite-Polymer Composite." *Clays and Clay Minerals, Clay Minerals Society*, 63(3), 172-189.

Cey B.D., Barbour S.L., and Hendry M.J., 2001. "Osmotic Flow through a Cretaceous Clay in Southern Saskatchewan, Canada." Canadian Geotechnical Journal, 38, 1025-1033.

Cotten, T.E., Davis, M.M., and Shackelford, C.D. 1998. "Effects of Test Duration and Specimen Length on Diffusion Testing of Unconfined Specimens." *Geotechnical Testing Journal*, 21(2), 79-94.

Creek, D., and Shackelford, C., 1992. "Permeability and Leaching Characteristics of Fly Ash Liner Materials." *Soils, Geology, and Foundations*, Geoenvironmental and Engineering Properties of Rock, Soil, and Aggregate, Transportation Research Record 1345, TRB, NRC, National Academy Press, Washington, DC, 74-83.

Crooks, V.E., and Quigley, R.M., 1984. "Saline Migration through Clay: A Comparative Laboratory and Field Investigation." *Canadian Geotechnical Journal*, 21, 349-362.

Daniel, D.E., 1987. "Earthen Liners for Land Disposal Facilities." *Geotechnical Practice for Waste disposal '87*, Woods. R.D. eds., GSP 13, ASCE, 21-39.

Daniel, D. E., 1993. "Clay Liners." *Geotechnical Practice for Waste Disposal*, Daniel, D.E., eds., Chapman & Hall, London, England, 137- 163.

Daniel, D.E., and Benson, C.H., 1990. "Water Content-Density Criteria for Compacted Soil Liners." *Journal of Geotechnical Engineering*, ASCE, 116(12), 1811-1830.

De Soto, I.S., Ruiz, A.I., Ayora, C., Garcia, R., Regadio, M., Cuevas, J., 2012. "Diffusion of Landfill Leachate through Compacted Natural Clays Containing Small Amounts of Carbonates and Sulfates." *Applied Geochemistry*, 27, 1202-1213

Di Emidio, G., Mazzieri, F., Verastegui-Flores, R.D., Van Impe, W., Bezuijen, A., 2015. "Polymer-Treated Bentonite Clay for Chemical-Resistant Geosynthetic Clay Liners." *Geosynthetics International*, 22 (1), 125-137.

Dominijanni, A. and Manassero, M., 2008. "Influence of Membrane Behavior on Contaminant Transport through Geosynthetic Clay Liners." *Characterization, Monitoring, and Modeling of GeoSystems*, Alshawabkeh, A.N. Reddy, K.R., and Khire, M.V. Eds., GeoCongress 2008, ASCE, Reston, Virginia, USA, 814-821.

Dominijanni, A. and Manassero, M., 2012. "Modelling the Swelling and Osmotic Properties of Clay Soils. Part I. The Phenomenological Approach." *International Journal of Engineering Science* 51, 32-50.

Dominijanni, A., Manassero, M, and Puma, S., 2013. "Coupled Chemical-Hydraulic-Mechanical Behavior of Bentonites." *Gèotechnique*, 63(3), 191-205.

Dow Chemical Company, 2000. "DOWICIL QK-20 Antimicrobial." Product Information, Form No. 253-01184-0100X/GW, Dow Chemical Company, Midland, MI.

Evans, J., Shackelford, C., Yeo, S., and Henning, J., 2008. "Membrane Behavior of Soil–Bentonite Slurry-Trench Cutoff Walls." *Soil and Sediment Contamination*, 17(4), 316–322.

Fritz, S., 1986. "Ideality of Clay Membranes in Osmotic Processes: A Review." *Clays and Clay Minerals*, 34(2), 214-223.

Garlanger, J.E., Cheung, F.K., and Bishar, S.T. 1987. "Quality Control Testing for a Sand-Bentonite Liner." *Geotechnical Practice for Waste Disposal '87*, Woods, R.D., ed., ASCE, New York, NY, 488-499.

Gillham, R.W., Robin, M.J.L., and Dytynyshyn, D.J., 1984. "Diffusion of Nonreactive and Reactive Solutes through Fine-Grained Barrier Materials." *Canadian Geotechnical Journal*, 21, 541-550.

Gipson, A.H., Jr. 1985. "Permeability Testing on Clayey Soil and Silty Sand-Bentonite Mixture

Using Acid Liquor." *Hydraulic Barriers in Soil and Rock*, STP 874, Johnson, A.I., Frobel, R.K., Cavalli, N.J., and Pettersson, C.B., eds., ASTM, West Conshohocken, Pa., 140-54.

Gleason, M.H., Daniel, D.E., and Eykholt, G.R., 1997. "Calcium and Sodium Bentonite for Hydraulic Containment Applications." *Journal of Geotechnical and Geoenvironmental Engineering*, 123(5), 438-445.

Groenevelt, P., and Elrick, D., 1976. "Coupling Phenomena in Saturated Homo-Ionic Montmorillonite: II. Theoretical." *Soil Science Society of America Journal*, 40(6), 820-823.

Haug, M.D. and Wong, L.C. 1992. "Impact of Molding Water Content on the Hydraulic Conductivity of Compacted Sand-Bentonite." *Canadian Geotechnical Journal*, 29(2), 253-262.

Henning, J., Evans, J., and Shackelford, C. (2006). "Membrane Behavior of Two Backfills from Field-Constructed Soil-Bentonite Cutoff Walls." *Journal of Geotechnical and Geoenvironmental Engineering*, 132(10), 1243–1249.

Howell, J.L. and Shackelford, C.D., 1997. "Hydraulic Conductivity of Sand Admixed with Processed Clay Mixtures." Proceedings, *14th International Conference on Soil Mechanics and Foundation Engineering*, Hamburg, Germany, Sept. 6-12, Balkema, A.A. Rotterdam, The Netherlands, Vol. 1, 307-310.

Howell, J.L., Shackelford, C.D., Amer, N.H., and Stern, R.T., 1997. "Compaction of Sand-Processed Clay Soil Mixtures." *Geotechnical Testing Journal*, 20(4), 443-458.

Kang, J., and Shackelford, C., 2009. "Clay Membrane Testing Using a Flexible-Wall Cell under Closed-System Boundary Conditions." *Applied Clay Science*, 44(1-2), 43-58.

Kang, J., and Shackelford, C., 2010. "Membrane Behavior of Compacted Clay Liners." *Journal of Geotechnical and Geoenvironmental Engineering*, 136(10), 1368-1382.

Kang, J., and Shackelford, C., 2011. "Consolidation Enhanced Membrane Behavior of a Geosynthetic Clay Liner." *Geotextiles and Geomembranes*, 29, 544-556.

Keijzer, T., Kleingeld, P., and Loch, J., 1999. "Chemical Osmosis in Compacted Clayey Material and the Prediction of Water Transport." *Engineering Geology,* 53(2), 151-159.

Keijzer, T., and Loch, J., 2001. "Chemical Osmosis in Compacted Dredging Sludge." *Soil Science Society of America Journal*, 65(4), 1045-1055.

Kemper, W., and Maasland, D., 1964. "Reduction in Salt Content of Solution Passing through Thin Films Adjacent to Charged Surfaces." *Proceedings of the Soil Science Society of America*, 28(3), 318-323.

Kemper, W. and Rollins, J., 1966. "Osmotic Efficiency Coefficients across Compacted Clays." *Proceedings of the Soil Science Society of America*, 30(5), 529-534.

Kemper, W., and Quirk, J., 1972. "Ion Mobilities and Electric Charge of External Clay Surfaces Inferred from Potential Differences and Osmotic Flow." *Soil Science Society of America*, 36(3), 426-433.

Kenney, T.C., van Veen, W.A., Swallow, M.A., and Sungaila, M.A. 1992. "Hydraulic Conductivity of Compacted Bentonite-Sand Mixtures." *Canadian Geotechnical Journal*, 29(3), 364-374.

Kraus, J.F., Benson, C.H., Erickson, A.E., and Chamberlain, E.J. 1997. "Freeze-Thaw Cycling and Hydraulic Conductivity of Bentonitic Barriers." *Journal of Geotechnical and Geoenvironmental Engineering*, 123(3), 229-238.

Lee, J.-M., and Shackelford, C.D., 2005. "Concentration Dependency of the Prehydration Effect for a Geosynthetic Clay Liner." *Soils and Foundations*, 45(4), 27-41.

Lo, I., Liljestrand, H., Daniel, D., 1994. "Waste-Soil Interactions and Adsorption Parameters for Pollutant transport through Montmorillonite and Modified Montmorillonite Clay Liner Materials." *Hydraulic Conductivity and Waste Contaminant Transport in Soil,*D.E. Daniel and S.J. Trautwein Eds., STP 1142, ASTM, West Conshohoken, PA, 422-438.

Lo, I., Luk, A., and Yang, X., 2004. "Migration of Heavy Metals in Saturated Sand and Bentonite/Soil Admixture." *Journal of Environmental Engineering*, 130(8), 906–909.

Lundgren, T.A. 1981. "Some Bentonite Sealants in Soil Mixed Blankets." Proceedings, *10th International Conference on Soil Mechanics and Foundation Engineering*, Stockholm, Sweden, June 15-19, Balkema, A. A. eds., Rotterdam, The Netherlands, Vol. 2, 349-354.

MacKay, R., 1946. ‘‘The Control of Impounding Structures on Ore Deposition.’’ *Economic Geology and the Bulletin of the Society of Economic Geologists,* Economic Geology, New Haven, CT, 13–46.

Malusis, M., and Shackelford, C., 2002a. "Chemico-Osmotic Efficiency of a Geosynthetic Clay Liner." *Journal of Geotechnical and Geoenvironmental Engineering*, 128(2), 97-106.

Malusis, M., and Shackelford, C., 2002b. "Coupling Effects during Steady-State Solute Diffusion through a Semipermeable Clay Membrane." *Environmental Science and Technology,* 36(6), 3212-1319.

Malusis, M.A., Kang, J.-B., and Shackelford, C.D., 2014. "Restricted Salt Diffusion in a Geosynthetic Clay Liner." *Environmental Geotechnics*, ICE, Thomas Telford Ltd., London, 2(2), 68-77.

Malusis, M., Shackelford, C., and Olsen, H., 2001. "Flow and Transport through Clay Membrane Barriers." *Geoenvironmental Engineering, Geoenvironmental Impact Management*, R. Yong and H. Thomas, Eds., *Thomas Telford Publ*., London, UK, 334-341.

Manassero, M. and Dominijanni, A., 2003. "Modelling the Osmosis Effect on Solute Migration through Porous Media." *Géotechnique*, 53(5), 481-492.

Mazzieri, F., Di Emidio, G., and Van Impe, P., 2010. "Diffusion of Calcium Chloride in a Modified Bentonite: Impact on Osmotic Efficiency and Hydraulic Conductivity." *Clays and Clay Minerals*; 58(3), 351-363.

Meier, A., Sample-Lord, K., Castelbaum, D., Kallase, S., Moran, B., Ray, T., and Shackelford, C., 2014. "Persistence of Semipermeable Membrane Behavior for a Geosynthetic Clay Liner." *Proceedings, 7th International Conference on Environmental Geotechnics*, A. Bouazza, S. Yuen, and B. Brown, Eds., Nov. 10-14, 2014, Melbourne, Australia (ISBN 978-1-922107-23-7), 496-503.

O'Sadnick, D.L., Simpson, B.E., and Kasel, G.K. 1995. "Evaluation and Performance of a Sand/Bentonite Liner." *Geoenvironment 2000*, Y. B. Acar and D. E. Daniel, eds., ASCE, New York, NY, 688-701.

Quigley, R., Yanful, E., and Fernandez, F., 1987. "Ion Transfer by Diffusion through Clayey Barriers." *Geotechnical Practice for Waste Disposal, Special Publication No. 13*, R. Woods, Ed., ASCE, New York, 137-158.

Rosanne, M., Mammar, N., Koudina, N., Prunet-Foch, B., Thovert, J.F., Tevissen, E., and Adler, P.M., 2003. "Transport Properties of Compacted Clays II. Diffusion." *Journal of Colloid and Interface Science,* 260, 195-203.

Rowe, R., and Badv, K., 1996. "Chloride Diffusion through Clayey Silt Underlain by Fine Sand or Silt." *Journal of Geotechnical Engineering*, 60-68.

Rowe, R.K. and Fraser, M.J., 1995. "Effect of Uncertainty in the Assessment of the Potential Impact of Waste Disposal Facilities." Proceedings, *Geoenvironmental 2000*, ASCE Specialty Conference, GSP 46, Vol. 1, New Orleans, LA, Feb, 270-284.

Saindon, R., and Whitworth, T.M., 2005. "Hyperfiltration of NaCl Solutions Using a Simulated Clay/Sand Mixture at Low Compaction Pressures." *Aquatic Geochemistry*, 11:433-444.

Sample-Lord, K., 2015. *Membrane Behavior and Diffusion in Unsaturated Sodium Bentonite*. PhD Dissertation, Colorado State University, Fort Collins, CO.

Shackelford, C., 1991. "Laboratory Diffusion Testing for Waste Disposal – A review." *Journal of Contaminant Hydrology*, 7(3), 177-217.

Shackelford, C., 1994. "Waste Soil Interactions that Alter Hydraulic Conductivity." *Hydraulic Conductivity and Waste Contaminant Transport in Soil,* Daniel, D.E. and Trautwein, S.J. eds., STP 1142, ASTM, West Conshohoken, PA, 111-168.

Shackelford, C., 2013. "Membrane Behavior in Engineered Bentonite-Based Containment Barriers: State of the Art." *Proceedings of Coupled Phenomena in Environmental Geotechnics (CPEG)*, M. Manassero, A. Dominijanni, S. Foti, and G. Musso, eds., July 1-3, Torino, Italy, CRC Press/Balkema, Taylor & Francis Group, London, 45-60.

Shackelford, C., 2014. "The ISSMGE Kerry Rowe Lecture: The Role of Diffusion in Environmental Geotechnics." *Canadian Geotechnical Journal*, NRC, 51(11), 1219-1242

Shackelford, C, Benson, C.H., Katsumi, T., Edil, T.B., and Lin, L. 2000. "Evaluating the Hydraulic Conductivity of GCLs Permeated with Non-standard Liquids." *Geotextiles and Geomembranes,* 18(2-4), 133-161.

Shackelford, C., and Daniel, D., 1991. "Diffusion in Saturated Soil. 1. Background." *Journal of Geotechnical Engineering*, 117(3), 467–484.

Shackelford, C., Daniel, D., Liljestrand, H., 1989. "Diffusion of Inorganic Chemical Species in Compacted Clay Soil." *Journal of Contaminant Hydrology*, 4 241-273.

Shackelford, C., and Lee, J., 2003. "The Destructive Role of Diffusion on Clay Membrane Behavior." *Clays and Clay Minerals*, 51(2), 187-197.

Shackelford, C., Malusis, M., and Olsen, H., 2003. "Clay Membrane Behavior for Geoenvironmental Containment." *Soil and Rock America Conference 2003*, P. J. Culligan, H. H. Einstein, and A. J. Whittle, Eds., Verlag Glückauf GMBH, Essen, Germany, Vol. 1, 767-774.

Shackelford, C. and Moore, S.M., 2013. "Fickian Diffusion of Radionuclides for Engineered Containment Barriers: Diffusion Coefficients, Porosities, and Complicating Issues." *Engineering Geology*, 152(1), 133-147.

Shackelford, C., Meier, A., Sample-Lord, K., 2016. "Limiting Membrane and Diffusion Behavior of a Geosynthetic Clay Liner," *Geotextiles and Geomembranes* (in review).

Stern, R.T. and Shackelford, C.D., 1998. "Permeation of Sand-Processed Clay Mixtures with Calcium Chloride Solutions." *Journal of Geotechnical and Geoenvironmental Engineering*, 124(3), 231-241.

Tang, Q., Katsumi, T., Inui, T., Li, Z., 2014a. "Membrane Behavior of Bentonite-Amended Compacted Clay." *Soils and Foundations*, Japanese Geotechnical Society, 54(3), 329-344.

Tang, Q., Katsumi, T., Inui, T., Takai, A., Li, Z., 2014b. "Influence of Compaction Degree on Membrane Behavior of Compacted Clay Amended with Bentonite." *Geo-Congress 2014*, February 23-26, 2014, Atlanta, Georgia, GSP 234, ASCE.

Tian, K., and Benson, C., 2015. "Effect of Low-Level Radioactive Waste Leachate on Hydraulic Conductivity of a Geosynthetic Clay Liner." *Geosynthetics 2015*, February 15-18, 2015, Portland, Oregon, Industrial Fabrics Association International, Roseville, MN, 236-244

Tong, S., 2015. "Standardized Hydraulic Conductivity Testing of Compacted Sand-Bentonite Mixtures." MS Thesis, Colorado State University, Fort Collins, CO.

Tong, S., and Shackelford, C., 2016. "Standardized Hydraulic Conductivity Testing of Compacted Sand-Bentonite Mixtures." *Geotechnical Testing Journal* (in-review).

van Olphen, H., 1963. *An Introduction to Clay Colloid Chemistry*. John Wiley & Sons, Inc., New York.

Yeo, S., Shackelford, C., and Evans, J., 2005. "Membrane Behavior of Model Soil-Bentonite Backfills." *Journal of Geotechnical and Geoenvironmental Engineering*, 131(4), 418-429.

Yesiller, N., and Shackelford, C.D., 2011. *Geoenvironmental Engineering* (Chapter 13). Geotechnical Engineering Handbook, Das, B.M., eds., J. Ross Publishing, Ft. Lauderdale, FL, 13-1 – 13-61.

APPENDIX A: METHOD OF REVERSE FITTING FOR DETERINATION OF STEADY-STATE NET ACCUMULATED SOLUTE FLUX

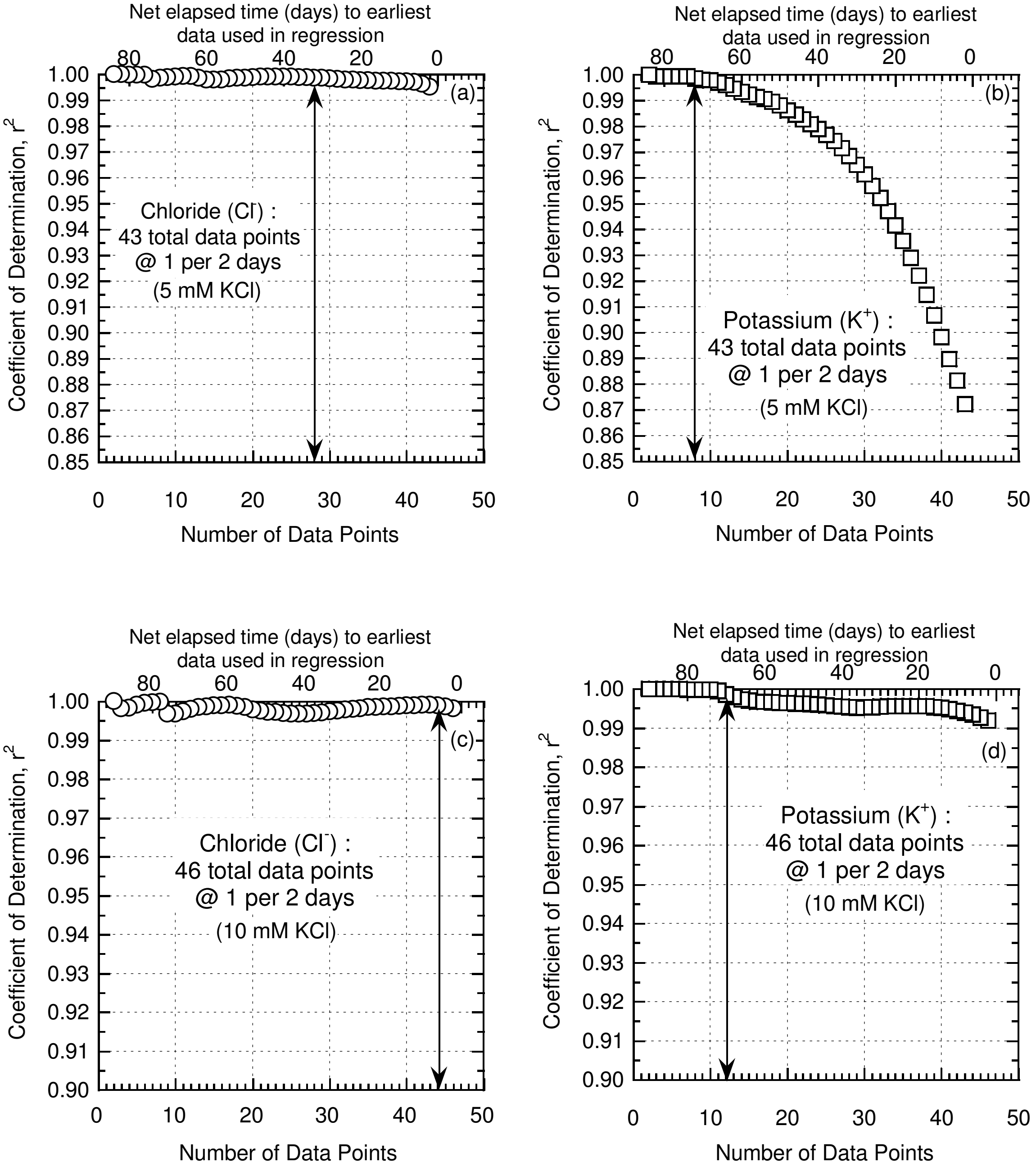

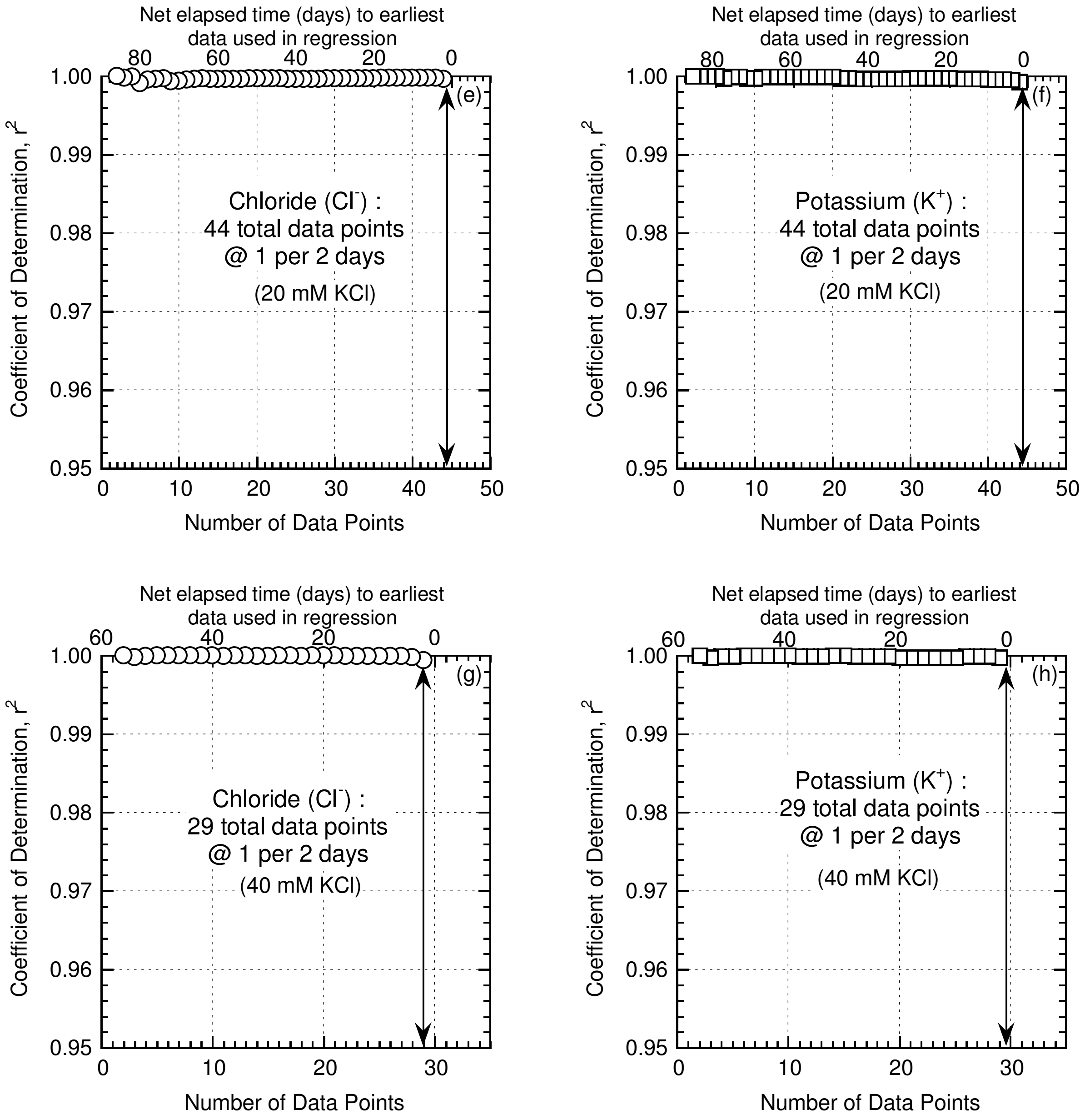
Net elapsed time (days) to earliest data used in regression
80
60
40
20
0
1.00
0.99
0.98
0.97
0.96
0.95
Coefficient of Determination, r²
(e)
Chloride (Cl⁻) :
44 total data points
@ 1 per 2 days
(20 mM KCl)
0
10
20
30
40
50
Number of Data Points
Net elapsed time (days) to earliest data used in regression
(f)
Potassium (K⁺) :
44 total data points
@ 1 per 2 days
(20 mM KCl)
Number of Data Points
Net elapsed time (days) to earliest data used in regression
60
40
20
0
(g)
Chloride (Cl⁻) :
29 total data points
@ 1 per 2 days
(40 mM KCl)
0
10
20
30
Number of Data Points
Net elapsed time (days) to earliest data used in regression
(h)
Potassium (K⁺) :
29 total data points
@ 1 per 2 days
(40 mM KCl)
Number of Data Points

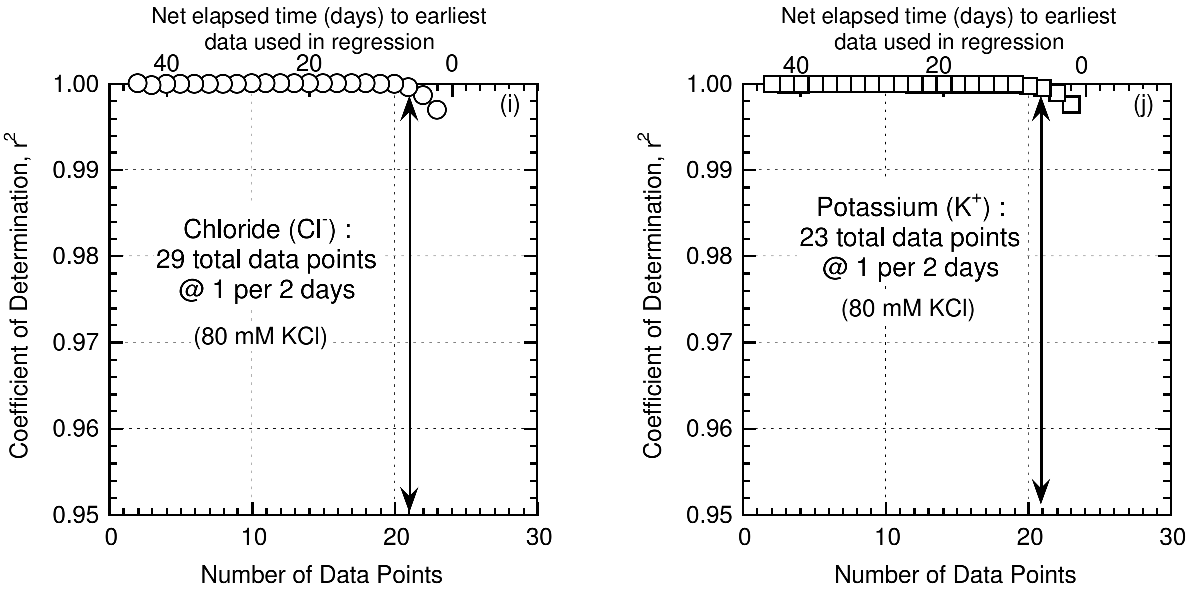

Figure A.1. Determination of steady-state net solute mass flux through the method of reverse fitting values of r^2: (a) Cl^- data for the 5 mM KCl stage; (b) K^+ data for the 5 mM KCl stage; (c) Cl^- data for the 10 mM KCl stage; (d) K^+ data for the 10 mM KCl stage; (e) Cl^- data for 20 mM KCl stage; (f) K^+ data for the 20 mM KCl stage; (g) Cl^- data for the 40 mM KCl stage; (h) K^+ data for the 40 mM KCl stage; (i) Cl^- data for the 80 mM KCl stage; (j) K^+ data for the 80 mM KCl stage.

APPENDIX B: COMPARISON OF CHEMICO-OSMOTIC EFFICIENCY COEFFICIENTS FOR DIFFERENT TYPES OF BENTONITE-BASED BARRIERS

Table B. 1. Tabulated values from the literature of membrane efficiency coefficients for different types of bentonite-based barriers.

Barrier Type	Reference	Cell Type[a]	Salt Type	Source Concentration, C_{ot} (mM)	Membrane Efficiency coefficient based on C_{ot}, ω_o	Average Source Concentration Across the Specimen, $C_{o,ave}$ (mM)	Membrane Efficiency coefficient based on C_{ave}, ω_{ave}	Porosity, *n*
Geosyntehtic Clay Liner (GCL)	Malusis and Shackelford (2002a)	RW	KCl	3.9	0.590	1.95	0.63	0.80
				8.7	0.46	4.35	0.49	0.79
				20	0.28	10	0.32	0.79
				47	0.12	23.5	0.14	0.78
				3.9	0.68	1.95	0.69	0.74
				6	0.56	3	0.58	
				8.7	0.51	4.35	0.53	
				20	0.3	10	0.32	
				47	0.14	23.5	0.16	
				3.9	0.48	1.95	0.52	0.86
				6	0.38	3	0.42	
				8.7	0.38	4.35	0.42	
				20	0.21	10	0.26	
				47	0.07	23.5	0.08	
	Kang and Shackelford	FW	KCl	3.9	0.427	1.95	0.561	0.81
				6	0.308	3	0.418	0.80

	(2011) also presented in Malusis et al. (2014)			8.7	0.202	4.35	0.286	0.79
				20	0.050	10	0.076	0.79
				47	0.010	23.5	0.015	0.79
				3.9	0.498	1.95	0.584	0.80
				6	0.375	3	0.461	0.80
				8.7	0.26	4.35	0.328	0.80
				20	0.113	10	0.152	0.80
				47	0.049	23.5	0.068	0.79
				3.9	0.634	1.95	0.719	0.77
				6	0.521	3	0.628	0.77
				8.7	0.390	4.35	0.484	0.76
				20	0.171	10	0.226	0.76
				47	0.070	23.5	0.098	0.76
				3.9	0.680	1.95	0.784	0.70
				6	0.545	3	0.635	0.68
				8.7	0.383	4.35	0.459	0.67
				20	0.180	10	0.230	0.66
				47	0.079	23.5	0.106	0.66
	Meier et al. (2014)	RW	KCl	20	0.096	10	0.12	0.79
				35	0.054	17.5	0.067	
				40	0.034	20	0.043	
				100	0.015	50	0.018	
				200	0.004	100	0.006	
				400	0.000087	200	0.000112	
Bentonite Amended Compacted	Kang and Shackelford (2010)	FW	KCl	3.9	0.763	1.95	0.973	0.36
				8.7	0.354	4.35	0.389	
				20	0.027	10	0.03	

Clay Liner (CCL)	Tang et al. (2014)	RW	KCl	0.5	0.880	0.25	1.03	0.44
				1	0.580	0.5	0.63	
				5	0.390	2.5	0.42	
				10	0.200	5	0.23	
				50	0.040	25	0.05	
				0.5	0.990	0.25	1.12	0.44
				1	0.620	0.5	0.66	
				5	0.350	2.5	0.39	
				10	0.200	5	0.24	
				50	0.040	25	0.05	
				0.5	0.920	0.25	1.01	0.47
				1	0.740	0.5	0.8	
				5	0.360	2.5	0.41	
				10	0.210	5	0.25	
				50	0.050	25	0.06	
				0.5	0.920	0.25	1.04	0.49
				1	0.530	0.5	0.59	
				5	0.370	2.5	0.43	
				10	0.230	5	0.26	
				50	0.060	25	0.07	
Compacted Natural Bentonites	Kemper and Rollins (1966)	RW	NaCl	--	--	1.9	0.98	0.80
				--	--	6	0.79	
				--	--	19	0.42	
				--	--	60	0.1	
				--	--	190	0.01	
			NaCl	--	--	1.9	0.77	0.84

				--	--	6	0.56	
				--	--	19	0.29	
				--	--	60	0.085	
				--	--			
			NaCl	--	--	1.9	0.68	0.91
				--	--	6	0.37	
				--	--	19	0.12	
				--	--	60	0.005	
	Kemper and Quirk (1972)	RW	NaCl	3	0.800	2	0.8	0.84
				10	0.500	6.5	0.5	
				30	0.250	20	0.25	
				100	0.030	65	0.03	
				300	0.003	200	0.003	
				1000	0.001	650	0.001	
			CsCl	3	0.250	2	0.25	0.84
				10	0.110	6.5	0.11	
				30	0.030	20	0.03	
				300	0.001	200	0.001	
			NaCl	3	0.210	2	0.21	0.91
				10	0.075	6.5	0.075	
				30	0.015	20	0.015	
				100	0.001	65	0.001	
	Keijzer et al. (1999)	FW	NaCl	600	--	350	0.003	0.35-0.638
				600	--	350	0.001	0.35-671
	Keijzer and Loch (2001)	FW	NaCl	100	--	55	0.015	0.555
	Dominijanni et al. (2013)	RW	NaCl	5.16	--	2.58	0.680	0.81
				10.27	--	5.135	0.580	

				20.24	--	10.12	0.330	
				51.94	--	25.97	0.140	
				109.31	--	54.66	0.050	
	Di Emidio et al. (2015)	RW	$CaCl_2$	1	--	0.5	0.29	0.718
				5	--	2.5	0	
Compacted Polymerized Bentonites	Bohnhoff and Shackelford (2013)	RW	KCl	4.7	0.800	2.35	0.84	0.92
				9.3	0.650	4.65	0.69	
				20	0.430	10	0.5	
				54	0.170	27	0.21	
				4.7	0.880	2.35	0.88	0.80
				9.3	0.730	4.65	0.76	
				20	0.460	10	0.51	
				54	0.200	27	0.25	
		FW		4.7	0.550	2.35	0.63	0.94-0.95
				9.3	0.320	4.65	0.45	
				20	0.140	10	0.22	
				54	0.040	27	0.07	
				4.7	0.460	2.35	0.45	0.78-0.84
				9.3	0.380	4.65	0.46	
				20	0.250	10	0.35	
				54	0.100	27	0.15	
	Di Emidio et al. (2015)	RW	$CaCl_2$	1	--	0.5	0.65	0.718
				5	--	2.5	0.13	
Compacted Sand-	Barbour and Fredlund (1989)	FW	NaCl	8	0.4	--	--	0.44
				9.5	0.06	--	--	
				50	0.04	--	--	

Bentonite Mixtures				100	0.03	--	--	
				400	0.00015	--	--	
				2000	0.00035	--	--	
				3000	0.00055	--	--	
				4000	0.00065	--	--	
				8	0.4	--	--	
				50	0.09	--	--	
				100	0.06	--	--	
	Saindon and Whitworth (2005)	RW	NaCl	1	0.030	--	--	unknown
				1	0.035	--	--	
				1	0.040	--	--	
				1	0.190	--	--	

[a] Cell types are designated as RW (rigid-wall) and FW (flexible-wall)

APPENDIC C: COMPARISON OF EFFECTIVE DIFFUSION COEFFICICENTS FOR CHLORIDE FOR DIFFERENT TYPES OF BENTONITE-BASED BARRIERS

Table C. 1. Tabulated values from the literature for effective diffusion coefficients for chloride for different types of bentonite-based barriers.

Barrier Type	Reference	Cell Type	Salt/ Contaminant	Source Cl^- Concentration (mM)	Effective Diffusion Coefficient based on ΔC_{ave}, D^*_{ave} ($x10^{-10}$ m2/s)	Porosity, *n*
Geosynthetic Clay Liners (GCLs)	Shackelford and Lee (2003)	RW	$CaCl_2$	5	1.21	0.72
	Malusis et al. (2014)	FW	KCl	3.9	1.26	0.80
				6	1.66	0.80
				8.7	2.08	0.79
				20	2.69	0.79
				47	2.80	0.79
				3.9	0.86	0.8-0.79
				6	1.39	
				8.7	1.71	
				20	2.12	
				47	2.41	
				3.9	0.72	0.77-0.76
				6	0.86	
				8.7	1.13	
				20	1.59	
				47	2.02	
				3.9	0.43	0.69
				6	0.64	0.68
				8.7	0.87	0.67
				20	1.18	0.66
				47	1.38	0.66
	Shackelford et al. (2016)	RW	KCl	21.1	1.108	0.79
				35.2	1.352	
				54.8	1.470	
				108.2	1.516	
				239.8	1.648	

				408.1	1.826	
Compacted Clay Liners (CCLs)	Crooks and Quigley (1984)	RW	NaCl	256.7	10	0.38
					6	
	Shackelford et al. (1989)	RW	Leachate	10	34	0.54
					0.47	0.54
					44	0.52
					15	0.47
					1.4	0.45
	Shackelford and Daniel (1991)	RW	Leachate	10	4.5	0.59
					10.4	0.58
					5.5	0.56
					8	0.54
					9.1	0.54
					10.6	0.57
					7.1	0.55
					4.7	0.47
	Rowe and Badv (1996)	RW	NaCl	50	5.7	0.287
					5.7	
	De Soto et al. (2012)	RW	Leachate	75	0.29	0.29
				250	0.15	0.41
Compacted Natural Bentonites	Rosanne et al. (2003)	RW	NaCl	1	3.75	0.56
				100	9	0.59
				100	1.85	0.49
				100	1.15	0.46
	Dominijanni et al. (2013)	RW	NaCl	10.27	2.54	0.81
				20.24	3.52	
				51.94	4.19	
				109.31	4.6	
	Di Emidio et al. 2015	RW	$CaCl_2$	1	0.40	0.72
				5	2.22	
				10	3.80	
Compacted Polymerized Bentonites	Mazzieri et al. (2010)	RW	$CalCl_2$	10	1.79	0.717
	Bohnhoff and Shackelford (2015)	RW	KCl	4.7	1	0.92
				9.3	1.5	
				20	1.4	

				54	2.2	
				4.7	0.37	0.8
				9.3	0.55	
				20	0.68	
				54	1	
		FW		4.7	1.7	0.94-0.95
				9.3	2.2	
				20	2.7	
				54	2.9	
				4.7	0.73	0.78-0.84
				9.3	0.99	
				20	1.4	
				54	1.6	
	Di Emidio et al. (2015)	RW	$CaCl_2$	1	0.44	0.72
				5	1.67	
				10	1.71	